

# Decoding FRB energetics and frequency features hidden by observational incompleteness

Chen-Ran Hu<sup>ID</sup><sup>1</sup>, Yong-Feng Huang<sup>ID</sup><sup>\*1,2,✉</sup>, Jin-Jun Geng<sup>ID</sup><sup>3</sup>, Chen Deng<sup>ID</sup><sup>1</sup>, Ze-Cheng Zou<sup>ID</sup><sup>1</sup>,  
Xiao-Fei Dong<sup>ID</sup><sup>1</sup>, Yi-Dan Wang<sup>ID</sup><sup>4,5</sup>, Pei Wang<sup>ID</sup><sup>†4,6,✉</sup>, Fan Xu<sup>ID</sup><sup>7</sup>, Lang Cui<sup>ID</sup><sup>8,9,10</sup>, Song-Bo  
Zhang<sup>ID</sup><sup>3</sup>, Xue-Feng Wu<sup>ID</sup><sup>‡3,11,✉</sup>

<sup>1</sup>*School of Astronomy and Space Science, Nanjing University, Nanjing 210023, China*

<sup>2</sup>*Key Laboratory of Modern Astronomy and Astrophysics (Nanjing University), Ministry of Education, China*

<sup>3</sup>*Purple Mountain Observatory, Chinese Academy of Sciences, Nanjing 210023, China*

<sup>4</sup>*CAS Key Laboratory of FAST, National Astronomical Observatories, Chinese Academy of Sciences, Beijing 100101, China*

<sup>5</sup>*University of Chinese Academy of Sciences, Beijing 100049, China*

<sup>6</sup>*Institute for Frontiers in Astronomy and Astrophysics, Beijing Normal University, Beijing 102206, China*

<sup>7</sup>*Department of Physics, Anhui Normal University, Wuhu 241002, China*

<sup>8</sup>*Xinjiang Astronomical Observatory, Chinese Academy of Sciences, 150 Science 1-Street, Urumqi 830011, China*

<sup>9</sup>*Key Laboratory of Radio Astronomy, Chinese Academy of Sciences, 150 Science 1-Street, Urumqi 830011, China*

<sup>10</sup>*Xinjiang Key Laboratory of Radio Astrophysics, 150 Science 1-Street, Urumqi 830011, China*

<sup>\*</sup>Email: hyf@nju.edu.cn, orcid.org/0000-0001-7199-2906

<sup>†</sup>Email: wangpei@nao.cas.cn, orcid.org/0000-0002-3386-7159

<sup>‡</sup>Email: xfwu@pmo.ac.cn, orcid.org/0000-0002-6299-1263

<sup>11</sup>*School of Astronomy and Space Sciences, University of Science and Technology of China, Hefei 230026, China*

**Fast radio bursts (FRBs) are fierce radio flashes lasting for a few milliseconds from the sky. Although their connection to strongly magnetized neutron stars has been strongly indicated, the exact triggering process and radiation mechanism are still unknown and highly debated. Due to their extremely short duration, the observation of FRBs has long been a difficult task even for large radio telescopes. The difficulty results from the fact that the information obtained in observations is always incomplete, since the telescope always has a limited flux sensitivity and finite operating frequency band. A pressing challenge is to decode the intrinsic features of FRBs from the incomplete observations. Here we establish an efficient methodology to overcome this problem, aiming at effectively correcting for the fluence and frequency cutoffs. Using this method, inverse modeling is performed on a large number of repeating bursts from FRB 20121102A to recover their intrinsic features. It is found that strong bursts intrinsically tend to concentrate their energy in a narrow band, while the spectral range of weak bursts can be either narrow or wide. However, when a weak burst has a broad spectrum, the wing of the spectrum can easily go undetected, resulting in a very narrow spectrum being observed. The narrow spectrum features observed in repeating FRBs are thus an observational selection effect. Underestimation of the burst energy caused by observational cutoffs is also corrected for, and the intrinsic burst energy distribution is re-constructed. It is also found that the bandwidth increases with the increasing central frequency in the Arecibo sample (1.15-1.73 GHz), but such a correlation is not observed in the FAST (1-1.5 GHz) and GBT (4-8 GHz) sample. It indicates the emission pattern of the FRB source might vary across**

## **different active periods and frequency bands.**

Fast radio bursts (FRBs) are cosmic explosions that release immense energy at radio wavelengths on a millisecond timescale. They are commonly classified as either non-repeating (one-off) or repeating sources. FRB 20121102A is one of the most notable repeating sources, which has been monitored extensively<sup>1-9</sup>. However, during the observing process, the detected bursts are often incompletely recorded due to limitations in telescope sensitivity and operating band<sup>3,10</sup>, which seriously restricts our exploration of the underlying physics. The large number of bursts from the same repeater provides us with an opportunity to reconstruct a “complete” sample. Utilizing observational data from the 305-m William E. Gordon Telescope at the Arecibo Observatory (Arecibo<sup>3</sup>), the Robert C. Byrd Green Bank Telescope (GBT<sup>9</sup>) and the Five-hundred-meter Aperture Spherical radio Telescope (FAST<sup>1</sup>), we have tried to correct for the observational cutoff effects on the bursts from FRB 20121102A through an inverse modeling process. Our reconstruction involves using mathematical and statistical techniques to recover the genuine burst properties from the observational data. Based on the reconstructed bursts, intrinsic energetics and frequency features are then analyzed.

### **Observational cutoff effect**

Observational cutoff primarily arises from the fluence threshold and band limitations of the telescope, leading to incompleteness in data acquisition. The spectra of the bursts from FRB 20121102A are found to be well described by the Gaussian function<sup>3,8,11-14</sup>. Our quantitative analysis based on the Bayesian Information Criterion (BIC)<sup>15</sup> also shows that the Gaussian model provides a better fit to the FRB spectra over the power-law and cutoff power-law models (Methods). Fig. 1 illustrates

the impact of observational cutoff on the burst, which can be caused by either sensitivity cutoff or operating-band cutoff. Due to the existence of the fluence threshold  $F_{\nu,\text{thre}}$ , the lower wings of the burst spectrum will be completely omitted in observations since they are beneath the threshold (i.e. sensitivity cutoff). Also, the operating-band cutoff leads to inaccurate estimations of the burst energy and bandwidth (e.g. the proper spectral boundaries  $\nu_\ell$  and  $\nu_h$  are cutoff to the observed spectral boundaries  $\nu_1$  and  $\nu_2$ ).

A connection between the observed spectrum and the intrinsic spectrum can be established by considering the Gaussian shape of the spectral energy distribution. The spectral parameters of intrinsic spectrum can be derived from observations by solving the following equation,

$$\sqrt{2\pi}F_{\nu,\text{thre}}\sigma_\nu e^{\left(\frac{\delta\nu}{2\sqrt{2}\sigma_\nu}\right)^2} \left[ \Phi\left(\frac{\nu_2 - \nu_p}{\sigma_\nu}\right) - \Phi\left(\frac{\nu_1 - \nu_p}{\sigma_\nu}\right) \right] = F_{\nu,\text{obs}}^{\text{equiv}} \delta\nu_{\text{obs}}, \quad (1)$$

where  $\Phi$  is the cumulative function of a standard Gaussian distribution,  $\nu_p$  is the peak frequency, and  $\sigma_\nu$  characterizes the intrinsic full width at half maximum (FWHM) of the spectrum.  $F_{\nu,\text{obs}}^{\text{equiv}}$  denotes the observed frequency-equivalent fluence,  $\delta\nu_{\text{obs}} = \nu_2 - \nu_1$  represents the observed bandwidth of the burst, and  $\delta\nu = \nu_h - \nu_\ell$  stands for the intrinsic bandwidth. It is worth noting that both  $\delta\nu$  and  $\delta\nu_{\text{obs}}$  depend on the telescopes used in the observation. We have utilized the algorithm of adaptive gradient descent (AGD<sup>16–18</sup>) to numerically solve the above equation (Methods). As illustrated in Fig. 1, we can also calculate the integrated fluence as

$$F = \int_0^\infty F_\nu d\nu = \sqrt{2\pi}F_{\nu,\text{thre}}\sigma_\nu e^{\left(\frac{\delta\nu}{2\sqrt{2}\sigma_\nu}\right)^2}, \quad (2)$$

where  $F_\nu$  is the monochromatic fluence at frequency  $\nu$ . By solving Equation (1) and Equation (2), we can further calculate the proper energy of the burst as

$$E = (10^{-20} \text{ erg}) \frac{4\pi}{1+z} \left( \frac{F}{\text{Jy} \cdot \text{ms} \cdot \text{MHz}} \right) \left( \frac{D_L}{\text{cm}} \right)^2, \quad (3)$$



where  $z$  and  $D_L$  correspond to the redshift and luminosity distance of the FRB source, respectively.

### Sensitivity cutoff

During nearly 59 hours of observations between December 2015 and October 2016, Arecibo detected 478 bursts from FRB 20121102A. The observations were performed with a fluence threshold of  $\sim 0.057$  Jy ms in an operating band of 1.15 – 1.73 GHz, providing measurements of  $\nu_1$ ,  $\nu_2$  and  $F_{\nu,\text{obs}}^{\text{equiv}}$  for the bursts<sup>3</sup>. For a specific burst, since  $F_{\nu,\text{obs}}^{\text{equiv}}$  is derived from  $\delta\nu_{\text{obs}}$  in the sample, we have  $F_{\nu,\text{thre}} = 0.057\sqrt{275\text{ MHz}/\delta\nu_{\text{obs}}}$  Jy ms (see Ref. <sup>3, 13, 19, 20</sup>). All these Arecibo bursts are influenced by sensitivity cutoff, while only a subset are affected by operating-band cutoff. Specifically, whether a burst is affected by operating-band cutoff can be determined by checking if the observed spectral boundaries reach the edges of the telescope’s operating band. We have reconstructed the intrinsic burst spectra of this Arecibo sample. Eight bursts were excluded as they are below the fluence threshold, which makes their observed parameters highly uncertain. Among the remaining bursts, 113 events are band-unlimited, which implies the absence of operating-band cutoff. They will be corrected for the sensitivity cutoff effect in this section. The other 357 bursts, which are band-limited, will be discussed in the section of Operating-band cutoff.

For band-unlimited bursts, we have  $\nu_p = \nu_{p,\text{obs}} = \frac{\nu_1 + \nu_2}{2}$ . Utilizing Equations (1) and (2), we can obtain the spectral solution of  $(F, \nu_p, \sigma_\nu)$  for each band-unlimited burst in the Arecibo sample. All physical quantities of the reconstructed band-unlimited bursts are displayed in Extended Data Fig. 10, together with pairwise correlation coefficients  $\tau_b$ . The derived  $(F, \nu_p, \sigma_\nu)$  and the observed physical quantities  $(F_{\nu,\text{obs}}^{\text{equiv}}, \delta\nu_{\text{obs}}, \Delta t_{\text{obs}}, W_{\text{obs}}^{\text{equiv}})$  are compared pairwise in Fig. 2a. Here,  $\Delta t_{\text{obs}}$  is

the waiting time and  $W_{\text{obs}}^{\text{equiv}}$  corresponds to the boxcar-equivalent pulse width. The Kendall tau method<sup>21–24</sup> is employed to calculate the correlation coefficient ( $\tau_b$ ) between the quantities and the corresponding hypothesis test results ( $p$ ). A correlation is deemed to exist when the absolute value of  $\tau_b$  exceeds 0.4, with positive and negative values indicating positive and negative correlations, respectively. The correlation is significant when  $p$  is below 0.05. For the statistically significant correlations, corresponding trendlines (dash-dotted lines) are plotted in the panels. In Fig. 2a, the correlation between  $F_{\nu, \text{obs}}^{\text{equiv}}$  and  $F$  can be approximated as  $F_{\nu, \text{obs}}^{\text{equiv}} = 0.0044F^{0.94}$ , which essentially indicates  $F_{\nu, \text{obs}}^{\text{equiv}} \propto \frac{F}{\delta f}$ . It means that for band-unlimited bursts, the method of estimating the burst energy by adopting the width of the operating band as the burst bandwidth is viable<sup>25</sup>. Interestingly, in the  $W_{\text{obs}}^{\text{equiv}}$  vs.  $F$  plane, the correlation is approximately  $F \propto W_{\text{obs}}^{\text{equiv}^2}$ . Considering that  $F_{\nu, \text{obs}}^{\text{equiv}} \propto \frac{F}{\delta f}$  and  $F_{\nu, \text{obs}}^{\text{equiv}} = S_\nu W_{\text{obs}}^{\text{equiv}}$  for band-unlimited bursts, where  $S_\nu$  represents the peak flux density, we have  $S_\nu \propto W_{\text{obs}}^{\text{equiv}}$ . It indicates that bursts with a higher energy tend to have a longer duration.

We have further analyzed the reconstructed band-unlimited bursts. The results are shown in Fig. 3. We define  $\frac{F}{\sigma_\nu}$  as the intrinsic frequency-averaged fluence and  $\frac{\delta\nu_{\text{obs}}}{\sigma_\nu}$  as the observed-to-intrinsic bandwidth ratio. In Fig. 3a, both  $F_{\nu, \text{obs}}^{\text{equiv}}$  and  $\frac{\delta\nu_{\text{obs}}}{\sigma_\nu}$  increase as  $\frac{F}{\sigma_\nu}$  increases. This is because a higher intrinsic frequency-averaged fluence of the burst results in an elevated fraction of its spectrum emerging above the telescope’s fluence threshold, leading to a higher observed-to-intrinsic bandwidth ratio. In fact, from Equation (2), we can easily derive

$$F/\sigma_\nu = \sqrt{2\pi}F_{\nu, \text{thre}}e^{\left(\frac{\delta\nu/\sigma_\nu}{2\sqrt{2}}\right)^2}. \quad (4)$$

For band-unlimited bursts,  $\delta\nu_{\text{obs}}$  is identical to  $\delta\nu$ . The correlation between  $F$  and  $\frac{\delta\nu_{\text{obs}}}{\sigma_\nu}$  (the inset of Fig. 3a) can then be well interpreted by Equation (4). In observations, high-energy bursts appear at the upper end of the corresponding curve only when  $\sigma_\nu$  is small, indicating that they are linked

with a narrower spectrum. However, low-energy bursts do not exhibit a specific dependence on the spectral width. This phenomenon also provides a satisfactory explanation for the negative correlation between  $F$  and  $\sigma_\nu$  as shown in Fig. 2b. In Fig. 3a, when  $\frac{\delta\nu_{\text{obs}}}{\sigma_\nu} < 1$  (the region to the left of the dashed line), bursts with lower energies are difficult to observe. In Fig. 3b, we see that bursts with a larger  $\sigma_\nu$  are predominantly distributed around the dashed line of  $\nu_p = f_{c,\text{Arecibo}}$  (the central frequency of Arecibo operating band). This is because the bursts with much larger  $\sigma_\nu$  that are far from the dashed line of  $\nu_p = f_{c,\text{Arecibo}}$  are subject to the operating-band cutoff and therefore are not included in the sample of band-unlimited bursts.

Due to the sensitivity cutoff, bursts with a large intrinsic spectral width  $\sigma_\nu$  (i.e. FWHM) may exhibit narrow observed bandwidths  $\delta\nu_{\text{obs}}$  (see the comparison between the size of the points and the dotted lines in Fig. 3b). This occurs because if they happen to have a low energy, the lower wings of their spectra fall below the fluence threshold, resulting in a narrower observed bandwidth. It can explain the finding that the bandwidths of repeating FRBs are generally narrower than those of non-repeating FRBs<sup>14</sup>, especially considering the possibility that non-repeating FRBs could be high-energy events from repeaters<sup>26</sup>. Particularly, when a non-repeating FRB represents the rarest and most extreme high-energy burst from a repeater, even if the intrinsic spectral width is narrow, the observed bandwidth can still be significantly broadened (see those points that are smaller in size but exhibit a color closer to the red end of the color scale in Fig. 3b). Based on this, we argue that the intrinsic spectral width  $\sigma_\nu$  is a more meaningful measure of the concentration level of energy per unit frequency, compared to the observed bandwidth  $\delta\nu_{\text{obs}}$ , as the latter phenomenologically characterizes the observed spectral range well. This is somewhat similar to our definition of the temporal width of a burst. The observed narrow bandwidth can also be attributed to the operating-

band cutoff, a point that will be discussed in detail in subsequent sections.

Adopting the shifted log-normal distribution function (Methods), the distributions of intrinsic energy and observed energy of the bursts are fitted through Markov Chain Monte Carlo (MCMC) simulations (Fig. 3c). We see that the energy loss caused by the sensitivity cutoff leads to distortion in the energy distribution. Specifically, compared to the intrinsic energy, the distribution of the observed energy has a wider range in the lower region, which is due to the energy loss caused by observational cutoff. With a total energy loss of  $1 - \left(\frac{\Sigma E_{\text{obs}}}{\Sigma E}\right)_{\text{band-unlimited}} = 0.05$ , the energy loss due to the sensitivity cutoff in band-unlimited bursts of the Arecibo sample is small. Naturally, for telescopes with a better fluence sensitivity, the energy loss due to the sensitivity cutoff will be even smaller. In general, sensitivity cutoff predominantly influences the observed bandwidth of the burst.

### **Operating-band cutoff**

In the Arecibo sample, nearly 75% of the bursts are band-limited, indicating that they are affected by both the sensitivity cutoff and the operating-band cutoff (see Fig. 1). The occurrence of the operating band can lead to significant variation of the spectral index, which may range from negative to positive values across bursts<sup>2,27</sup>. This can also explain why some bursts can be well fitted by a power-law spectrum, while others cannot<sup>28,29</sup>. Additionally, operating-band cutoff can cause distortion of bursts on the  $\nu_{\ell}-\nu_h$  plane (i.e. the lower boundary of intrinsic spectrum plotted versus the upper boundary of intrinsic spectrum).

Based on Bayesian inference, we have reconstructed the intrinsic 2D Gaussian distribution

of  $(\nu_\ell, \nu_h)$  (Methods). The blue contour lines in Fig. 4a depict the reconstructed  $(\nu_\ell, \nu_h)$  distribution. Due to the influence of the operating band limits, the band-limited bursts are squeezed from their intrinsic distribution to the observed distribution (the yellow-orange-red contour lines). Specifically, these band-limited bursts can be classified into three categories as  $\nu_\ell < f_\ell < \nu_h < f_h$ ,  $f_\ell < \nu_\ell < f_h < \nu_h$  and  $\nu_\ell < f_\ell < f_h < \nu_h$ , inherently occupying their respective regions but being squeezed towards the operating band limits (the orange dashed lines) and clustered there, as indicated by the arrows. Such a phenomenon can also be observed in the subplots of Fig. 4a, where the intrinsic 1D distributions of  $\nu_\ell$  and  $\nu_h$  (the blue solid lines) are squeezed and distorted into the observed 1D distributions (green histograms). The reconstructed distribution of  $(\nu_\ell, \nu_h)$ , denoted as  $f_N(\nu_\ell, \nu_h) \sim N(\nu_\ell, \nu_h; \mu_{\nu_\ell}, \mu_{\nu_h}, \sigma_{\nu_\ell}, \sigma_{\nu_h}, \rho)$ , can be described by

$$f_N(\nu_\ell, \nu_h) = \frac{1}{2\pi\sigma_{\nu_\ell}\sigma_{\nu_h}\sqrt{1-\rho^2}} \exp \left\{ -\frac{1}{2(1-\rho^2)} \left[ \frac{(\nu_\ell - \mu_{\nu_\ell})^2}{\sigma_{\nu_\ell}^2} - \frac{2\rho(\nu_\ell - \mu_{\nu_\ell})(\nu_h - \mu_{\nu_h})}{\sigma_{\nu_\ell}\sigma_{\nu_h}} + \frac{(\nu_h - \mu_{\nu_h})^2}{\sigma_{\nu_h}^2} \right] \right\}. \quad (5)$$

According to Equation (5), there should also exist undetected bursts with  $\nu_\ell < \nu_h < f_\ell < f_h$  or  $f_\ell < f_h < \nu_\ell < \nu_h$ , corresponding to the pink region in the main plot of Fig. 4a. The parameters of  $N(\nu_\ell, \nu_h; \mu_{\nu_\ell}, \mu_{\nu_h}, \sigma_{\nu_\ell}, \sigma_{\nu_h}, \rho)$  are well constrained, as shown in Fig. 4b. By numerically integrating Equation (5) over the undetectable region employing the optimal parameters provided in Fig. 4b, we derived a 1.64% probability of undetected bursts for the Arecibo sample, which mainly satisfying  $f_\ell < f_h < \nu_\ell < \nu_h$ . For the band-limited bursts, the probabilities corresponding to the cases of  $\nu_\ell < f_\ell < \nu_h < f_h$ ,  $f_\ell < \nu_\ell < f_h < \nu_h$  and  $\nu_\ell < f_\ell < f_h < \nu_h$  are 5.67%, 66.24%, and 0.79%, respectively. This indicates that, given that the burst is detected, there is a 73.92% probability that it is affected by the operating-band cutoff. This probability is primarily governed by the scenario of  $f_\ell < \nu_\ell < f_h < \nu_h$ , which is in line with the observations. Note that the effect of operating-band cutoff in a sample depends not only on the telescope's operating band range but

also on the intrinsic spectra of the bursts, which may vary across different periods.

Since  $(\nu_p, \delta\nu)$  (i.e. the peak frequency and the intrinsic bandwidth) is a linear transformation of  $(\nu_\ell, \nu_h)$ , we can derive the  $(\nu_p, \delta\nu)$  distribution  $N(\nu_p, \delta\nu; \mu_{\nu_p}, \mu_{\delta\nu}, \sigma_{\nu_p}, \sigma_{\delta\nu}, k)$  from the  $(\nu_\ell, \nu_h)$  distribution as (Methods)

$$f_N(\nu_p, \delta\nu) = \frac{1}{2\pi\sigma_{\nu_p}\sigma_{\delta\nu}\sqrt{1-k^2}} \exp\left\{-\frac{1}{2(1-k^2)}\left[\frac{(\nu_p - \mu_{\nu_p})^2}{\sigma_{\nu_p}^2} - \frac{2k(\nu_p - \mu_{\nu_p})(\delta\nu - \mu_{\delta\nu})}{\sigma_{\nu_p}\sigma_{\delta\nu}} + \frac{(\delta\nu - \mu_{\delta\nu})^2}{\sigma_{\delta\nu}^2}\right]\right\}. \quad (6)$$

Here  $\mu_{\nu_p} = \frac{\mu_{\nu_\ell} + \mu_{\nu_h}}{2}$ ,  $\mu_{\delta\nu} = \mu_{\nu_h} - \mu_{\nu_\ell}$ ,  $\sigma_{\nu_p} = \sqrt{(\sigma_{\nu_\ell}^2 + \sigma_{\nu_h}^2 + 2\rho\sigma_{\nu_\ell}\sigma_{\nu_h})/4}$ ,  $\sigma_{\delta\nu} = \sqrt{\sigma_{\nu_\ell}^2 + \sigma_{\nu_h}^2 - 2\rho\sigma_{\nu_\ell}\sigma_{\nu_h}}$  and  $k = (\sigma_{\nu_h}^2 - \sigma_{\nu_\ell}^2) / \sqrt{(\sigma_{\nu_\ell}^2 + \sigma_{\nu_h}^2)^2 - 4\rho^2\sigma_{\nu_\ell}^2\sigma_{\nu_h}^2}$ . By substituting the optimal parameters from Fig. 4b into Equation (6), we obtained the intrinsic distribution of  $(\nu_p, \delta\nu)$  as demonstrated in Fig. 4c. Similar to the intrinsic distribution of  $(\nu_\ell, \nu_h)$ , distortion due to operating-band cutoff leads to an underestimation of  $\delta\nu$ , as the peak of its intrinsic distribution should be nearly twice as that being observed. In essence, it is interesting to note that  $\delta\nu$  exhibits a gradual increase with the rise of  $\nu_p$ , with a correlation coefficient of  $k = 0.44$ , which is not observationally obvious due to the presence of the operating-band cutoff. Considering the results of ‘‘intrinsic spectral width versus observed bandwidth’’ in the section of Sensitivity cutoff, the observed narrow spectrum features of repeating FRBs<sup>14,28</sup> are more likely originated from observational cutoff effects.

We have also estimated the intrinsic energy of these band-limited bursts. Although  $\nu_\ell$  and/or  $\nu_h$  of a specific burst are unknown, the distribution of  $(\nu_\ell, \nu_h)$  can be reconstructed. Thus, for all possible combinations of  $(\nu_\ell, \nu_h)$ , we can convolve the spectral solution with the corresponding probability density to obtain the expected value of the integrated fluence for a specific burst as (see

Methods)

$$E(F) = \begin{cases} \frac{\iint_{\nu_\ell < f_\ell < f_h < \nu_h} F(\nu_\ell, \nu_h, F_{\nu_{\text{obs}}}^{\text{equiv}}; F_{\nu_{\text{thre}}}) \times f_N(\nu_\ell, \nu_h) d\nu_\ell d\nu_h}{\iint_{\nu_\ell < f_\ell < f_h < \nu_h} f_N(\nu_\ell, \nu_h) d\nu_\ell d\nu_h}, & \nu_\ell < f_\ell < f_h < \nu_h, \\ \frac{\int_{\nu_\ell < f_\ell} F(\nu_\ell, \nu_h, F_{\nu_{\text{obs}}}^{\text{equiv}}; F_{\nu_{\text{thre}}}) \times \left[ f_N(\nu_\ell, \nu_h) / \varphi\left(\frac{\nu_h - \mu_{\nu_h}}{\sigma_{\nu_h}}\right) \right] d\nu_\ell}{\int_{\nu_\ell < f_\ell} \left[ f_N(\nu_\ell, \nu_h) / \varphi\left(\frac{\nu_h - \mu_{\nu_h}}{\sigma_{\nu_h}}\right) \right] d\nu_\ell}, & \nu_\ell < f_\ell < \nu_h < f_h, \\ \frac{\int_{\nu_h > f_h} F(\nu_\ell, \nu_h, F_{\nu_{\text{obs}}}^{\text{equiv}}; F_{\nu_{\text{thre}}}) \times \left[ f_N(\nu_\ell, \nu_h) / \varphi\left(\frac{\nu_\ell - \mu_{\nu_\ell}}{\sigma_{\nu_\ell}}\right) \right] d\nu_h}{\int_{\nu_h > f_h} \left[ f_N(\nu_\ell, \nu_h) / \varphi\left(\frac{\nu_\ell - \mu_{\nu_\ell}}{\sigma_{\nu_\ell}}\right) \right] d\nu_h}, & f_\ell < \nu_\ell < f_h < \nu_h. \end{cases} \quad (7)$$

Here the function  $\varphi$  is the probability density function (PDF) of the standard Gaussian distribution.

Combining the above equation with Equation (3), a reasonable estimation of the intrinsic energy of the band-limited burst can be obtained.

In Fig. 5a, we see that the decrease of  $\delta\nu_{\text{obs}}$  leads to a decrease in  $\frac{E}{E_{\text{obs}}}$ , indicating a stronger energy loss stemming from operating-band cutoff. In extreme cases, such a energy loss can even exceed one order of magnitude. Additionally, band-limited bursts with a smaller  $\delta\nu_{\text{obs}}$  tend to have a higher  $\nu_{\text{p,obs}}$ , suggesting that the primary range of the 1D distribution of  $\nu_h$  is higher than Arecibo's operating band. On the other hand, bursts with  $\nu_{\text{p,obs}}$  smaller than  $f_{\text{c,Arecibo}}$  (1440 MHz) correspond to the condition of  $\nu_\ell < f_\ell < \nu_h < f_h$ , and they tend to align closely with the  $E = E_{\text{obs}}$  line, indicating that the primary range of the 1D distribution of  $\nu_\ell$  almost coincides with Arecibo's operating band. For band-limited bursts with the same  $E$ , the energy loss (quantified by  $\frac{E}{E_{\text{obs}}}$ ) is mainly influenced by  $\nu_{\text{p,obs}}$ , which reflects the relation between  $(\nu_\ell, \nu_h)$  and the telescope's operating band. Low-energy bursts cannot possess excessively large values of  $\frac{E}{E_{\text{obs}}}$ , as they fall below the telescope's sensitivity. High-energy bursts exhibit a tendency for  $\frac{E}{E_{\text{obs}}}$  to be skewed towards either larger or smaller values. As mentioned in the section of Sensitivity cutoff, high-energy bursts tend to concentrate more energy within a narrower spectrum. Hence, they are more sensitive to the operating-band cutoff. Some of them may only lose a negligible portion of energy when the spectrum wing is cutoff, while others can experience a significant energy loss when the spectrum's

central portion is cutoff.

The intrinsic energy and observed energy distributions of all the Arecibo bursts are compared in Fig 5b. The distributions are fitted with a shifted log-normal function. Comparing with the intrinsic energy, the distribution of the observed energy is shifted towards lower values and exhibits an expanded range due to the observational cutoff effect, mainly induced by the operating band cutoff. The high-energy end of the observed distribution profile displays some anomalous substructures, which arise from the effect that a part of high-energy bursts are observed as low-energy bursts. In the Arecibo sample, the observational cutoff effect leads to an energy loss of  $1 - \left(\frac{\Sigma E_{\text{obs}}}{\Sigma E}\right)_{\text{detected}} = 0.39$  for the detected bursts, which means the cutoff effect is really significant. To meet the requirement of energy budget of radio and X-ray emissions from the central engine, additional energy mechanisms beyond the magnetar magnetosphere energy supply may be required, particularly for highly active sources<sup>30–32</sup>.

The operating-band cutoff renders some bursts undetectable (1.64%). Moreover, there should be additional undetectable bursts whose intensity falls below the fluence threshold. To consider these bursts, we employed the standard log-normal distribution function to fit the proper energy through MCMC methods. The fitted parameters are shown in Fig. 5c. While the standard log-normal distribution function may not fit the distribution profile as perfectly as the shifted log-normal distribution function, it allows for the potential presence of undetectable low-energy bursts (Methods). Distinguishing from the undetected bursts, there may exist unidentified bursts in the current observational data (e.g. extremely short-duration bursts<sup>33,34</sup>), which need to be identified using advanced data processing methods<sup>3,9</sup> and would update our understanding of FRB energy,



waiting time and event rate.

## GBT and FAST Samples

We have also applied the reconstruction methodology to other samples. During a 6-hour observation on August 26, 2017, GBT detected 93 bursts from FRB 20121102A in the 4-8 GHz operating band, providing measurements of  $\nu_1$ ,  $\nu_2$  and  $F_{\nu, \text{obs}}^{\text{equiv}}$  for each burst<sup>9</sup>. We reconstructed the intrinsic distribution of  $(\nu_\ell, \nu_h)$  for the GBT sample. The results are shown in Extended Data Fig. 7a. The model parameters are well constrained and shown in Extended Data Fig. 7b. The intrinsic distribution of  $(\nu_p, \delta\nu)$  was obtained by using Equation (6) and is shown in Extended Data Fig. 7d. In contrast to the Arecibo sample in the L-band (1-2 GHz) where  $\delta\nu$  slowly increases with the increasing  $\nu_p$ , for the bursts in the C-band (4-8 GHz),  $\delta\nu$  does not increase with the increasing  $\nu_p$ . In the GBT sample, many weak bursts were identified by utilizing machine learning method. Therefore, the fluence threshold could be complicated for these bursts<sup>19,20</sup>. An advantage of our method is its ability to adapt to the fluence threshold variation in a limited range across bursts (Methods).

During the 59.5 hours of observation spanning from 29 August to 29 October 2019, FAST detected 1652 bursts from FRB 20121102A in the 1 – 1.5 GHz operating band, providing measurements of  $F_{\nu, \text{obs}}^{\text{equiv}}$  for all bursts<sup>1,13,19,20</sup>. We reprocessed the data and extracted  $\nu_1$  and  $\nu_2$  of the bursts (Supplementary Table 1). For the FAST sample,  $F_{\nu, \text{obs}}^{\text{equiv}}$  is calculated by using the telescope operating band  $\delta f$ , thereby a fluence threshold of 0.015 Jy ms can be applied to each burst<sup>1</sup>. After excluding indeterminate bursts that are below this fluence threshold or have an observed bandwidth lower than 20 MHz (approximately 2.30% of the total sample), the intrinsic distribution of  $(\nu_\ell, \nu_h)$

was reconstructed (Extended Data Fig. 8a), and relevant parameters were derived (Extended Data Fig. 8b). Comparing with the Arecibo sample, which is also in the L-band,  $\delta\nu$  of the FAST sample does not increase with the increasing  $\nu_p$  (Extended Data Fig. 8d). Also, the intrinsic distributions of  $(\nu_\ell, \nu_h)$  and  $(\nu_p, \delta\nu)$  differ markedly for the Arecibo and FAST samples. Combined with the GBT sample, it is found that FRBs exhibit differing behaviors during different active periods and across different frequency ranges. It suggests that repeaters may reside in complex environments and involve various magnetospheric activities<sup>35–38</sup> or plasma instabilities<sup>39–41</sup>. Coordinated observations across low- and high-frequency radio bands<sup>29,42,43</sup> may provide critical evidence to diagnose the mechanisms. Alternatively, an intrinsic evolutionary process of the repeating source<sup>44</sup> itself could explain the observed diversity, necessitating extensive follow-up monitoring of well-localized repeating FRBs with high burst rates to reveal the enigma.

For the FAST sample, the energy loss due to operating-band cutoffs on the bursts is small (Extended Data Fig. 9a). This is due to the that the intrinsic frequency distribution of the bursts and the operating band range of FAST are largely matched (Extended Data Fig. 8a). It leads to a 28.65% ratio for the operating-band cutoff in detected bursts, and a 0.96% ratio for non-detections. In Extended Data Fig. 9b, for the detected bursts, the energy loss is  $1 - \left(\frac{\Sigma E_{\text{obs}}}{\Sigma E}\right)_{\text{detected}} = 0.05$ . The intrinsic energy distribution can be well fitted with a standard log-normal function (Extended Data Fig. 9c).

To conclude, observational cutoffs can lead to underestimation of the energy release from repeaters. We propose a new method to inverse model the intrinsic properties of repeating FRBs from incomplete observational data in this study. It facilitates the joint analysis of data from

various telescopes. Three incomplete samples affected by observational cutoffs were effectively reconstructed. It is found that the narrow spectrum feature of repeating FRBs arises from the observational selection effect, while only high-energy bursts are intrinsically narrow in spectrum. It is also found that repeating FRB sources may have different behaviors in different active periods and across different frequency bands. Our methodology would have a wide application when more and more observational data of repeating FRBs are available in the future.

## References

1. Li, D. et al. A bimodal burst energy distribution of a repeating fast radio burst source. *Nature* **598**, 267-271 (2021). 2107.08205.
2. Spitler, L. G. et al. A repeating fast radio burst. *Nature* **531**, 202-205 (2016). 1603.00581.
3. Hewitt, D. M. et al. Arecibo observations of a burst storm from FRB 20121102A in 2016. *Mon. Not. R. Astron. Soc.* **515**, 3577-3596 (2022). 2111.11282.
4. Michilli, D. et al. An extreme magneto-ionic environment associated with the fast radio burst source FRB 121102. *Nature* **553**, 182-185 (2018). 1801.03965.
5. Hilmarsson, G. H. et al. Rotation Measure Evolution of the Repeating Fast Radio Burst Source FRB 121102. *Astrophys. J. Lett.* **908**, L10 (2021). 2009.12135.
6. Rajwade, K. M. et al. Possible periodic activity in the repeating FRB 121102. *Mon. Not. R. Astron. Soc.* **495**, 3551-3558 (2020). 2003.03596.

7. Spitler, L. G. et al. Detection of Bursts from FRB 121102 with the Effelsberg 100 m Radio Telescope at 5 GHz and the Role of Scintillation. *Astrophys. J.* **863**, 150 (2018). 1807.03722.
8. Gajjar, V. et al. Highest Frequency Detection of FRB 121102 at 4-8 GHz Using the Break-through Listen Digital Backend at the Green Bank Telescope. *Astrophys. J.* **863**, 2 (2018). 1807.03722.
9. Zhang, Y. G. et al. Fast Radio Burst 121102 Pulse Detection and Periodicity: A Machine Learning Approach. *Astrophys. J.* **866**, 149 (2018). 1809.03043.
10. Keane, E. F. & Petroff, E. Fast radio bursts: search sensitivities and completeness. *Mon. Not. R. Astron. Soc.* **447**, 2852-2856 (2015). 1409.6125.
11. Law, C. J. et al. A Multi-telescope Campaign on FRB 121102: Implications for the FRB Population. *Astrophys. J.* **850**, 76 (2017). 1705.07553.
12. Josephy, A. et al. CHIME/FRB Detection of the Original Repeating Fast Radio Burst Source FRB 121102. *Astrophys. J. Lett.* **882**, L18 (2019). 1906.11305.
13. Lyu, F. et al. Confining Burst Energy Function and Spectral Fringe Pattern of FRB 20121102A with Multifrequency Observations. *Astrophys. J.* **941**, 127 (2022). 2305.02598.
14. Pleunis, Z. et al. Fast Radio Burst Morphology in the First CHIME/FRB Catalog. *Astrophys. J.* **923**, 1 (2021). 2106.04356.
15. Liddle, A. R. Information criteria for astrophysical model selection. *Mon. Not. R. Astron. Soc.* **377**, L74-L78 (2007). astro-ph/0701113.

16. Duchi, J. C., Hazan, E. & Singer, Y. Adaptive Subgradient Methods for Online Learning and Stochastic Optimization. *J. Mach. Learn. Res.* **12**, 2121-2159 (2011). <https://dl.acm.org/doi/10.5555/1953048.2021068>.
17. Zeiler, M. D. ADADELTA: An Adaptive Learning Rate Method. [arXiv e-prints arXiv:1212.5701](https://arxiv.org/abs/1212.5701) (2012). 1212.5701.
18. Kingma, D. P. & Ba, J. Adam: A Method for Stochastic Optimization. [arXiv e-prints arXiv:1412.6980](https://arxiv.org/abs/1412.6980) (2014). 1412.6980.
19. Caleb, M. et al. Are the distributions of fast radio burst properties consistent with a cosmological population?. *Mon. Not. R. Astron. Soc.* **458**, 708-717 (2016). 1512.02738.
20. Li, X.-J., Dong, X.-F., Zhang, Z.-B. & Li, D. Long and Short Fast Radio Bursts Are Different from Repeating and Nonrepeating Transients. *Astrophys. J.* **923**, 230 (2021). 2110.07227.
21. Kendall, M. G. A New Measure of Rank Correlation. *Biometrika* **30**, 81-93 (1938). <http://www.jstor.org/stable/2332226>.
22. Kendall, M. G. The Treatment of Ties in Ranking Problems. *Biometrika* **33**, 239-251 (1945). <http://www.jstor.org/stable/2332303>.
23. Kendall, M. G. Rank Correlation Methods. (Charles Griffin, 1970).
24. Xue, Y.-J. & Wu, X.-P. The  $L_X$ -T,  $L_X$ - $\sigma$ , and  $\sigma$ -T Relations for Groups and Clusters of Galaxies. *Astrophys. J.* **538**, 65-71 (2000). astro-ph/0002446.

25. Zhang, Y.-K. et al. FAST Observations of an Extremely Active Episode of FRB 20201124A. II. Energy Distribution. Research in Astronomy and Astrophysics **22**, 124002 (2022). 2210.03645.
26. Kirsten, F. et al. A link between repeating and non-repeating fast radio bursts through their energy distributions. Nature Astronomy **8**, 337-346 (2024). 2306.15505.
27. Zhang, B. The physics of fast radio bursts. Reviews of Modern Physics **95**, 035005 (2023). 2212.03972.
28. CHIME/FRB Collaboration et al. The First CHIME/FRB Fast Radio Burst Catalog. Astrophys. J. Suppl. **257**, 59 (2021). 2106.04352.
29. Law, C. J. et al. A Multi-telescope Campaign on FRB 121102: Implications for the FRB Population. Astrophys. J. **850**, 76 (2017). 1705.07553.
30. Zhang, B. The physical mechanisms of fast radio bursts. Nature **587**, 45-53 (2020). 2011.03500.
31. Hu, C.-P. et al. Rapid spin changes around a magnetar fast radio burst. Nature **626**, 500-504 (2024). 2402.09291.
32. Wang, P. et al. X-Ray Hardening Preceding the Onset of SGR 1935+2154's Radio Pulsar Phase. Astrophys. J. Suppl. **275**, 39 (2024). 2308.08832.
33. Snelders, M. P. et al. Detection of ultra-fast radio bursts from FRB 20121102A. Nature Astronomy **7**, 1486-1496 (2023). 2307.02303.

34. Hewitt, D. M. et al. Dense forests of microshots in bursts from FRB 20220912A. Mon. Not. R. Astron. Soc. **526**, 2039-2057 (2023). 2308.12118.
35. Luo, R. et al. Diverse polarization angle swings from a repeating fast radio burst source. Nature **586**, 693-696 (2020). 2011.00171.
36. Chime/Frb Collaboration et al. Sub-second periodicity in a fast radio burst. Nature **607**, 256-259 (2022). 2107.08463.
37. Zhang, Y.-K. et al. FAST Observations of FRB 20220912A: Burst Properties and Polarization Characteristics. Astrophys. J. **955**, 142 (2023). 2304.14665.
38. Nimmo, K. et al. Magnetospheric origin of a fast radio burst constrained using scintillation. Nature **637**, 48-51 (2025). 2406.11053.
39. Beloborodov, A. M. A Flaring Magnetar in FRB 121102?. Astrophys. J. Lett. **842**, L26 (2017). 1702.08644.
40. Michilli, D. et al. An extreme magneto-ionic environment associated with the fast radio burst source FRB 121102. Nature **553**, 182-185 (2018). 1801.03965.
41. Niu, C.-H. et al. A repeating fast radio burst associated with a persistent radio source. Nature **606**, 873-877 (2022). 2110.07418.
42. Caleb, M. et al. Simultaneous multi-telescope observations of FRB 121102. Mon. Not. R. Astron. Soc. **496**, 4565-4573 (2020). 2006.08662.

43. Pearlman, A. B. et al. Multiwavelength Radio Observations of Two Repeating Fast Radio Burst Sources: FRB 121102 and FRB 180916.J0158+65. *Astrophys. J. Lett.* **905**, L27 (2020). 2009.13559.
44. Yang, Y.-P. & Zhang, B. Fast Radio Bursts and Their High-energy Counterparts from Magnetar Magnetospheres. *Astrophys. J.* **919**, 89 (2021). 2104.01925.
45. Hu, C.-R. & Huang, Y.-F. A Comprehensive Analysis of Repeating Fast Radio Bursts. *Astrophys. J. Suppl.* **269**, 17 (2023). 2212.05242.



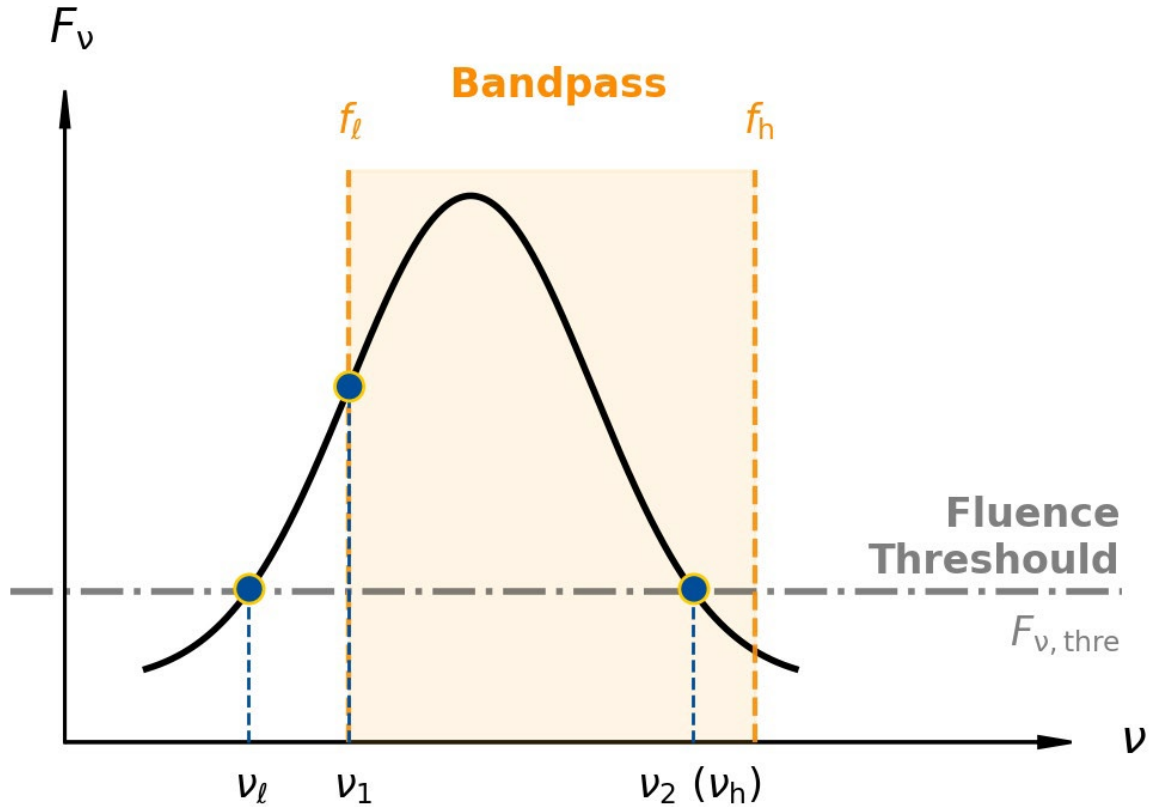


Figure 1: A schematic illustration of the observational cutoff of FRBs on the  $F_\nu$ - $\nu$  plane. The solid black curve represents the intrinsic spectrum of the burst. The dashed gray line represents the fluence threshold  $F_{\nu, \text{thre}}$  of the telescope. The orange shaded region shows the operating band of the telescope, with lower and upper limits denoted as  $f_\ell$  and  $f_h$ , respectively. The spectrum of the burst intersects with  $F_\nu = F_{\nu, \text{thre}}$  at two frequencies,  $\nu_\ell$  and  $\nu_h$ , which define the intrinsic bandwidth of the burst. Under the influence of both the sensitivity cutoff and operating-band cutoff, the observed bandwidth is determined by  $\nu_1$  and  $\nu_2$ . Note that this figure only shows one of the six possible cases, determined by the relationship of  $\nu_\ell$ ,  $\nu_h$ ,  $f_\ell$  and  $f_h$ .

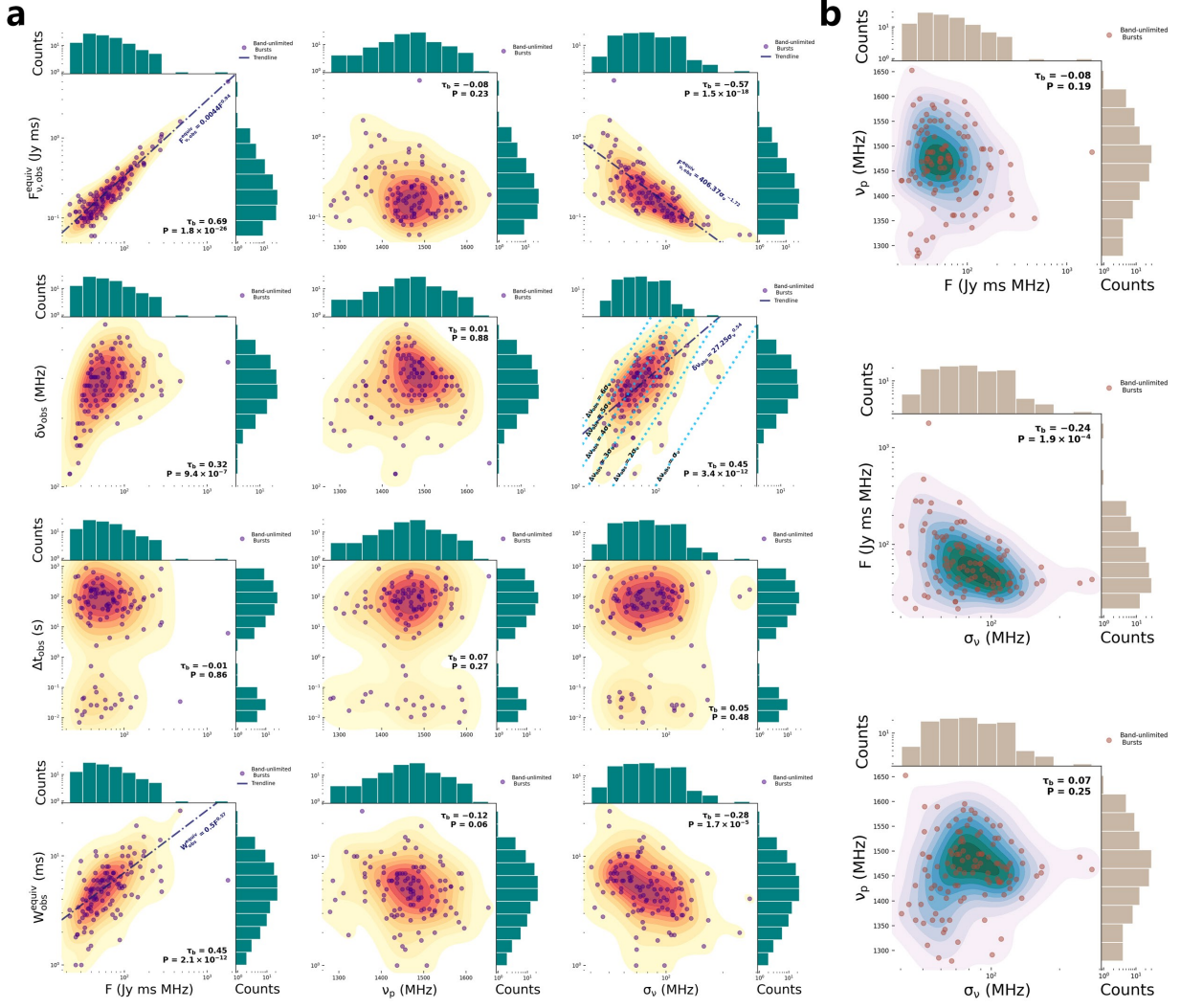


Figure 2: Comparison between the observed parameters ( $F_{\nu, \text{obs}}^{\text{equiv}}$ ,  $\delta\nu_{\text{obs}}$ ,  $\Delta t_{\text{obs}}$ ,  $W_{\text{obs}}^{\text{equiv}}$ ) and the derived spectral parameters ( $F$ ,  $\nu_p$ ,  $\sigma_\nu$ ) for the band-unlimited bursts of FRB 20121102A observed by Arecibo. Panel a: The pairwise comparison between ( $F_{\nu, \text{obs}}^{\text{equiv}}$ ,  $\delta\nu_{\text{obs}}$ ,  $\Delta t_{\text{obs}}$ ,  $W_{\text{obs}}^{\text{equiv}}$ ) and ( $F$ ,  $\nu_p$ ,  $\sigma_\nu$ ). Each main plot illustrates the 2D distribution of the band-unlimited bursts. The contour lines correspond to the kernel density estimation (KDE) of the distribution. 1D histograms are also plotted along the axes. The correlation coefficient ( $\tau_b$ ) is calculated for each pair of parameters by using the Kendall tau method. The corresponding coincidence probability ( $p$ ) is also calculated and marked. A trendline (dash-dotted line) is plotted when the correlation is statistically significant. Panel b: A pairwise plot for the three parameters of ( $F$ ,  $\nu_p$ ,  $\sigma_\nu$ ).

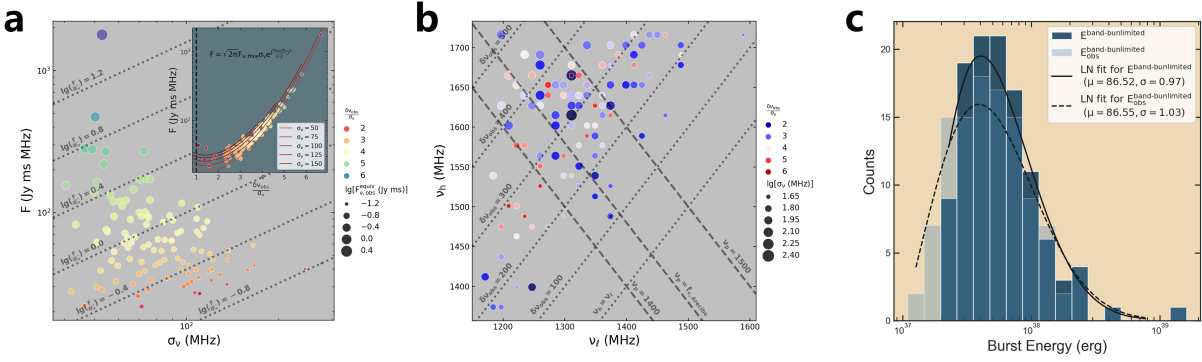


Figure 3: **Effects of sensitivity cutoff and the characteristics of reconstructed band-unlimited bursts.** Panel a: The distribution of band-unlimited bursts on the  $F$ - $\sigma_v$  plane. The data points are color-coded based on  $\frac{\delta v_{\text{obs}}}{\sigma_v}$  and their sizes are proportional to  $\lg [F_{\nu, \text{obs}}^{\text{equiv}} \text{ (Jy ms)}]$ . The inset plots the data points on the  $F$ - $\frac{\delta v_{\text{obs}}}{\sigma_v}$  plane. Panel b: The distribution of band-unlimited bursts on the  $\nu_h$ - $\nu_\ell$  plane, with data points color-coded based on  $\frac{\delta v_{\text{obs}}}{\sigma_v}$  and scaled in size proportional to  $\lg [\sigma_v \text{ (MHz)}]$ . Panel c: Observed energy distribution as compared with the intrinsic energy distribution for band-unlimited bursts.

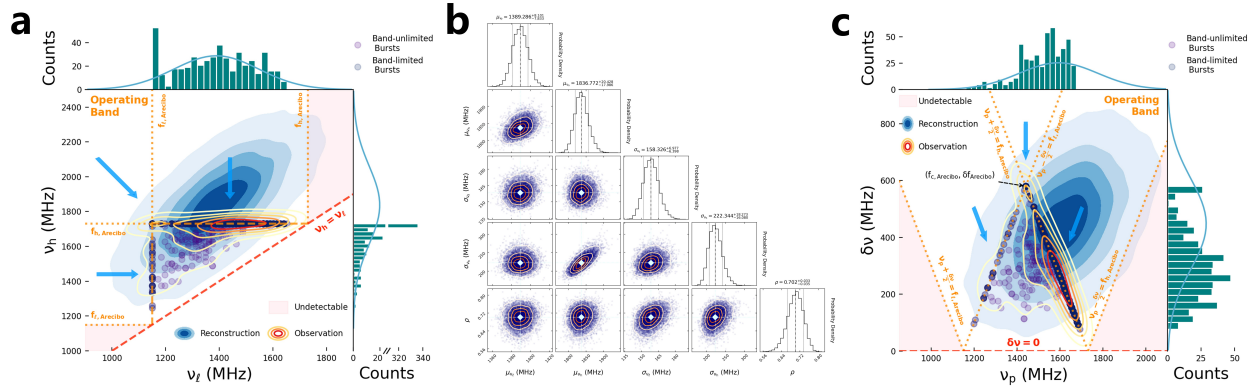


Figure 4: **Operating-band cutoff effects on burst distribution and the reconstructed intrinsic profile (Arecibo sample).** Panel a: The distribution of observed bursts on the  $\nu_h$ - $\nu_\ell$  plane. The yellow-orange-red contour lines represent the KDE, while the blue contour lines show their intrinsic distribution. 1D histograms of the bursts are shown along the axes. The dashed orange lines stand for the operating band limits of Arecibo, corresponding to  $\nu_\ell = f_\ell$ ,  $\nu_\ell = f_h$ ,  $\nu_h = f_\ell$  and  $\nu_h = f_h$ . The region below the red dashed line is non-physical, while the pink region is undetectable. Panel b: Constraints on the parameters of the reconstructed intrinsic distribution function  $N(\nu_\ell, \nu_h; \mu_{\nu_\ell}, \mu_{\nu_h}, \sigma_{\nu_\ell}, \sigma_{\nu_h}, \rho)$ . Panel c: The observed distribution of bursts on the  $\delta\nu$ - $\nu_p$  plane. The line styles are similar to that of Panel (a). Comparing with Panel (a), we see that the accumulation caused by distortion in the 1D histograms of  $\nu_p$  and  $\delta\nu$  is not restricted to the edge bin of the observed histogram, but can occur in every bin. Such histograms can be effectively explained by the “squeezing” effect. The point  $(f_{c,Arecibo}, \delta f_{Arecibo})$  represents the central frequency and width of Arecibo operating band.

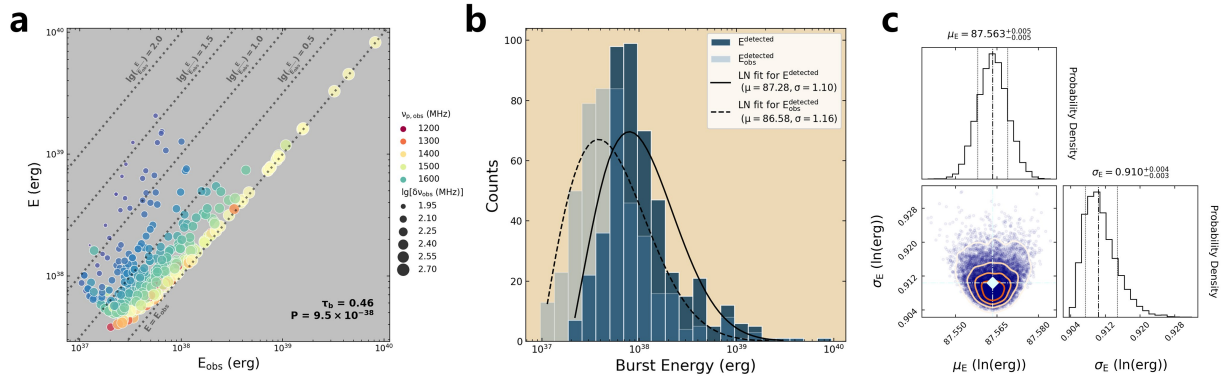


Figure 5: **Effects of operating-band cutoff on FRB energetics (Arecibo sample).** Panel a: The distribution of band-limited bursts on the  $E$ - $E_{\text{obs}}$  plane. The data points are color-coded based on  $\nu_{\text{p,obs}}$  and scaled in size proportional to  $\lg(\delta\nu_{\text{obs}})$ . Panel b: Observed energy distribution as compared with the recovered intrinsic energy distribution for detected bursts, including band-unlimited bursts and band-limited bursts. A shifted log-normal function is used to fit the distribution. Panel c: Constraints on the parameters of the standard log-normal distribution for the proper energy.

## Methods

**Spectrum profile of FRBs** We use the Bayesian Information Criterion (BIC) to analyze the spectrum shape of FRBs. For the 1652 FAST bursts, a precise temporal windowing was implemented to extract the spectra with minimized noise contamination. This was achieved by performing Gaussian fit to individual pulse profile, determining the time range centered on the pulse peak and measure the FWHM. Approximately 13% of bursts were excluded from the analysis due to their irregular pulse morphologies that prevent a reliable determination of their temporal boundaries.

For the remaining 87% of the sample, we fit their spectra with three spectral models (Gaussian, powerlaw, and cutoff powerlaw) and assessed the goodness of fit by using BIC<sup>15</sup>. Each burst received model rankings (1st to 3rd) based on ascending BIC values, where a lower BIC value indicates a better fit. Extended Data Fig. 1 presents the statistical distribution of these model rankings for four different spectral extraction methods. The upper panels demonstrate the spectra extracted in 1 – 1.5 GHz, contrasting temporal windows defined by the pulse FWHM versus twice the FWHM (i.e. 2FWHM). Both upper panels show that the Gaussian function is better than the powerlaw and cutoff powerlaw models. To investigate the impact of the operating bandwidth on the spectrum profile, we have also restricted the spectrum range in 1.05 – 1.45 GHz (the lower panels). We see that a narrower band increases the goodness of both the powerlaw and the cutoff powerlaw models, particularly for bursts exhibiting incomplete Gaussian profiles where the spectral peak falls outside the restricted band, resulting in quasi-powerlaw morphologies. However, the Gaussian function is still the best spectrum model.

Extended Data Fig. 2 shows the dynamical spectra of some typical bright bursts which ex-

hibit a Gaussian spectrum. Those bursts with the central frequency near the operating band edges display a truncated Gaussian profile. When restricting the spectral extraction to a narrower frequency range, these truncated bursts can exhibit a pseudo-powerlaw spectrum. It clearly demonstrates how the operating band limitation affects the observed spectral morphologies. Note that for both powerlaw and cutoff powerlaw models, the absolute value of the powerlaw index should be smaller than 0.1. Otherwise, the spectrum will be too flat to be fitted with our models.

**Theoretical modeling and analytical extensions of FRB Spectra** Fig. 1 illustrates the effect of observational cutoff on the FRB spectrum. The frequencies at which the spectrum intersects with the horizontal line of  $F_{\nu, \text{thre}}$  are denoted as  $\nu_\ell$  and  $\nu_h$ . The existence of the operating-band cutoff implies that the observed spectrum will be in a frequency range of  $\nu_1 < \nu < \nu_2$ , with the boundary frequencies determined by

$$\nu_1 = \begin{cases} f_\ell, & \nu_\ell \leq f_\ell, \\ \nu_\ell, & \nu_\ell > f_\ell, \end{cases} \quad (8)$$

$$\nu_2 = \begin{cases} \nu_h, & \nu_h \leq f_h, \\ f_h, & \nu_h > f_h. \end{cases} \quad (9)$$

Here  $f_\ell$  and  $f_h$  represent the lower and upper limits of the operating band, respectively.

The redshifted intrinsic burst spectrum can be described by a Gaussian function as <sup>13</sup>

$$F_\nu = \frac{F}{\sqrt{2\pi}\sigma_\nu} e^{-\frac{(\nu-\nu_p)^2}{2\sigma_\nu^2}}, \quad (10)$$

where  $F_\nu$  is the monochromatic fluence at frequency  $\nu$ ,  $F = \int_0^\infty F_\nu d\nu$  is the integrated fluence,  $\nu_p$  is the peak frequency.  $\sigma_\nu$  characterizes the FWHM of the spectrum, which is a more meaningful measure of the spectral width than the observed bandwidth of the burst ( $\delta\nu_{\text{obs}}$ ).

According to Fig. 1, we can easily derive the following equations that connect the observed spectral parameters with the intrinsic ones,

$$\nu_p = \frac{\nu_\ell + \nu_h}{2}, \quad (11)$$

$$F_\nu(\nu_\ell) = F_\nu(\nu_h) = F_{\nu, \text{thre}}, \quad (12)$$

$$\int_{\nu_1}^{\nu_2} \frac{F}{\sqrt{2\pi}\sigma_\nu} e^{-\frac{(\nu-\nu_p)^2}{2\sigma_\nu^2}} d\nu = F_{\nu, \text{obs}}^{\text{equiv}} \delta\nu_{\text{obs}}. \quad (13)$$

Here  $F_{\nu, \text{obs}}^{\text{equiv}}$  represents the frequency-equivalent fluence derived from the observation, and  $\delta\nu_{\text{obs}} = \nu_2 - \nu_1$  represents the observed bandwidth of the burst. For convenience, the observed burst energy is often averaged over the observed burst bandwidth (e.g. Ref. <sup>3</sup>) or the telescope's operating band (e.g. Ref. <sup>1</sup>), yielding the commonly used frequency-equivalent fluence of  $F_{\nu, \text{obs}}^{\text{equiv}}$ . Equation (13) delineates that only a fraction of  $F$  is detectable under the impact of sensitivity and operating-band cutoffs. Note that Equation (13) allows for the substitution of  $\delta\nu_{\text{obs}}$  with the width of the operating band  $\delta f$ , depending on whether  $F_{\nu, \text{obs}}^{\text{equiv}}$  is derived from  $\delta\nu_{\text{obs}}$  or  $\delta f$ <sup>25</sup>. From Equations (10), (11), (12) and (13), we can derive Equations (1) and (2).

We define  $\frac{F}{\sigma_\nu}$  as the intrinsic frequency-averaged fluence, and use  $\frac{\delta\nu_{\text{obs}}}{\sigma_\nu}$  to denote the observed-to-intrinsic bandwidth ratio. According to Equation (10), the monochromatic fluence at the peak frequency can be calculated as  $F_{\nu_p} = \frac{1}{\sqrt{2\pi}} \frac{F}{\sigma_\nu}$ . The observed-to-intrinsic fluence ratio is  $\frac{F_{\nu, \text{obs}}^{\text{equiv}}}{F/\sigma_\nu}$ . The observed-to-intrinsic energy ratio, denoted as  $\frac{E_{\text{obs}}}{E}$ , is expressed as  $\frac{F_{\nu, \text{obs}}^{\text{equiv}} \times \delta\nu_{\text{obs}}}{F}$ , where  $E_{\text{obs}}$  represents the observed burst energy. Combining Equations (1) and (2), we get

$$\frac{E_{\text{obs}}}{E} = \Phi\left(\frac{\nu_2 - \nu_p}{\sigma_\nu}\right) - \Phi\left(\frac{\nu_1 - \nu_p}{\sigma_\nu}\right). \quad (14)$$



For band-unlimited bursts, we have  $\nu_1 = \nu_\ell$  and  $\nu_2 = \nu_h$ . Equation (14) can be further expressed as

$$\left(\frac{E_{\text{obs}}}{E}\right)_{\text{band-unlimited}} = \text{erf}\left(\frac{\delta\nu/\sigma_\nu}{2\sqrt{2}}\right), \quad (15)$$

where  $\text{erf}(x) = \frac{2}{\sqrt{\pi}} \int_0^x e^{-\eta^2} d\eta$  stands for the Gauss error function. According to the definition of  $\frac{E_{\text{obs}}}{E}$ , we can further have

$$\frac{E_{\text{obs}}}{E} = \frac{F_{\nu,\text{obs}}^{\text{equiv}}}{F/\sigma_\nu} \times \frac{\delta\nu_{\text{obs}}}{\sigma_\nu}. \quad (16)$$

Consequently, from Equations (15) and (16), we derive

$$\left(\frac{F_{\nu,\text{obs}}^{\text{equiv}}}{F/\sigma_\nu}\right)_{\text{band-unlimited}} = \frac{\text{erf}\left(\frac{\delta\nu/\sigma_\nu}{2\sqrt{2}}\right)}{\delta\nu/\sigma_\nu}. \quad (17)$$

From Extended Data Fig. 3, we see that the vast majority of band-unlimited Arecibo bursts have a  $\frac{E_{\text{obs}}}{E}$  value above 0.68, corresponding to  $\frac{\delta\nu_{\text{obs}}}{\sigma_\nu} > 2$  (also see the  $\delta\nu_{\text{obs}}-\sigma_\nu$  plot in Fig. 2a). The distribution of  $\frac{\delta\nu_{\text{obs}}}{\sigma_\nu}$  exhibits a prominent peak around 4, which aligns with  $\frac{E_{\text{obs}}}{E} = 0.95$ . It should be emphasized that as  $\frac{E_{\text{obs}}}{E}$  and  $\frac{\delta\nu_{\text{obs}}}{\sigma_\nu}$  increase simultaneously,  $\frac{F_{\nu,\text{obs}}^{\text{equiv}}}{F/\sigma_\nu}$  decreases in the range of (0, 0.4], indicating a finite energy being spread over a broader observed bandwidth.

**Numerical solution of the Gaussian spectrum** When  $\nu_p$  is available, Equation (1) can be used to determine  $\sigma_\nu$  from the observed spectrum, yielding the unique solution  $(F, \nu_p, \sigma_\nu)$  for the Gaussian spectrum of the burst. The algorithm of AGD<sup>16-18</sup> is frequently employed for numerically solving such equations and is also commonly used in machine learning. In such a process, it is necessary to define a loss function to measure the discrepancy between the trial solution and the true solution. From Equation (1), we can define the loss function as

$$L = \left( \sqrt{2\pi} F_{\nu,\text{thre}} \sigma_\nu \left[ \Phi\left(\frac{\nu_2 - \nu_p}{\sigma_\nu}\right) - \Phi\left(\frac{\nu_1 - \nu_p}{\sigma_\nu}\right) \right] - F_{\nu,\text{obs}}^{\text{equiv}} \delta\nu_{\text{obs}} e^{-\left(\frac{\delta\nu}{2\sqrt{2}\sigma_\nu}\right)^2} \right)^2. \quad (18)$$

To avoid encountering excessively large values beyond the computational capabilities, we transform the exponential function into its reciprocal. When the loss function  $L(\sigma_v)$  equals 0,  $\sigma_v$  will be the true solution of Equation (1).

In accordance with the naming convention for symbols used in machine learning, we denote the value of the trial solution at the  $t$ -th step as  $w^t$ , which is equivalent to  $\sigma_v^t$ . Furthermore, we can derive the gradient of the loss function with respect to the trial solution at the  $t$ -th step as

$$g^t = \frac{\partial L(w^t)}{\partial w^t} = 2 \left( \sqrt{2\pi} F_{v,\text{thre}} w^t \left[ \Phi \left( \frac{v_2 - v_p}{w^t} \right) - \Phi \left( \frac{v_1 - v_p}{w^t} \right) \right] - F_{v,\text{obs}}^{\text{equiv}} \delta v_{\text{obs}} e^{-\left( \frac{\delta v}{2\sqrt{2}w^t} \right)^2} \right) \\ \left\{ \sqrt{2\pi} F_{v,\text{thre}} \left[ \Phi \left( \frac{v_2 - v_p}{w^t} \right) - \Phi \left( \frac{v_1 - v_p}{w^t} \right) \right] + \sqrt{2\pi} F_{v,\text{thre}} w^t \left[ \frac{v_1 - v_p}{\sqrt{2\pi} (w^t)^2} e^{-\left( \frac{v_1 - v_p}{\sqrt{2}w^t} \right)^2} - \frac{v_2 - v_p}{\sqrt{2\pi} (w^t)^2} e^{-\left( \frac{v_2 - v_p}{\sqrt{2}w^t} \right)^2} \right] \right. \\ \left. - F_{v,\text{obs}}^{\text{equiv}} \delta v_{\text{obs}} e^{-\left( \frac{\delta v}{2\sqrt{2}w^t} \right)^2} \frac{\delta v^2}{4 (w^t)^3} \right\}. \quad (19)$$

During the training process of AGD, the learning rate  $\eta^t = \frac{\eta^0}{\sqrt{t+1}}$  is dynamically adjusted by considering the root mean square of the previous gradients  $\sigma^t = \sqrt{\frac{1}{t+1} \sum_{i=0}^t (g^i)^2}$ . Consequently, the trial solution  $w^t$  undergoes optimal adjustments at each step, with substantial updates when it deviates significantly from the true solution and smaller updates as it approaches the true solution, i.e.

$$w^{t+1} = w^t - \frac{\eta^t}{\sigma^t} g^t = w^t - \frac{\eta^0}{\sqrt{\sum_{i=0}^t (g^i)^2}} g^t. \quad (20)$$

Throughout the training and equation-solving process, the initial value of the learning rate,  $\eta^0$ , plays a crucial role. If  $\eta^0$  is set to a very large value, the training may fail to converge to the true solution. On the other hand, if it is set too small, the training time might become unacceptably long although a convergence is possible. Moreover, since the true solution will be used in the integral term of Equation (5) for convolution (we need to numerically solve the true solution for every point in the 2D integration region), we should balance the computational efficiency and accuracy.

Thus, we made some modifications to AGD. Extended Data Fig. 4 illustrates the behavior of the loss function  $L(w^i)$  with respect to the trial solution  $w^i$ , which shows no clear evidence of the true solution in linear space. It implies that directly using AGD may fail to find the true solution unless  $\eta^0$  is set extremely small. However, setting  $\eta^0$  to such a small value can result in a significant increase in computation time. In our modification, we first try to identify the neighborhood of the true solution quickly based on the slope changes of  $L(w^t)$  in the logarithmic space. Then, within this neighborhood, we assign an initial trial solution  $w^0$  and a small  $\eta^0$  to efficiently obtain a high-precision solution. It should be noted that the point (0, 0) in Extended Data Fig. 4 corresponds to a non-physical solution, which particularly affects the training process when the true solution neighborhood is close to this point. Therefore, we need to incorporate a boundary condition during the training.

**Standard/Shifted log-normal distribution function** The standard log-normal distribution  $LN(x; \mu_{LN}, \sigma_{LN})$  and the shifted log-normal distribution  $LN(x; \delta, \mu_{LN}^s, \sigma_{LN}^s)$  (where the superscript "s" denotes "shifted") are used to fit the distribution of many key parameters in this study. These two distribution function differ only by a location parameter  $\delta$ . Their PDFs are expressed as

$$f_{LN}(x) = \frac{1}{\sqrt{2\pi}\sigma_{LN}x} e^{-\frac{(\ln x - \mu_{LN})^2}{2\sigma_{LN}^2}}, \quad x > 0, \sigma_{LN} > 0, \quad (21)$$

$$f_{LN}^s(x) = \frac{1}{\sqrt{2\pi}\sigma_{LN}^s(x - \delta)} e^{-\frac{[\ln(x - \delta) - \mu_{LN}^s]^2}{2(\sigma_{LN}^s)^2}}, \quad x > \delta, \sigma_{LN}^s > 0. \quad (22)$$

The introduction of the parameter  $\delta$  in the PDF of the shifted log-normal distribution allows for a better fit to the observed distribution profile. However, it also restricts the range of  $x$  values and lacks consideration for potential low values of  $x$  that have not been observed. In order to simplify

the fitting process and improve the accuracy, Equation (22) can be transformed into

$$f_{LN}^s(z) = \frac{1}{\sqrt{2\pi}M\sigma_{LN}^s} e^{-\frac{\ln^2 z}{2(\sigma_{LN}^s)^2}}, \quad (23)$$

where  $z = \frac{x-\delta}{M}$  and  $M = e^{\mu_{LN}^s}$ .

Considering the influence of statistical fluctuations on the observed distribution, we fit the log-normal distribution through MCMC simulations based on Bayesian inference. The logarithmic formulation of Bayes' theorem is expressed below, which offers computational simplicity and reduces risk of memory overflow in machine-based calculations,

$$\ln [P(\theta|D)] = \ln [P(D|\theta)] + \ln [P(\theta)] - \ln [P(D)]. \quad (24)$$

Here  $\theta$  represents the model parameters of the log-normal distribution function, and  $D$  stands for the observed data.  $P(\theta|D)$  is the posterior, which refers to our updated knowledge about the probability distribution of the model parameters based on the available data.  $P(D|\theta)$  is the likelihood, corresponding to the distribution that the data will exhibit given the model parameters. It follows the Poisson distribution of

$$\ln [P(D|\theta)] = \sum_i \left[ \ln(\lambda_i^{k_i}) - \ln(k_i!) - \lambda_i \right], \quad (25)$$

$$\lambda_i = \frac{N}{\int_{X_0}^{X_{n+1}} f_{LN}^{(s)}(x; \theta) dx} \int_{X_i}^{X_{i+1}} f_{LN}^{(s)}(x; \theta) dx. \quad (26)$$

To obtain better estimates of the model parameters, it is necessary to divide the observational data into  $n$  bins. The boundaries of the  $i$ -th bin are denoted as  $X_i$  and  $X_{i+1}$ .  $\lambda_i$  is the theoretical count of data in the  $i$ -th bin, while  $k_i = N_i$  represents the corresponding observed count. Empirically, the number of bins is usually taken as  $n = \lceil \sqrt{N} \rceil$  (i.e., rounding up the square root of  $N$ ), where

$N = \sum_i N_i$ .  $f_{LN}^{(s)}$  denotes the log-normal distribution function  $f_{LN}^s(x)$  or  $f_{LN}(x)$ , depending on which is utilized. The prior  $P(\theta)$  is typically characterized by a uniform distribution,

$$\ln [P(\theta)] = \begin{cases} -\ln(b-a), & a < \theta < b, \\ -\infty, & \text{otherwise.} \end{cases} \quad (27)$$

The range  $[a, b]$  of  $\theta$  can be set by considering the distribution of the observed data. For instance,  $\mu_{LN}^{(s)}$  should not exceed the maximum and minimum values of the data,  $3\sigma_{LN}^{(s)}$  should lie between 0 and the natural logarithm of the maximum value in the data, and  $\delta$  generally should match the minimum value in the data. The evidence  $P(D)$  refers to the probability of the observed facts, which should equal a constant  $C$ . Since the PDF's global integral is 1, the sum of  $P(\theta|D)$  over all conditions should be 1, i.e.  $\sum P(\theta|D) = 1$ . Furthermore, according to Equation (24), we have  $\sum [P(D|\theta)P(\theta)] = C$ , from which we can obtain the value of  $P(D)$ . In practice, to improve the efficiency, we can treat constant terms (such as the values of  $P(\theta)$  with  $\theta$  between  $a$  and  $b$ ) as 1 initially and then scale each  $P(\theta|D)$  proportionally so that  $\sum P(\theta|D) = 1$ .

Using this method, we can derive the probability distribution of the model parameters for the log-normal distribution and determine the parameters with the highest probability, known as the maximum likelihood estimation.

**Reconstructing the 2D Gaussian distribution of  $(\nu_\ell, \nu_h)$**  As shown in Extended Data Fig. 5a, the band-limited bursts exhibit an unnatural accumulation along the lines  $\nu_1 = f_\ell$  and  $\nu_2 = f_h$ , which correspond to the Arecibo operating band limits. According to Equations (8) and (9), the portion of the spectrum below  $f_\ell$  or above  $f_h$  cannot be detected, meaning that frequencies  $\nu_\ell$  below  $f_\ell$  and  $\nu_h$  above  $f_h$  are observationally identified as  $f_\ell$  and  $f_h$ , respectively. It leads to such an accumulation. The histograms in the subplots of Extended Data Fig. 5a reveal that the cutoff for

$\nu_h$  is significantly greater than that for  $\nu_\ell$ , both of which could ideally follow normal distributions according to their observed distribution profiles<sup>45</sup>. In Extended Data Fig. 5b which focuses on the band-unlimited bursts, the region of their KDE that separate from the operating band limits (below the blue dash-dotted line) exhibits a 2D Gaussian distribution.

Our objective is to inverse model and derive the 2D Gaussian distribution  $N(\nu_\ell, \nu_h; \mu_{\nu_\ell}, \mu_{\nu_h}, \sigma_{\nu_\ell}, \sigma_{\nu_h}, \rho)$  from the observational data of  $(\nu_1, \nu_2)$ . Here, the five model parameters are denoted as  $\theta$ . The reconstruction is done based on Bayes' theorem (see Equation (24)). The expression of the likelihood  $P(D|\theta)$  is slightly revised to adapt the 2D data,

$$\ln [P(D|\theta)] = \sum_i \sum_j [\ln(\lambda_{ij}^{k_{ij}}) - \ln(k_{ij}!) - \lambda_{ij}], \quad (28)$$

$$\lambda_{ij} = \frac{N \iint_{\nu_\ell < \nu_h} f_N(\nu_\ell, \nu_h; \theta) d\nu_\ell d\nu_h}{\iint_{(\nu_\ell < \nu_h) \wedge (\nu_\ell < f_h) \wedge (\nu_h > f_\ell)} f_N(\nu_\ell, \nu_h; \theta) d\nu_\ell d\nu_h} \int_{Y_i}^{Y_{i+1}} \int_{X_j}^{X_{j+1}} f_N(\nu_\ell, \nu_h; \theta) d\nu_\ell d\nu_h, \quad (29)$$

$$X_j = \begin{cases} \mu_{\nu_\ell} - 5\sigma_{\nu_\ell}, & j = 1, \\ f_\ell + \frac{(j-1)(f_h - f_\ell)}{n}, & 2 \leq j \leq n + 1, \end{cases} \quad (30)$$

$$Y_i = \begin{cases} f_\ell + \frac{(i-1)(f_h - f_\ell)}{n}, & 1 \leq i \leq n, \\ \mu_{\nu_h} + 5\sigma_{\nu_h}, & i = n + 1. \end{cases} \quad (31)$$

In Extended Data Fig. 6a, we divide the  $\nu_h$ - $\nu_\ell$  plane into  $n \times n$  grids (MCMC sampling subdomains). Here, the region enclosed by orange dashed lines represents the operating band. For the grids in the  $j$ -th column, both the left boundary  $X_j$  and the right boundary  $X_{j+1}$  are obtained using Equation (30). Similarly, for the grids in the  $i$ -th row, both the lower boundary  $Y_i$  and the upper boundary  $Y_{i+1}$  are calculated using Equation (31). Note that due to the operating-band

cutoff in observations, the probability density within the detectable region but outside the operating band region is squeezed towards the boundaries of the operating band region (along the direction indicated by the dark gray arrows), as displayed intuitively in Fig. 4a. Therefore, to establish the connection between the observed 2D distribution and the intrinsic 2D distribution, we need to extend these boundaries in the opposite direction of the arrows. As described in Equation (30),  $X_j$  should be  $-\infty$  when  $j = 1$ , but to avoid non-physical situations in practice, we set  $X_j = \mu_{\nu_\ell} - 5\sigma_{\nu_\ell}$ . Similarly, in Equation (31), we set  $Y_{i=n+1} = \mu_{\nu_h} + 5\sigma_{\nu_h}$ .  $\lambda_{ij}$  in Equation (29) represents the theoretical count of data points within the grid of the  $i$ -th row and  $j$ -th column for a given PDF related to the parameter set  $\theta$ . Correspondingly,  $k_{ij} = N_{ij}$  is the observed count.  $N = \sum_i \sum_j N_{ij}$  is the total count of detected bursts in the sample whose intensity exceed the fluence threshold, corresponding to the region of  $(\nu_\ell < \nu_h) \wedge (\nu_\ell < f_h) \wedge (\nu_h > f_\ell)$ . The region of  $\nu_\ell < \nu_h$  corresponds to the physically valid region, where both detectable and undetectable events could exist. The region below the line of  $\nu_h = \nu_\ell$  is the non-physical region, which also needs to be considered to provide feedback to the PDF candidate in order to obtain a desired PDF that avoids this region as much as possible. This implies that the theoretical count in this region should be equal to the observed count, which is 0. It is worth noting that, for the  $n \times n$  MCMC sampling subdomains, we can still empirically determine  $n$  through  $n = \lceil \sqrt{N} \rceil$ .

Using the above method, we can obtain the maximum likelihood estimation of  $\theta$  for the 2D Gaussian distribution of  $(\nu_\ell, \nu_h)$ . The derived model parameters are shown in Fig. 4b for the Arecibo sample, in Extended Data Fig. 7b for the GBT sample, and in Extended Data Fig. 8b for the FAST sample.  $\nu_p$  is available for the GBT bursts, but note that  $\nu_h - \nu_p$  and  $\nu_p - \nu_\ell$  usually are not equal for the band-unlimited bursts. The reason is that the lower fluence of the spectral wings

is more affected by noise, causing different degrees of signal masking in the noise on the two sides of the spectral wings. This is especially true for weak bursts found through machine learning in the GBT sample. To account for this effect, adjustments were made to  $\nu_1$  and  $\nu_2$  based on  $\nu_p$  to ensure integrality in the spectral frequency range. Concretely, for a band-unlimited burst in the GBT sample, for the two parameters of  $\nu_1$  and  $\nu_2$ , the one closer to  $\nu_p$  was adjusted away from  $\nu_p$  (within the range of the operating band) to maximize the symmetry of  $\nu_1$  and  $\nu_2$  with respect to  $\nu_p$ . The model parameters constrained from the adjusted sample show minor differences asv compared to those derived from the original sample (see Extended Data Fig. 7b and Extended Data Fig. 7c). To visually evaluate the reconstruction model, the reconstructed theoretical count and the observed count are directly compared in each MCMC sampling subdomain, as shown in Extended Data Fig. 6b for the Arecibo sample, in Extended Data Fig. 6c for the GBT sample, and in Extended Data Fig. 6d for the FAST sample. These three figures correspond to Fig. 4a, Extended Data Fig. 7a, and Extended Data Fig. 8a, respectively.

Additionally, such a grid-based counting method can accommodate to some extent the variation of the fluence threshold within the same sample. Substituting Equation (12) into Equation (10), we have

$$F_{\nu,\text{thre}} = \frac{F}{\sqrt{2\pi}\sigma_\nu} e^{-\frac{(\nu_\ell - \nu_p)^2}{2\sigma_\nu^2}}, \quad (32)$$

where  $\nu_\ell$  can also be replaced by  $\nu_h$ . Across the bursts, when  $F_{\nu,\text{thre}}$  changes by a mount of  $\Delta F_{\nu,\text{thre}}$ , we have

$$F_{\nu,\text{thre}} + \Delta F_{\nu,\text{thre}} = \frac{F}{\sqrt{2\pi}\sigma_\nu} e^{-\frac{(\nu_\ell + \Delta\nu_\ell - \nu_p)^2}{2\sigma_\nu^2}}. \quad (33)$$

Dividing Equation (33) by Equation (32) and assuming  $\Delta\nu_\ell \leq \frac{\delta f}{n}$  (where  $\frac{\delta f}{n}$  is the side length of



each grid), we get

$$\frac{\Delta F_{v,\text{thre}}}{F_{v,\text{thre}}} \leq \frac{\delta f}{2n} \frac{\delta v}{\sigma_v^2}, \quad (34)$$

where we have taken the first-order Maclaurin approximation for the exponential term and neglected other smaller terms. In this way, we can estimate the maximum allowable relative change in  $F_{v,\text{thre}}$  for grid-based counting, by considering the sample conditions and the side length of the grid.

**Transforming  $(v_\ell, v_h)$  distribution to  $(v_p, \delta v)$  distribution** Let  $(x, y)$  be a 2D random variable with a joint probability density of  $f(x, y)$ , and  $(u, v)$  be a 2D random variable with a joint probability density of  $F(u, v)$ . Assuming that  $(x, y)$  and  $(u, v)$  are connected by the functions of  $u = u(x, y)$ ,  $v = v(x, y)$  and the unique inverse functions of  $x = x(u, v)$ ,  $y = y(u, v)$ . Then the Jacobian determinant of the transformation is

$$J = \frac{\partial(x, y)}{\partial(u, v)} = \begin{vmatrix} \partial x / \partial u & \partial x / \partial v \\ \partial y / \partial u & \partial y / \partial v \end{vmatrix} = \left( \frac{\partial(u, v)}{\partial(x, y)} \right)^{-1} = \begin{vmatrix} \partial u / \partial x & \partial v / \partial x \\ \partial v / \partial x & \partial v / \partial y \end{vmatrix}^{-1}. \quad (35)$$

Here we have assumed that all the relevant partial derivatives are continuous. If the Jacobian determinant is non-zero, then the joint probability density  $F(u, v)$  can be calculated as

$$F(u, v) = f(x(u, v), y(u, v)) |J|. \quad (36)$$

In Equation (36), it is not necessary for  $x$  and  $y$  to be mutually independent.

In this study, the distribution of  $(v_\ell, v_h)$  follows  $N(v_\ell, v_h; \mu_{v_\ell}, \mu_{v_h}, \sigma_{v_\ell}, \sigma_{v_h}, \rho)$ . Also, the variable of  $(v_p, \delta v)$  is connected with  $(v_\ell, v_h)$  as  $v_p = (v_\ell + v_h) / 2$  and  $\delta v = v_h - v_\ell$ , with the corresponding unique inverse functions given by  $v_\ell = v_p - \delta v / 2$  and  $v_h = v_p + \delta v / 2$ . Then, according to Equations

(5) and (36), we can derive the joint probability density of  $(v_p, \delta v)$  as

$$\begin{aligned}
f_N(v_p, \delta v) &= \frac{1}{2\pi\sigma_{v_\ell}\sigma_{v_h}\sqrt{1-\rho^2}} \exp \left\{ -\frac{1}{2(1-\rho^2)} \left[ \frac{(v_p - \delta v/2 - \mu_{v_\ell})^2}{\sigma_{v_\ell}^2} \right. \right. \\
&\quad \left. \left. - \frac{2\rho(v_p - \delta v/2 - \mu_{v_\ell})(v_p + \delta v/2 - \mu_{v_h})}{\sigma_{v_\ell}\sigma_{v_h}} + \frac{(v_p + \delta v/2 - \mu_{v_h})^2}{\sigma_{v_h}^2} \right] \right\} \\
&= \frac{1}{2\pi\sigma_{v_\ell}\sigma_{v_h}\sqrt{1-\rho^2}} \exp \left\{ -\frac{\mathcal{A}v_p^2 + \mathcal{B}(\delta v)^2 + \mathcal{C}v_p\delta v + \mathcal{D}v_p + \mathcal{E}\delta v + \mathcal{F}}{2(1-\rho^2)} \right\}.
\end{aligned} \tag{37}$$

Here  $\mathcal{A} = \frac{1}{\sigma_{v_\ell}^2} + \frac{1}{\sigma_{v_h}^2} - \frac{2\rho}{\sigma_{v_\ell}\sigma_{v_h}}$ ,  $\mathcal{B} = \frac{1}{4} \left( \frac{1}{\sigma_{v_\ell}^2} + \frac{1}{\sigma_{v_h}^2} + \frac{2\rho}{\sigma_{v_\ell}\sigma_{v_h}} \right)$ ,  $\mathcal{C} = \frac{1}{\sigma_{v_h}^2} - \frac{1}{\sigma_{v_\ell}^2}$ ,  $\mathcal{D} = 2 \left[ -\frac{\mu_{v_\ell}}{\sigma_{v_\ell}^2} - \frac{\mu_{v_h}}{\sigma_{v_h}^2} + \frac{\rho(\mu_{v_\ell} + \mu_{v_h})}{\sigma_{v_\ell}\sigma_{v_h}} \right]$ ,  $\mathcal{E} = \frac{\mu_{v_\ell}}{\sigma_{v_\ell}^2} - \frac{\mu_{v_h}}{\sigma_{v_h}^2} + \frac{\rho(\mu_{v_\ell} - \mu_{v_h})}{\sigma_{v_\ell}\sigma_{v_h}}$ , and  $\mathcal{F} = \frac{\mu_{v_\ell}^2}{\sigma_{v_\ell}^2} + \frac{\mu_{v_h}^2}{\sigma_{v_h}^2} - \frac{2\rho\mu_{v_\ell}\mu_{v_h}}{\sigma_{v_\ell}\sigma_{v_h}}$ . Since  $(v_p, \delta v)$  is a linear transformation of  $(v_\ell, v_h)$ , it should also follow a 2D Gaussian distribution, denoted as  $f_N(v_p, \delta v) \sim N(v_p, \delta v; \mu_{v_p}, \mu_{\delta v}, \sigma_{v_p}, \sigma_{\delta v}, k)$ . Integrating the PDF of a 2D Gaussian distribution over one of the two random variables yields the PDF of a 1D Gaussian distribution for that variable, i.e.,  $f_N(\delta v) \sim N(\delta v; \mu_{\delta v}, \sigma_{\delta v})$  and  $f_N(v_p) \sim N(v_p; \mu_{v_p}, \sigma_{v_p})$ . As a result, we have

$$f_N(\delta v) = \int_{-\infty}^{\infty} f_N(v_p, \delta v) dv_p = \frac{1}{\sqrt{2\pi}\sigma_{\delta v}} e^{-\frac{(\delta v - \mu_{\delta v})^2}{2\sigma_{\delta v}^2}}, \tag{38}$$

$$f_N(v_p) = \int_{-\infty}^{\infty} f_N(v_p, \delta v) d\delta v = \frac{1}{\sqrt{2\pi}\sigma_{v_p}} e^{-\frac{(v_p - \mu_{v_p})^2}{2\sigma_{v_p}^2}}. \tag{39}$$

This can help us determine the model parameters in the expression of  $N(v_p, \delta v; \mu_{v_p}, \mu_{\delta v}, \sigma_{v_p}, \sigma_{\delta v}, k)$ .

We can separate the variable  $v_p$  in the expression of  $f_N(v_p, \delta v)$  by using Equation (37). Substituting the resulting expression into Equation (38), we get

$$\frac{1}{\sqrt{2\pi}\sqrt{\sigma_{v_\ell}^2 + \sigma_{v_h}^2 - 2\rho\sigma_{v_\ell}\sigma_{v_h}}} \exp \left[ -\frac{(\mathcal{B} - \frac{\mathcal{C}^2}{4\mathcal{A}})(\delta v)^2 + (\mathcal{E} - \frac{\mathcal{C}\mathcal{D}}{2\mathcal{A}})\delta v + (\mathcal{F} - \frac{\mathcal{D}^2}{4\mathcal{A}})}{2(1-\rho^2)} \right] = \frac{1}{\sqrt{2\pi}\sigma_{\delta v}} e^{-\frac{(\delta v - \mu_{\delta v})^2}{2\sigma_{\delta v}^2}}. \tag{40}$$

Utilizing the commonly-used method of factorization in polynomial division, we can easily derive

$$\mathcal{B} - \frac{\mathcal{C}^2}{4\mathcal{A}} = \frac{1-\rho^2}{\sigma_{v_\ell}^2 + \sigma_{v_h}^2 - 2\rho\sigma_{v_\ell}\sigma_{v_h}}, \quad \mathcal{E} - \frac{\mathcal{C}\mathcal{D}}{2\mathcal{A}} = -\frac{2(\mu_{v_h} - \mu_{v_\ell})(1-\rho^2)}{\sigma_{v_\ell}^2 + \sigma_{v_h}^2 - 2\rho\sigma_{v_\ell}\sigma_{v_h}} \quad \text{and} \quad \mathcal{F} - \frac{\mathcal{D}^2}{4\mathcal{A}} = \frac{(\mu_{v_h} - \mu_{v_\ell})^2(1-\rho^2)}{\sigma_{v_\ell}^2 + \sigma_{v_h}^2 - 2\rho\sigma_{v_\ell}\sigma_{v_h}}. \quad \text{Thus, Equation}$$

(40) can be simplified as

$$\frac{1}{\sqrt{2\pi} \sqrt{\sigma_{v_\ell}^2 + \sigma_{v_h}^2 - 2\rho\sigma_{v_\ell}\sigma_{v_h}}} \exp \left\{ -\frac{[\delta v - (\mu_{v_h} - \mu_{v_\ell})]^2}{2(\sigma_{v_\ell}^2 + \sigma_{v_h}^2 - 2\rho\sigma_{v_\ell}\sigma_{v_h})} \right\} = \frac{1}{\sqrt{2\pi}\sigma_{\delta v}} e^{-\frac{(\delta v - \mu_{\delta v})^2}{2\sigma_{\delta v}^2}}. \quad (41)$$

By matching the terms on both sides of Equation (41), we get  $\mu_{\delta v} = \mu_{v_h} - \mu_{v_\ell}$  and  $\sigma_{\delta v} = \sqrt{\sigma_{v_\ell}^2 + \sigma_{v_h}^2 - 2\rho\sigma_{v_\ell}\sigma_{v_h}}$ .

Similarly, by separating the variable  $\delta v$  in the expression of  $f_N(v_p, \delta v)$  using Equation (37) and substituting the result into Equation (39), we ultimately get

$$\frac{1}{\sqrt{2\pi} \sqrt{(\sigma_{v_\ell}^2 + \sigma_{v_h}^2 + 2\rho\sigma_{v_\ell}\sigma_{v_h})/4}} \exp \left\{ -\frac{\left(v_p - \frac{\mu_{v_\ell} + \mu_{v_h}}{2}\right)^2}{2\left[(\sigma_{v_\ell}^2 + \sigma_{v_h}^2 + 2\rho\sigma_{v_\ell}\sigma_{v_h})/4\right]} \right\} = \frac{1}{\sqrt{2\pi}\sigma_{v_p}} e^{-\frac{(v_p - \mu_{v_p})^2}{2\sigma_{v_p}^2}}. \quad (42)$$

Hence, we have  $\mu_{v_p} = \frac{\mu_{v_\ell} + \mu_{v_h}}{2}$  and  $\sigma_{v_p} = \sqrt{(\sigma_{v_\ell}^2 + \sigma_{v_h}^2 + 2\rho\sigma_{v_\ell}\sigma_{v_h})/4}$ . By matching the exponential terms of Equations (37) and (6), we get  $\mathcal{A} = \frac{1-\rho^2}{1-k^2} \frac{1}{\sigma_{v_p}^2}$  and  $C = \frac{1-\rho^2}{1-k^2} \left(-\frac{2k}{\sigma_{v_p}\sigma_{\delta v}}\right)$ . Take the ratio of  $C$  to  $\mathcal{A}$  and substitute the definitions of  $\mathcal{A} = \frac{1}{\sigma_{v_\ell}^2} + \frac{1}{\sigma_{v_h}^2} - \frac{2\rho}{\sigma_{v_\ell}\sigma_{v_h}}$  and  $C = \frac{1}{\sigma_{v_h}^2} - \frac{1}{\sigma_{v_\ell}^2}$  into the resulting equation, combining the obtained expressions of  $\sigma_{v_p} = \sqrt{(\sigma_{v_\ell}^2 + \sigma_{v_h}^2 + 2\rho\sigma_{v_\ell}\sigma_{v_h})/4}$  and  $\sigma_{\delta v} = \sqrt{\sigma_{v_\ell}^2 + \sigma_{v_h}^2 - 2\rho\sigma_{v_\ell}\sigma_{v_h}}$ , we can derive

$$k = -\frac{C\sigma_{\delta v}}{2\mathcal{A}\sigma_{v_p}} = \frac{\sigma_{v_h}^2 - \sigma_{v_\ell}^2}{\sqrt{(\sigma_{v_\ell}^2 + \sigma_{v_h}^2)^2 - 4\rho^2\sigma_{v_\ell}^2\sigma_{v_h}^2}}. \quad (43)$$

In this way, based on the model parameters of the  $(v_\ell, v_h)$  distribution, we can get the expressions for all the five model parameters of  $(v_p, \delta v)$  distribution.

**Estimation of integrated fluence for band-limited bursts** Given  $v_\ell$  and  $v_h$ , the values of  $v_1$  and  $v_2$  can be determined through Equations (8) and (9) respectively, which in turn yield  $\delta v_{\text{obs}}$ . Similarly,  $v_p$  can be obtained using Equation (11). Furthermore, using  $F_{v_{\text{obs}}}^{\text{equiv}}$ , Equation (1) can be solved, and the solution can be substituted into Equation (2) to obtain the burst's integrated fluence  $F(v_\ell, v_h, F_{v_{\text{obs}}}^{\text{equiv}}; F_{v_{\text{thre}}})$ . In the case of a band-limited burst, considering  $v_\ell$  and/or  $v_h$  are unknown,

we can employ Equation (5) to convolve  $F(\nu_\ell, \nu_h, F_{\nu_{\text{obs}}}^{\text{equiv}}; F_{\nu_{\text{thre}}})$  with  $f_N(\nu_\ell, \nu_h)$  to derive the expected value of the integrated fluence,  $E(F)$  (i.e. Equation (7)). Since band-limited bursts are classified into three categories based on their positions in the  $\nu_h-\nu_\ell$  plane (corresponding to the three conditions in Equation (7)), we only consider the convolution of the other variable when one of  $\nu_\ell$  and  $\nu_h$  is known. The denominator terms in Equation (7) represent the conditional probabilities guided by the potential distribution domains in the  $\nu_h-\nu_\ell$  plane.

**Data Availability** The Arecibo and GBT data can be obtained from the corresponding references. We reprocessed the FAST data and extracted the frequency properties of the bursts, which are presented in Supplementary Table 1.

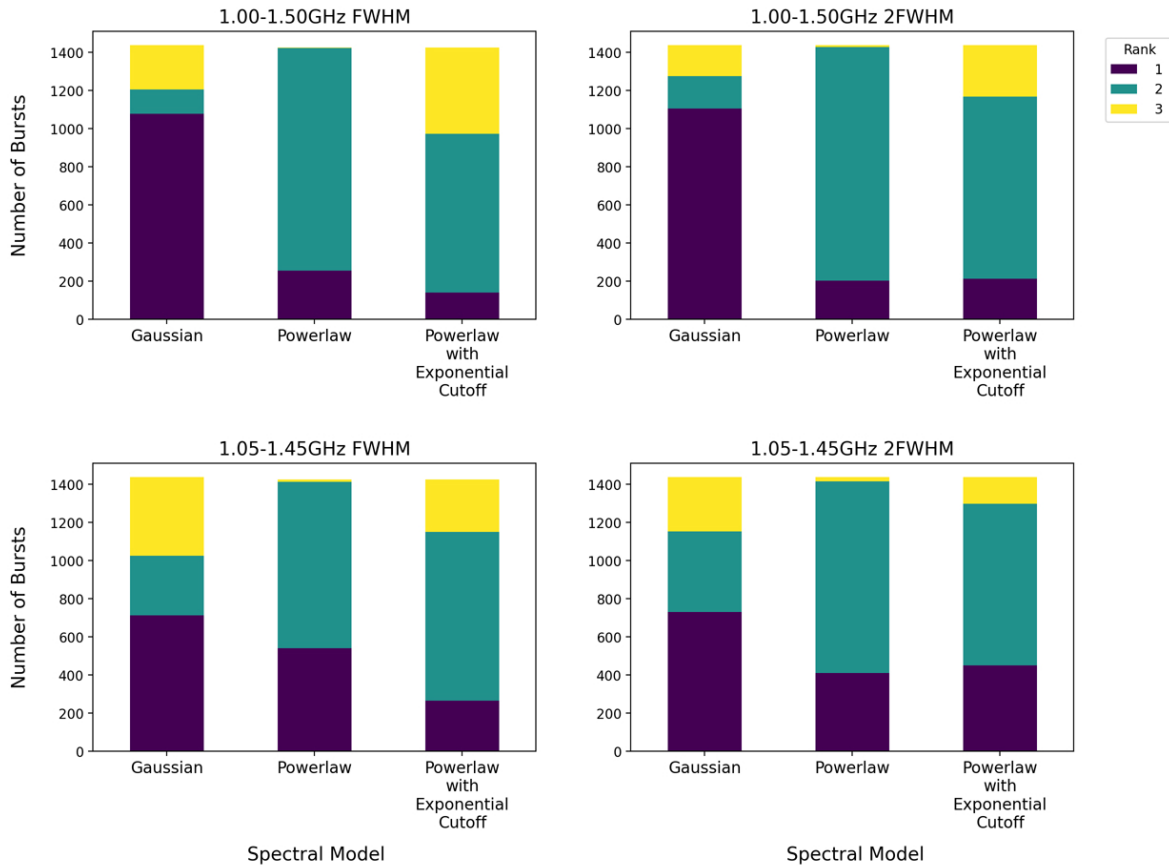
**Code Availability** Results can be fully reproduced using the methodology described in Methods, based on Python 3.7.9 and the publicly available Python packages NumPy 1.21.5, SciPy 1.9.1, emcee 3.1.4, pandas 1.4.4, Seaborn 0.11.2 and Matplotlib 3.5.2.

**Acknowledgements** This work is supported by the National Natural Science Foundation of China (Grant Nos. 12041306, 12233002, 12273113), by the National SKA Program of China Nos. 2020SKA0120300, by the National Key R&D Program of China (2021YFA0718500), and the CAS Project for Young Scientists in Basic Research (Grant No. YSBR-063). PW acknowledges support from the National Natural Science Foundation of China (NSFC) Programs No.11988101, 12041303, the CAS Youth Interdisciplinary Team, the Youth Innovation Promotion Association CAS (id. 2021055), and the Cultivation Project for FAST Scientific Payoff and Research Achievement of CAMS-CAS. YFH acknowledges the support from the Xinjiang Tianchi Program. JJG acknowledges support from the Youth Innovation Promotion Association (2023331). This work made use of data from FAST, Arecibo and GBT.

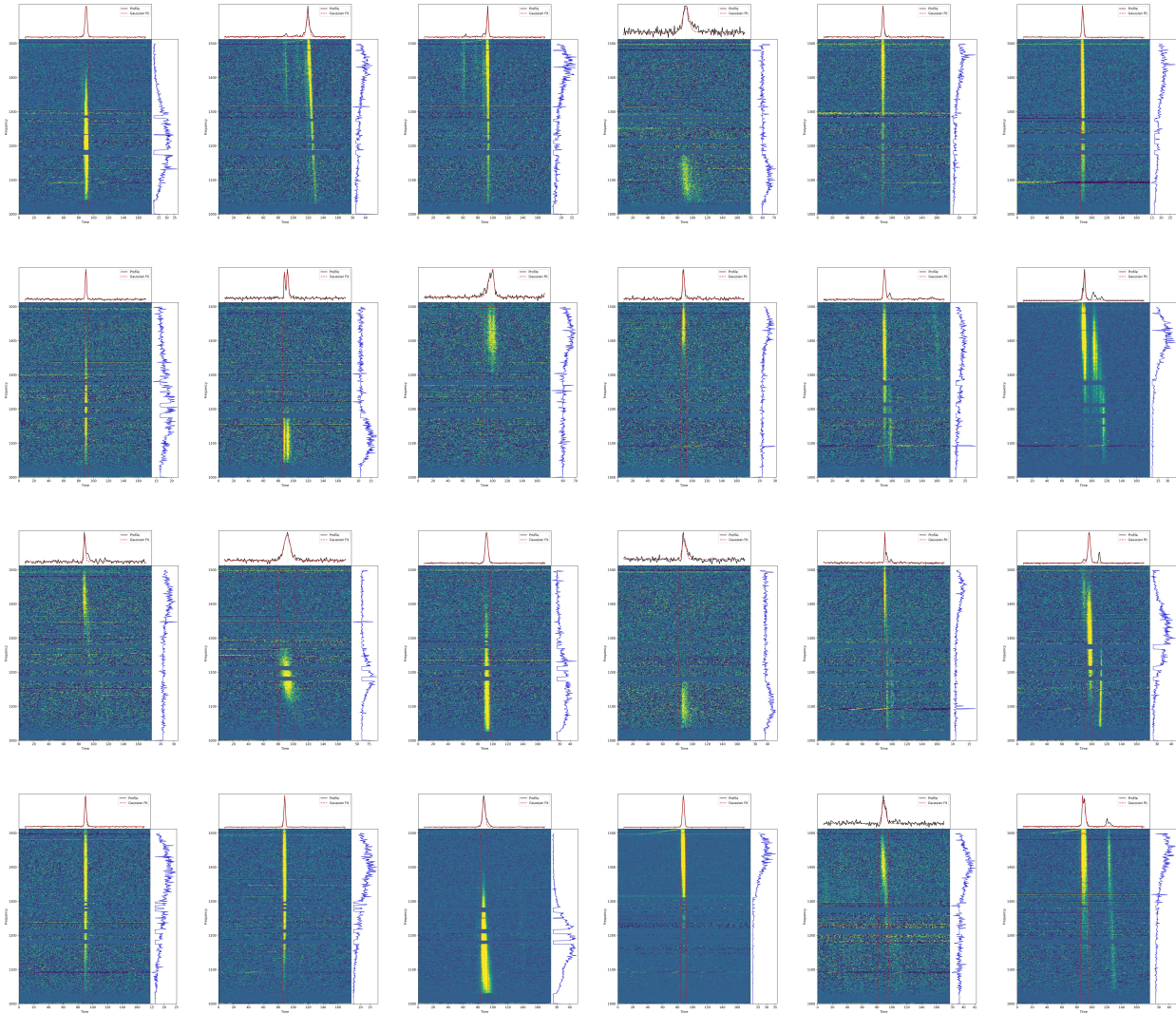
**Author Contributions** CRH and YFH proposed the idea of applying inverse modeling to study FRBs with observational cutoffs. PW and YDW reprocessed the FAST data. CRH, XFD, and PW developed the inversion model. CRH, CD and JJG performed the numerical calculations. CRH, JJG, XFW, ZCZ, LC and FX led the theoretical analysis of the energetics and frequency characteristics of the reconstructed bursts. XFW and SBZ guided the astrophysical feasibility. All authors participated in the discussions, analyses, and manuscript writing.

**Competing Interests** The authors declare no competing interests.

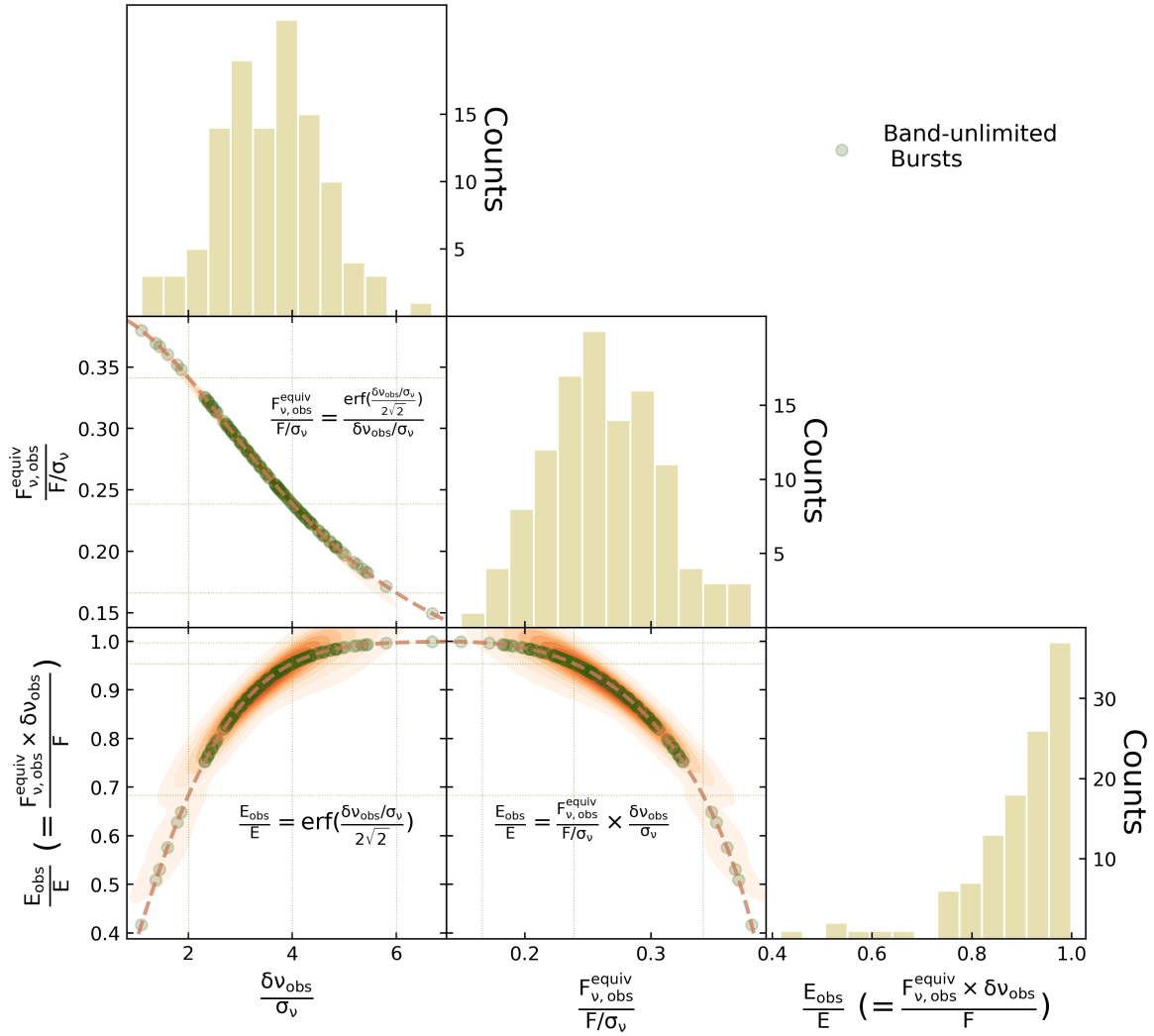
**Correspondence** Correspondence and requests for materials should be addressed to Yong-Feng Huang (hyf@nju.edu.cn), Pei Wang (wangpei@nao.cas.cn) and Xue-Feng Wu (xfwu@pmo.ac.cn).



**Extended Data Fig. 1. Spectral model rank distribution (FAST sample).** The four panels correspond to different spectral extraction methods. The upper and lower panels represent frequency ranges of 1.0 – 1.5 GHz and 1.05 – 1.45 GHz, respectively, while the left and right panels correspond to temporal windows of the pulse FWHM and twice the pulse FWHM, both centered at the pulse peak. Each panel shows the distribution of goodness-of-fit rankings for the three spectral models, with a higher count of top rankings indicating a better model performance.

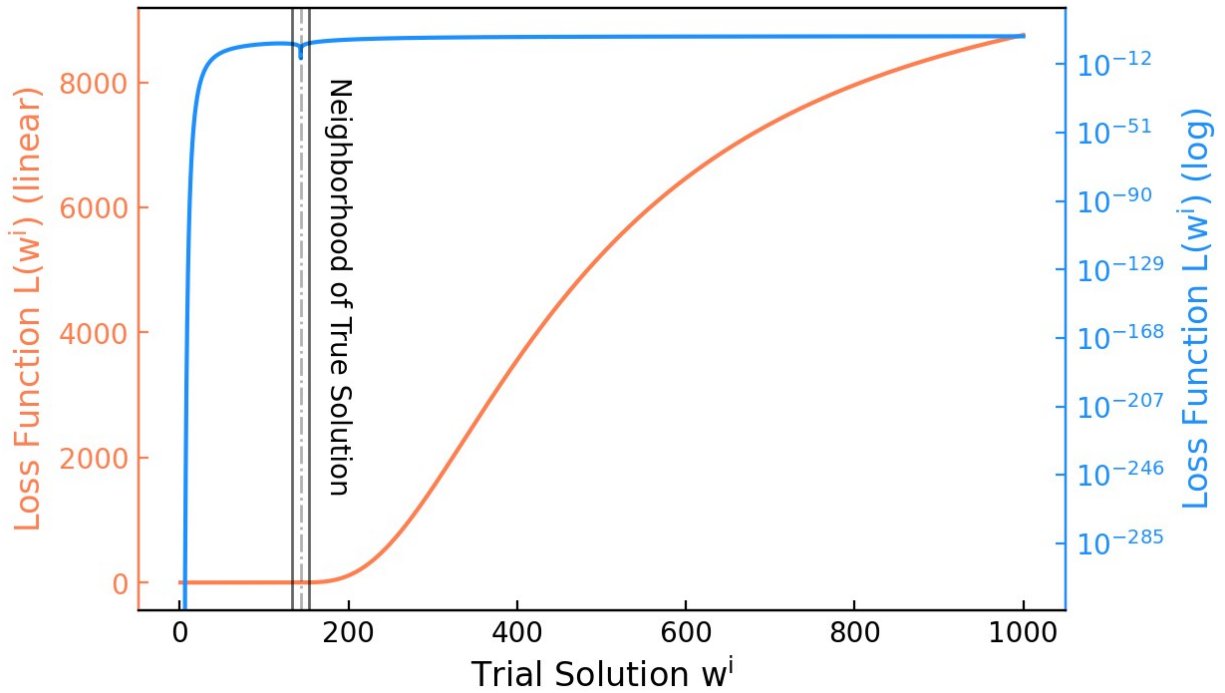


**Extended Data Fig. 2. Typical bright bursts exhibiting a Gaussian spectral profile (FAST sample).** The bursts exhibit either a complete or an incomplete Gaussian spectral profile. The spectral extraction was performed by restricting the temporal window to twice the pulse FWHM centered at the pulse peak, together with a frequency range of 1 – 1.5 GHz.

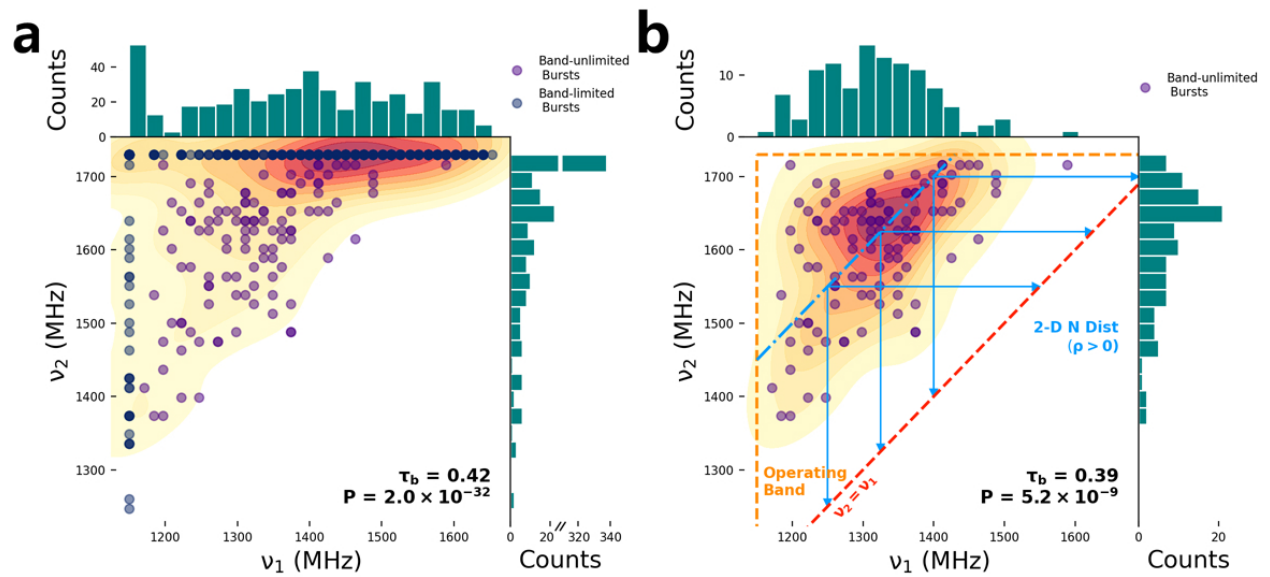


**Extended Data Fig. 3. The distribution of three observed-to-intrinsic ratios and their correlations (Arecibo sample).**

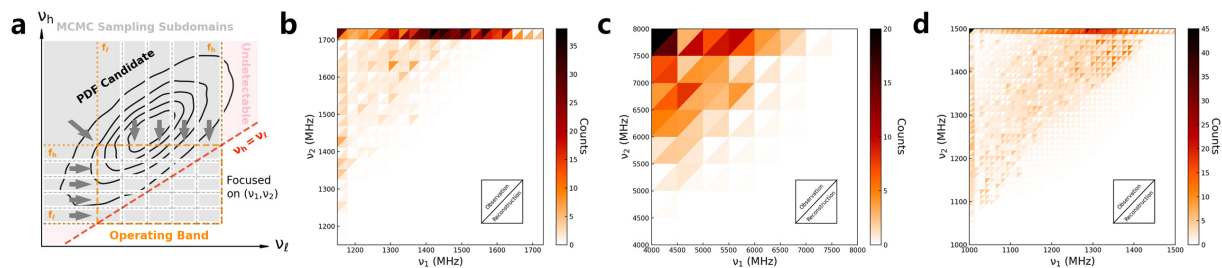




**Extended Data Fig. 4. Response of the loss function to different trial solutions.** This figure shows how  $L(w^i)$  behaves with different  $w^i$  for a burst. The loss function is shown in both linear (the orange curve with respect to the orange vertical axis) and logarithmic (the blue curve with respect to the blue vertical axis) scales.

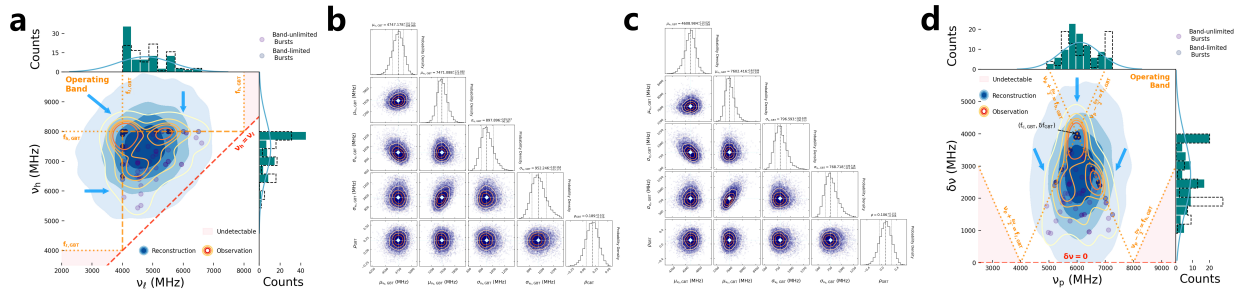


**Extended Data Fig. 5. Impact of operating-band cutoff on bursts (Arecibo sample).** Panel a: The distribution of detected bursts on the  $\nu_2$ - $\nu_1$  plane. The contour lines represent their KDE, and the corresponding 1D histograms are plotted along the axes. Panel b: The distribution of band-unlimited bursts on the  $\nu_2$ - $\nu_1$  plane. The orange dashed lines stand for the operating band limits of Arecibo, corresponding to  $\nu_1 = f_\ell$  and  $\nu_2 = f_h$ .



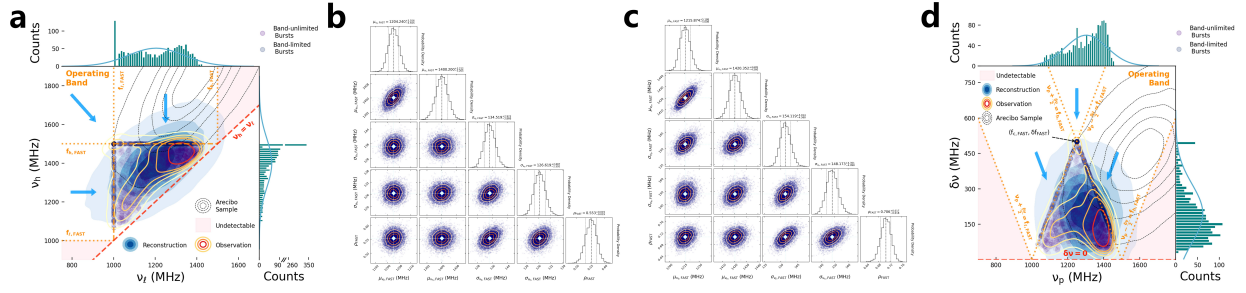
**Extended Data Fig. 6. Grid-based inverse modeling of 2D Gaussian Distribution of  $(\nu_\ell, \nu_h)$ .**

Panel a: A schematic illustration on how the  $\nu_h$ - $\nu_\ell$  plane is divided into subregions for PDF candidate integrations, which enable a direct comparison with observations to provide feedback for MCMC sampling. Panel b: A direct comparison between the theoretical counts and the observed counts in each subregion for the Arcicibo sample. In each grid, the top-left corner stands for the observed count, while the bottom-right corner stands for the theoretical count (calculated from the reconstructed  $(\nu_\ell, \nu_h)$  distribution, as shown in Fig. 4a). Panel c: A direct comparison between the theoretical counts and the observed counts in each subregion for the GBT sample. The corresponding reconstructed distribution is shown in Extended Data Fig. 7a. Panel d: A direct comparison between the theoretical counts and the observed counts in each subregion for the FAST sample. The corresponding reconstructed distribution is shown in Extended Data Fig. 8a.



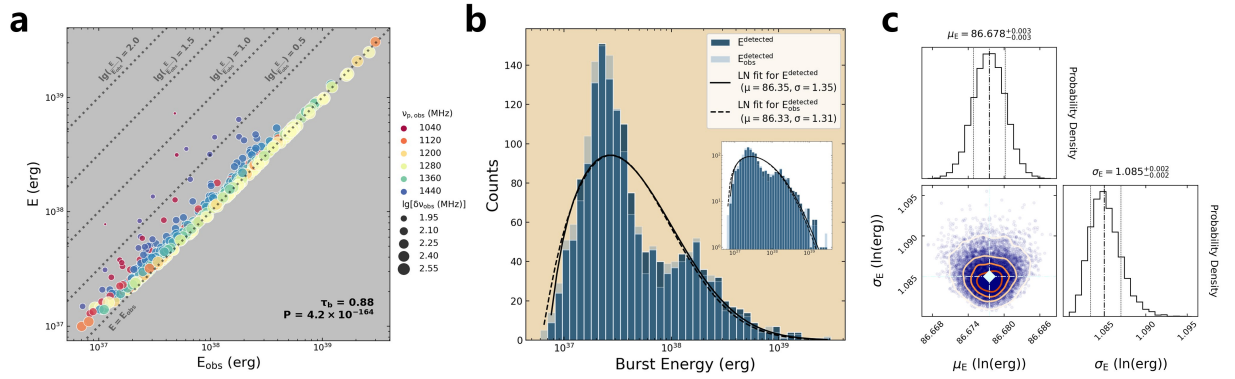
**Extended Data Fig. 7. Operating-band cutoff effects on the burst distribution (GBT sample).**

Panel a: The observed distribution of bursts on the  $\nu_h$ - $\nu_\ell$  plane, overlaid with yellow-orange-red contour lines demonstrating the KDE. The blue contour lines depict the intrinsic distribution. 1D histograms of observed bursts and corresponding intrinsic 1D distributions are also plotted along the axes. The orange dashed lines are the operating-band limits of GBT. The region below the red dashed line is non-physical, while the pink region is undetectable.  $\nu_1$  and  $\nu_2$  have been adjusted based on  $\nu_p$  to maximize the integrity of the observed frequency range. In the subplots, histograms delineated by the dashed outline correspond to bursts before adjustment. Panel b: Constraints on the parameters of  $N(\nu_\ell, \nu_h; \mu_{\nu_\ell}, \mu_{\nu_h}, \sigma_{\nu_\ell}, \sigma_{\nu_h}, \rho)$ , which is the reconstructed intrinsic distribution of  $(\nu_\ell, \nu_h)$ . Panel c: Constraints on the parameters of  $N(\nu_\ell, \nu_h; \mu_{\nu_\ell}, \mu_{\nu_h}, \sigma_{\nu_\ell}, \sigma_{\nu_h}, \rho)$  for the sample before adjustment. Panel d: The observed distribution of bursts on the  $\delta\nu$ - $\nu_p$  plane, where the data points align with  $\delta\nu_{\text{obs}} = \nu_2 - \nu_1$  and  $\nu_{p,\text{obs}} = \frac{\nu_1 + \nu_2}{2}$ . The dashed-outlined histogram on the  $\nu_p$  axis corresponds to the provided  $\nu_p$  values, and the histogram on the  $\delta\nu$  axis represents the  $\delta\nu$  values of the sample before adjustment. Other graphical elements are similar to those in Panel (a).



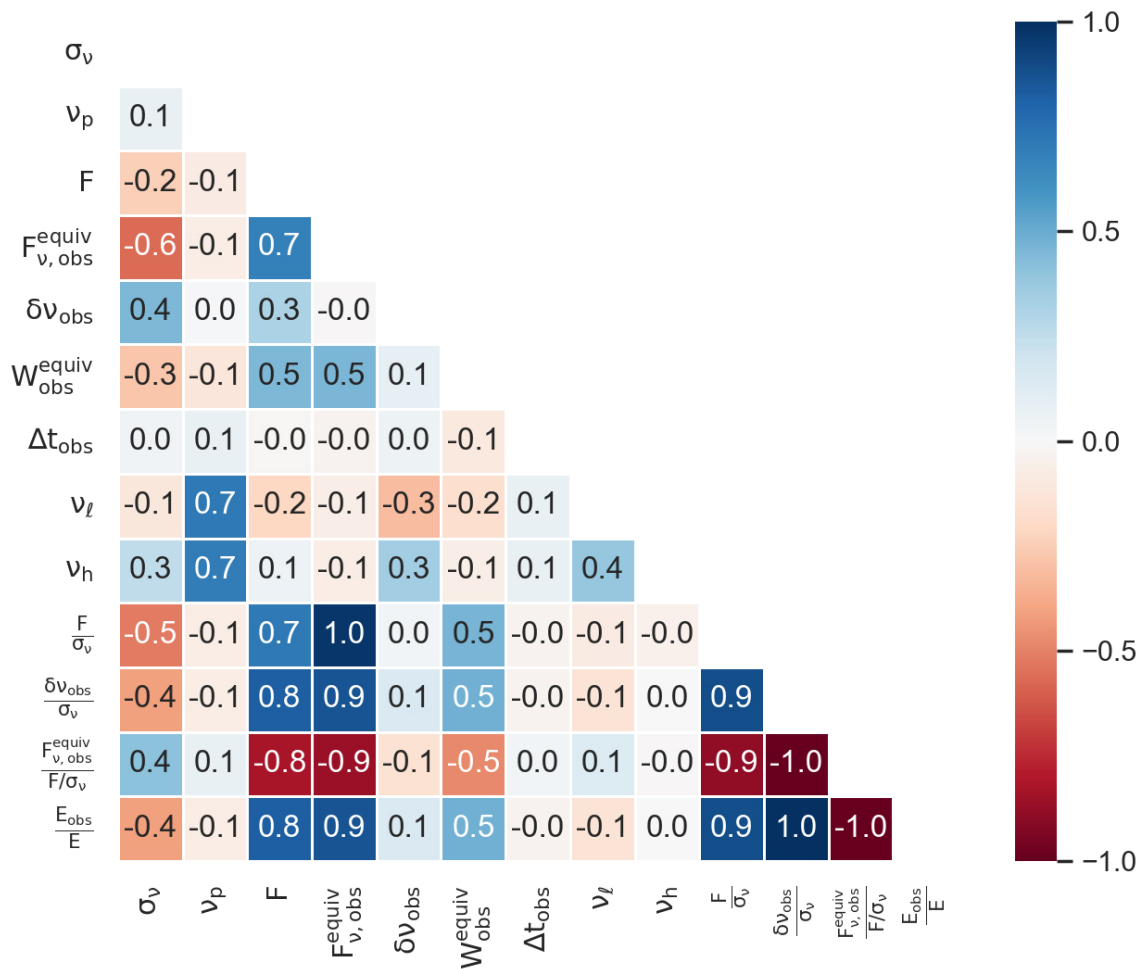
**Extended Data Fig. 8. Operating-band cutoff effects on the burst distribution (FAST sample).**

Panel a: The observed distribution of bursts on the  $\nu_h$ - $\nu_\ell$  plane, overlaid with yellow-orange-red contour lines demonstrating the KDE. The blue contour lines depict the intrinsic distribution, in contrast to the black dashed contour lines, which represent the intrinsic distribution of the Arecibo sample. 1D histograms of observed bursts and corresponding intrinsic 1D distributions are also plotted along the axes. The orange dashed lines are the operating-band limits of FAST. The region below the red dashed line is non-physical, while the pink region is undetectable. Panel b: Constraints on the parameters of  $N(\nu_\ell, \nu_h; \mu_{\nu_\ell}, \mu_{\nu_h}, \sigma_{\nu_\ell}, \sigma_{\nu_h}, \rho)$ , which is the reconstructed intrinsic distribution of  $(\nu_\ell, \nu_h)$ . Panel c: Constraints on the parameters of  $N(\nu_\ell, \nu_h; \mu_{\nu_\ell}, \mu_{\nu_h}, \sigma_{\nu_\ell}, \sigma_{\nu_h}, \rho)$  for the sample in the operating band of 1.05 – 1.45 GHz. The full operating band of FAST is 1 – 1.5 GHz, but note that the measurement is more precise within its central band of 1.05 – 1.45 GHz. We thus have artificially cutoff  $\nu_1$  and  $\nu_2$  into the central band and used them to constrain the parameters of the  $\nu_h$ - $\nu_\ell$  distribution. The results are largely consistent with that derived based on the original sample. Panel d: The observed distribution of bursts on the  $\delta\nu$ - $\nu_p$  plane, where the data points align with  $\delta\nu_{\text{obs}} = \nu_2 - \nu_1$  and  $\nu_{p,\text{obs}} = \frac{\nu_1 + \nu_2}{2}$ . Other graphical elements are similar to that in Panel (a).



**Extended Data Fig. 9. Effects of operating-band cutoff on FRB energetics (FAST sample).**

Panel a: The distribution of band-limited bursts on the  $E$ - $E_{\text{obs}}$  plane. The data points are color-coded based on  $\nu_{p,\text{obs}}$  and scaled in size proportional to  $\lg(\delta\nu_{\text{obs}})$ . Panel b: Observed energy distribution as compared with the intrinsic energy distribution for detected bursts, including band-unlimited bursts and band-limited bursts. A shifted log-normal function is used to fit the distribution. The inset displays the same histogram but with the vertical axis in logarithmic scale. Panel c: Constraints on the parameters of the standard log-normal distribution of the intrinsic energy.



**Extended Data Fig. 10. Diagonal correlation matrix of the parameters of the reconstructed band-unlimited bursts (Arecibo sample).** The color bar corresponds to the correlation coefficient ( $\tau_b$ ) computed utilizing the Kendall tau method.

## Extended Data

Supplementary Table 1: **Characteristic frequencies of FRB 20121102A bursts detected by FAST.**

**Supplementary Table 1:**

Burst ID <sup>a</sup>	$\nu_1^b$ (MHz)	$\nu_2^b$ (MHz)	$\nu_{p,obs}$ (MHz)	Burst ID <sup>a</sup>	$\nu_1^b$ (MHz)	$\nu_2^b$ (MHz)	$\nu_{p,obs}$ (MHz)
1	1069 (34)	1143 (36)	1106 (25)	73	1417 (12)	1489 (4)	1453 (6)
2	1253 (35)	1469 (9)	1361 (18)	74	1235 (12)	1362 (15)	1299 (10)
3	1027 (4)	1468 (16)	1248 (8)	75	1330 (19)	1409 (14)	1370 (12)
4	1350 (36)	1428 (19)	1389 (20)	76	1072 (11)	1160 (22)	1116 (12)
5	1350 (6)	1413 (17)	1381 (20)	77	1387 (16)	1435 (11)	1411 (10)
6	1376 (97)	1468 (20)	1422 (50)	78	1052 (7)	1280 (183)	1166 (91)
7	1245 (26)	1391 (18)	1318 (16)	79	1203 (13)	1321 (13)	1262 (9)
8	1374 (3)	1433 (3)	1403 (2)	80	1372 (16)	1472 (6)	1422 (9)
9	1346 (14)	1484 (16)	1415 (11)	81	1054 (68)	1497 (3)	1276 (34)
10	1073 (46)	1175 (54)	1124 (36)	82	1051 (7)	1231 (10)	1141 (6)
11	1005 (2)	1497 (6)	1251 (3)	83	1038 (24)	1309 (55)	1173 (30)
12	1399 (9)	1475 (4)	1437 (5)	84	1238 (11)	1425 (6)	1331 (6)
13	1236 (10)	1386 (8)	1311 (6)	85	1149 (6)	1434 (12)	1292 (7)
14	1263 (20)	1398 (27)	1331 (17)	86	1047 (9)	1329 (17)	1188 (10)
15	1211 (18)	1409 (10)	1310 (10)	87	1159 (73)	1350 (10)	1255 (37)
16	1135 (12)	1252 (8)	1194 (7)	88	1247 (14)	1470 (5)	1359 (8)
17	1168 (28)	1361 (17)	1264 (16)	89	1163 (15)	1321 (20)	1242 (13)
18	1189 (21)	1436 (6)	1312 (11)	90	1342 (7)	1477 (7)	1410 (5)
19	1281 (35)	1413 (11)	1347 (18)	91	1260 (12)	1464 (17)	1362 (10)
20	1102 (12)	1370 (15)	1236 (9)	92	1214 (3)	1334 (3)	1274 (2)
21	1392 (26)	1482 (11)	1437 (14)	93	1345 (26)	1395 (20)	1370 (17)
22	1110 (3)	1499 (1)	1305 (1)	94	1293 (9)	1499 (2)	1396 (4)
23	1094 (24)	1499 (1)	1297 (12)	95	1015 (11)	1224 (23)	1120 (13)
24	1186 (55)	1394 (19)	1290 (29)	96	1009 (3)	1230 (28)	1120 (14)
25	1126 (46)	1244 (37)	1185 (29)	97	1287 (9)	1455 (7)	1371 (6)
26	1161 (24)	1304 (22)	1233 (16)	98	1151 (12)	1238 (6)	1195 (7)
27	1117 (13)	1233 (8)	1175 (8)	99	1030 (37)	1314 (53)	1172 (33)
28	1070 (14)	1189 (139)	1130 (70)	100	1005 (3)	1316 (34)	1161 (17)
29	1013 (4)	1282 (15)	1147 (8)	101	1277 (12)	1463 (6)	1370 (7)
30	1021 (4)	1178 (9)	1099 (5)	102	1268 (30)	1398 (13)	1333 (16)
31	1379 (15)	1480 (7)	1429 (8)	103	1289 (4)	1492 (6)	1390 (4)
32	1114 (6)	1404 (15)	1259 (8)	104	1302 (49)	1439 (23)	1370 (27)
33	1098 (7)	1266 (12)	1182 (7)	105	1349 (6)	1376 (13)	1362 (7)
34	1011 (9)	1065 (3)	1038 (5)	106	1402 (23)	1479 (13)	1441 (13)
35	1271 (19)	1424 (15)	1348 (12)	107	1178 (40)	1423 (28)	1301 (24)
36	1017 (11)	1099 (20)	1058 (11)	108	1091 (12)	1363 (55)	1227 (28)
37	1327 (16)	1498 (2)	1413 (8)	109	1376 (19)	1482 (6)	1429 (10)
38	1309 (34)	1454 (29)	1382 (22)	110	1085 (4)	1241 (5)	1163 (3)
39	1187 (28)	1364 (9)	1276 (15)	111	1269 (8)	1447 (12)	1358 (7)
40	1008 (5)	1067 (2)	1038 (3)	112	1214 (24)	1437 (15)	1326 (14)
41	1250 (36)	1401 (26)	1326 (22)	113	1216 (9)	1444 (22)	1330 (12)
42	1251 (6)	1487 (6)	1369 (4)	114	1197 (13)	1378 (38)	1288 (20)
43	1241 (36)	1316 (24)	1279 (22)	115	1334 (4)	1486 (6)	1410 (4)
44	1050 (26)	1123 (37)	1086 (23)	116	1264 (63)	1420 (23)	1342 (33)
45	1226 (13)	1290 (6)	1258 (7)	117	1348 (145)	1470 (17)	1409 (73)
46	1199 (7)	1397 (19)	1298 (10)	118	1427 (11)	1478 (5)	1452 (6)
47	1017 (4)	1209 (11)	1113 (6)	119	1168 (16)	1266 (24)	1217 (14)
48	1011 (4)	1220 (10)	1116 (5)	120	1019 (9)	1172 (35)	1095 (18)
49	1152 (25)	1398 (26)	1275 (18)	121	1258 (3)	1319 (4)	1288 (2)
50	1007 (4)	1378 (41)	1193 (21)	122	1291 (20)	1497 (3)	1394 (10)
51	1387 (8)	1455 (8)	1421 (6)	123	1337 (11)	1421 (7)	1379 (7)
52	1167 (32)	1499 (1)	1333 (16)	124	1003 (1)	1191 (5)	1097 (3)
53	1325 (12)	1478 (10)	1401 (8)	125	1318 (34)	1483 (17)	1401 (19)
54	1141 (9)	1284 (12)	1212 (8)	126	1332 (25)	1424 (17)	1378 (15)
55	1354 (25)	1430 (22)	1392 (17)	127	1311 (19)	1494 (4)	1402 (10)
56	1320 (4)	1498 (2)	1409 (2)	128	1327 (2)	1452 (3)	1389 (2)
57	1288 (6)	1499 (2)	1393 (3)	129	1278 (30)	1468 (19)	1373 (18)
58	1040 (23)	1117 (33)	1078 (20)	130	1114 (32)	1417 (24)	1265 (20)
59	1047 (15)	1104 (7)	1075 (8)	131	1067 (41)	1329 (51)	1198 (33)
60	1235 (32)	1496 (3)	1366 (16)	132	1069 (21)	1193 (11)	1131 (12)
61	1040 (9)	1217 (10)	1129 (7)	133	1223 (16)	1465 (21)	1344 (13)
62	1095 (16)	1278 (12)	1186 (10)	134	1348 (20)	1481 (11)	1415 (11)
63	1367 (16)	1491 (5)	1429 (8)	135	1140 (15)	1266 (15)	1203 (11)
64	1289 (14)	1499 (2)	1394 (7)	136	1255 (17)	1479 (8)	1367 (9)
65	1102 (17)	1180 (63)	1141 (33)	137	1316 (14)	1499 (2)	1408 (7)
66	1178 (11)	1483 (3)	1331 (6)	138	1003 (2)	1283 (19)	1143 (10)
67	1366 (36)	1485 (25)	1425 (22)	139	1261 (25)	1493 (4)	1377 (12)
68	1358 (20)	1480 (4)	1419 (10)	140	1179 (47)	1368 (33)	1274 (29)
69	1337 (24)	1486 (3)	1411 (12)	141	1087 (11)	1151 (7)	1119 (7)
70	1227 (24)	1448 (27)	1337 (18)	142	1096 (23)	1173 (14)	1135 (14)



Supplementary Table 1:

Burst ID <sup>a</sup>	$\nu_1^b$ (MHz)	$\nu_2^b$ (MHz)	$\nu_{p,obs}$ (MHz)	Burst ID <sup>a</sup>	$\nu_1^b$ (MHz)	$\nu_2^b$ (MHz)	$\nu_{p,obs}$ (MHz)
71	1157 (51)	1452 (16)	1304 (27)	143	1311 (24)	1411 (19)	1361 (15)
72	1265 (14)	1481 (5)	1373 (8)	144	1299 (31)	1464 (31)	1382 (22)
145	1372 (13)	1449 (11)	1411 (8)	217	1290 (22)	1363 (29)	1326 (18)
146	1371 (21)	1490 (7)	1430 (11)	218	1165 (16)	1444 (19)	1304 (13)
147	1216 (44)	1353 (17)	1285 (24)	219	1178 (24)	1390 (19)	1284 (15)
148	1327 (8)	1378 (13)	1353 (7)	220	1120 (20)	1416 (19)	1268 (14)
149	1291 (11)	1489 (3)	1390 (6)	221	1137 (9)	1341 (5)	1239 (5)
150	1349 (151)	1473 (21)	1411 (76)	222	1057 (25)	1175 (122)	1116 (62)
151	1374 (17)	1486 (10)	1430 (10)	223	1071 (7)	1466 (4)	1268 (4)
152	1347 (7)	1430 (15)	1388 (8)	224	1071 (7)	1466 (4)	1268 (4)
153	1263 (33)	1414 (26)	1339 (21)	225	1378 (21)	1449 (10)	1413 (12)
154	1192 (18)	1406 (25)	1299 (15)	226	1318 (14)	1363 (4)	1341 (7)
155	1343 (5)	1490 (3)	1416 (3)	227	1264 (54)	1442 (32)	1353 (32)
156	1113 (42)	1449 (9)	1281 (21)	228	1191 (19)	1341 (19)	1266 (13)
157	1263 (38)	1495 (5)	1379 (19)	229	1173 (18)	1362 (11)	1267 (10)
158	1177 (17)	1316 (19)	1246 (13)	230	1443 (3)	1462 (5)	1453 (3)
159	1138 (14)	1315 (9)	1226 (8)	231	1300 (23)	1493 (4)	1397 (12)
160	1345 (29)	1462 (19)	1404 (17)	232	1016 (3)	1429 (20)	1223 (10)
161	1077 (11)	1250 (20)	1163 (11)	233	1008 (5)	1429 (20)	1219 (11)
162	1052 (23)	1499 (1)	1275 (12)	234	1090 (9)	1244 (11)	1167 (7)
163	1035 (14)	1499 (1)	1267 (7)	235	1076 (9)	1247 (11)	1162 (7)
164	1345 (17)	1482 (7)	1414 (9)	236	1030 (19)	1340 (17)	1185 (13)
165	1418 (2)	1452 (3)	1435 (2)	237	1045 (34)	1336 (17)	1191 (19)
166	1352 (9)	1473 (8)	1412 (6)	238	1356 (20)	1428 (11)	1392 (12)
167	1330 (33)	1487 (5)	1409 (17)	239	1304 (16)	1484 (6)	1394 (8)
168	1212 (17)	1473 (8)	1343 (9)	240	1155 (9)	1275 (15)	1215 (9)
169	1174 (26)	1455 (17)	1315 (16)	241	1186 (16)	1381 (11)	1283 (10)
170	1150 (9)	1297 (6)	1223 (5)	242	1044 (27)	1127 (6)	1086 (14)
171	1364 (64)	1459 (23)	1411 (34)	243	1211 (31)	1319 (4)	1265 (16)
172	1348 (16)	1430 (17)	1389 (12)	244	1420 (5)	1468 (4)	1444 (3)
173	1230 (6)	1340 (4)	1285 (3)	245	1400 (10)	1485 (6)	1442 (6)
174	1096 (3)	1287 (9)	1191 (5)	246	1177 (29)	1454 (23)	1315 (18)
175	1280 (17)	1415 (7)	1347 (9)	247	1160 (20)	1442 (19)	1301 (14)
176	1215 (13)	1499 (1)	1357 (6)	248	1172 (22)	1443 (17)	1308 (14)
177	1387 (20)	1447 (25)	1417 (16)	249	1157 (13)	1445 (19)	1301 (12)
178	1219 (35)	1328 (32)	1273 (24)	250	1255 (10)	1406 (9)	1330 (7)
179	1059 (19)	1217 (6)	1138 (10)	251	1287 (23)	1467 (7)	1377 (12)
180	1300 (19)	1361 (14)	1331 (12)	252	1139 (3)	1251 (2)	1195 (2)
181	1009 (4)	1136 (10)	1073 (5)	253	1389 (12)	1489 (6)	1439 (7)
182	1004 (2)	1106 (10)	1055 (5)	254	1352 (18)	1493 (5)	1422 (9)
183	1305 (95)	1435 (33)	1370 (50)	255	1314 (6)	1465 (4)	1389 (4)
184	1109 (18)	1297 (8)	1203 (10)	256	1343 (24)	1434 (37)	1389 (22)
185	1095 (18)	1281 (15)	1188 (12)	257	1037 (6)	1120 (8)	1078 (5)
186	1417 (7)	1471 (11)	1444 (7)	258	1033 (14)	1243 (13)	1138 (10)
187	1104 (28)	1189 (49)	1147 (28)	259	1272 (35)	1410 (14)	1341 (19)
188	1182 (13)	1499 (1)	1341 (7)	260	1067 (39)	1217 (53)	1142 (33)
189	1078 (15)	1380 (16)	1229 (11)	261	1308 (17)	1464 (8)	1386 (9)
190	1311 (31)	1489 (4)	1400 (16)	262	1017 (5)	1128 (7)	1072 (4)
191	1073 (10)	1379 (125)	1226 (63)	263	1356 (30)	1485 (4)	1421 (15)
192	1270 (17)	1458 (9)	1364 (10)	264	1006 (3)	1483 (13)	1245 (7)
193	1335 (37)	1484 (11)	1409 (19)	265	1070 (84)	1267 (36)	1168 (46)
194	1347 (29)	1414 (18)	1381 (17)	266	1390 (17)	1465 (20)	1428 (13)
195	1030 (9)	1140 (6)	1085 (5)	267	1166 (47)	1368 (21)	1267 (26)
196	1329 (7)	1486 (5)	1408 (4)	268	1051 (2)	1224 (155)	1137 (78)
197	1367 (8)	1492 (5)	1430 (5)	269	1414 (22)	1464 (15)	1439 (13)
198	1077 (34)	1213 (74)	1145 (41)	270	1124 (3)	1215 (49)	1169 (24)
199	1246 (32)	1314 (28)	1280 (21)	271	1236 (21)	1409 (21)	1322 (15)
200	1196 (38)	1452 (19)	1324 (21)	272	1220 (32)	1413 (18)	1317 (18)
201	1193 (92)	1408 (40)	1301 (50)	273	1354 (37)	1487 (13)	1420 (20)
202	1369 (47)	1455 (32)	1412 (28)	274	1213 (36)	1306 (36)	1260 (25)
203	1250 (45)	1480 (18)	1365 (24)	275	1314 (37)	1489 (3)	1401 (19)
204	1280 (23)	1499 (1)	1389 (11)	276	1347 (4)	1433 (3)	1390 (2)
205	1297 (9)	1499 (1)	1398 (4)	277	1383 (7)	1465 (25)	1424 (13)
206	1155 (13)	1433 (4)	1294 (7)	278	1259 (12)	1333 (7)	1296 (7)
207	1292 (17)	1389 (9)	1340 (10)	279	1352 (6)	1493 (4)	1422 (4)
208	1241 (12)	1368 (13)	1305 (9)	280	1195 (9)	1304 (9)	1249 (7)
209	1277 (24)	1498 (3)	1387 (12)	281	1151 (9)	1289 (12)	1220 (7)
210	1069 (10)	1128 (23)	1098 (13)	282	1106 (25)	1355 (22)	1231 (17)
211	1093 (8)	1164 (8)	1128 (6)	283	1043 (13)	1386 (25)	1215 (14)
212	1039 (2)	1145 (3)	1092 (2)	284	1334 (15)	1381 (10)	1358 (9)
213	1246 (13)	1443 (17)	1345 (11)	285	1088 (22)	1317 (59)	1203 (32)
214	1358 (20)	1431 (15)	1394 (13)	286	1299 (10)	1489 (6)	1394 (6)
215	1058 (10)	1101 (25)	1080 (13)	287	1326 (33)	1384 (6)	1355 (17)
216	1013 (4)	1163 (29)	1088 (15)	288	1346 (22)	1410 (40)	1378 (23)
289	1330 (11)	1490 (5)	1410 (6)	361	1239 (23)	1332 (8)	1285 (12)
290	1320 (14)	1486 (5)	1403 (7)	362	1131 (25)	1330 (11)	1231 (13)
291	1152 (10)	1262 (15)	1207 (9)	363	1292 (3)	1377 (3)	1334 (2)
292	1137 (12)	1277 (14)	1207 (9)	364	1356 (39)	1465 (3)	1410 (20)
293	1345 (8)	1475 (9)	1410 (6)	365	1357 (14)	1493 (5)	1425 (8)

Supplementary Table 1:

Burst ID <sup>a</sup>	$\nu_1^b$ (MHz)	$\nu_2^b$ (MHz)	$\nu_{p,obs}$ (MHz)	Burst ID <sup>a</sup>	$\nu_1^b$ (MHz)	$\nu_2^b$ (MHz)	$\nu_{p,obs}$ (MHz)
294	1365 (10)	1496 (5)	1431 (5)	366	1384 (8)	1475 (20)	1430 (11)
295	1059 (21)	1172 (10)	1115 (12)	367	1261 (28)	1345 (39)	1303 (24)
296	1119 (13)	1163 (27)	1141 (15)	368	1003 (1)	1409 (4)	1206 (2)
297	1319 (14)	1470 (8)	1394 (8)	369	1331 (23)	1396 (14)	1364 (14)
298	1192 (12)	1296 (21)	1244 (12)	370	1376 (36)	1448 (20)	1412 (21)
299	1123 (9)	1282 (12)	1202 (7)	371	1255 (57)	1408 (17)	1331 (30)
300	1124 (20)	1231 (14)	1177 (12)	372	1195 (17)	1304 (14)	1249 (11)
301	1236 (8)	1324 (5)	1280 (5)	373	1258 (27)	1487 (6)	1373 (14)
302	1175 (32)	1252 (33)	1214 (23)	374	1418 (13)	1483 (9)	1450 (8)
303	1073 (26)	1195 (31)	1134 (20)	375	1006 (4)	1429 (6)	1217 (3)
304	1017 (11)	1454 (24)	1235 (13)	376	1278 (46)	1397 (18)	1338 (25)
305	1120 (13)	1460 (11)	1290 (9)	377	1166 (11)	1341 (7)	1253 (7)
306	1330 (12)	1488 (4)	1409 (6)	378	1009 (6)	1483 (12)	1246 (6)
307	1415 (2)	1452 (2)	1434 (2)	379	1312 (15)	1430 (19)	1371 (12)
308	1126 (3)	1429 (4)	1277 (3)	380	1073 (13)	1138 (9)	1105 (8)
309	1358 (25)	1415 (21)	1386 (16)	381	1401 (11)	1490 (4)	1446 (6)
310	1071 (64)	1499 (1)	1285 (32)	382	1277 (34)	1393 (12)	1335 (18)
311	1177 (37)	1272 (39)	1225 (27)	383	1318 (12)	1409 (20)	1364 (12)
312	1340 (27)	1435 (16)	1388 (16)	384	1200 (35)	1392 (12)	1296 (18)
313	1152 (14)	1346 (21)	1249 (13)	385	1272 (37)	1499 (1)	1386 (19)
314	1194 (25)	1361 (9)	1278 (13)	386	1262 (3)	1380 (2)	1321 (2)
315	1156 (12)	1355 (9)	1255 (7)	387	1056 (2)	1096 (2)	1076 (2)
316	1187 (98)	1439 (4)	1313 (49)	388	1049 (6)	1210 (17)	1129 (9)
317	1014 (4)	1184 (8)	1099 (5)	389	1183 (37)	1372 (31)	1278 (24)
318	1017 (8)	1155 (18)	1086 (10)	390	1017 (4)	1172 (32)	1094 (16)
319	1317 (14)	1374 (6)	1346 (8)	391	1390 (34)	1458 (22)	1424 (20)
320	1031 (21)	1499 (1)	1265 (11)	392	1009 (5)	1048 (3)	1028 (3)
321	1347 (17)	1412 (4)	1379 (9)	393	1153 (3)	1499 (1)	1326 (2)
322	1386 (17)	1438 (28)	1412 (16)	394	1056 (42)	1499 (1)	1278 (21)
323	1298 (14)	1484 (4)	1391 (7)	395	1392 (16)	1441 (14)	1417 (11)
324	1293 (16)	1484 (4)	1388 (8)	396	1119 (9)	1171 (4)	1145 (5)
325	1036 (17)	1097 (13)	1067 (11)	397	1126 (9)	1213 (13)	1170 (8)
326	1026 (17)	1084 (13)	1055 (11)	398	1244 (9)	1434 (13)	1339 (8)
327	1101 (10)	1499 (1)	1300 (5)	399	1090 (53)	1240 (45)	1165 (35)
328	1326 (14)	1467 (7)	1396 (8)	400	1161 (4)	1442 (5)	1301 (3)
329	1131 (5)	1482 (6)	1307 (4)	401	1048 (7)	1499 (1)	1274 (4)
330	1367 (36)	1420 (19)	1394 (20)	402	1111 (6)	1196 (8)	1154 (5)
331	1365 (19)	1438 (26)	1402 (16)	403	1303 (25)	1407 (11)	1355 (14)
332	1004 (2)	1203 (7)	1104 (4)	404	1190 (8)	1407 (10)	1299 (6)
333	1300 (35)	1435 (29)	1368 (22)	405	1248 (18)	1432 (16)	1340 (12)
334	1153 (27)	1472 (19)	1313 (16)	406	1003 (2)	1499 (1)	1251 (1)
335	1090 (12)	1208 (135)	1149 (68)	407	1006 (3)	1499 (1)	1252 (2)
336	1112 (3)	1212 (5)	1162 (3)	408	1313 (8)	1411 (11)	1362 (7)
337	1133 (13)	1254 (7)	1194 (7)	409	1319 (16)	1404 (10)	1361 (10)
338	1044 (2)	1150 (3)	1097 (2)	410	1315 (15)	1489 (14)	1402 (10)
339	1015 (8)	1399 (14)	1207 (8)	411	1313 (16)	1408 (9)	1361 (9)
340	1012 (3)	1226 (21)	1119 (10)	412	1077 (16)	1166 (4)	1121 (8)
341	1305 (13)	1468 (7)	1386 (7)	413	1259 (13)	1385 (6)	1322 (7)
342	1204 (18)	1316 (24)	1260 (15)	414	1291 (31)	1498 (3)	1394 (16)
343	1295 (54)	1395 (19)	1345 (28)	415	1256 (28)	1311 (11)	1284 (15)
344	1126 (6)	1499 (1)	1312 (3)	416	1387 (18)	1450 (17)	1418 (12)
345	1055 (23)	1194 (31)	1125 (19)	417	1363 (21)	1427 (21)	1395 (15)
346	1354 (25)	1487 (7)	1420 (13)	418	1335 (26)	1405 (20)	1370 (17)
347	1042 (30)	1111 (24)	1077 (19)	419	1396 (24)	1470 (15)	1433 (14)
348	1353 (50)	1478 (30)	1416 (29)	420	1402 (14)	1471 (7)	1436 (8)
349	1307 (6)	1437 (6)	1372 (4)	421	1159 (15)	1355 (5)	1257 (8)
350	1327 (9)	1408 (7)	1368 (6)	422	1389 (10)	1436 (14)	1413 (9)
351	1119 (23)	1176 (28)	1147 (18)	423	1076 (5)	1105 (24)	1091 (12)
352	1256 (18)	1387 (16)	1321 (12)	424	1355 (3)	1442 (2)	1398 (2)
353	1036 (2)	1121 (3)	1078 (2)	425	1079 (46)	1450 (16)	1265 (25)
354	1058 (18)	1161 (30)	1109 (18)	426	1252 (136)	1428 (22)	1340 (69)
355	1003 (1)	1258 (22)	1131 (11)	427	1407 (12)	1487 (6)	1447 (7)
356	1006 (4)	1367 (5)	1187 (3)	428	1397 (67)	1466 (9)	1432 (34)
357	1271 (64)	1462 (26)	1366 (34)	429	1386 (7)	1446 (11)	1416 (7)
358	1014 (15)	1221 (10)	1118 (9)	430	1022 (8)	1499 (1)	1260 (4)
359	1285 (26)	1482 (8)	1384 (13)	431	1233 (16)	1334 (12)	1283 (10)
360	1103 (11)	1340 (16)	1221 (10)	432	1401 (15)	1457 (10)	1429 (9)
433	1333 (21)	1417 (10)	1375 (11)	505	1078 (10)	1182 (70)	1130 (36)
434	1120 (90)	1499 (1)	1310 (45)	506	1002 (1)	1499 (1)	1251 (1)
435	1010 (14)	1499 (1)	1255 (7)	507	1102 (74)	1490 (6)	1296 (37)
436	1026 (4)	1299 (6)	1163 (4)	508	1198 (43)	1499 (1)	1349 (21)
437	1381 (3)	1443 (3)	1412 (2)	509	1146 (25)	1291 (16)	1219 (15)
438	1144 (24)	1499 (1)	1322 (12)	510	1279 (10)	1497 (3)	1388 (5)
439	1139 (2)	1262 (7)	1200 (4)	511	1227 (63)	1453 (13)	1340 (32)
440	1373 (5)	1485 (15)	1429 (8)	512	1263 (42)	1432 (44)	1348 (30)
441	1205 (10)	1340 (57)	1273 (29)	513	1325 (53)	1412 (28)	1368 (30)
442	1342 (27)	1393 (14)	1368 (15)	514	1191 (4)	1280 (7)	1236 (4)
443	1351 (37)	1409 (19)	1380 (21)	515	1347 (11)	1427 (11)	1387 (8)
444	1339 (3)	1441 (4)	1390 (3)	516	1009 (3)	1127 (21)	1068 (10)

Supplementary Table 1:

Burst ID <sup>a</sup>	$\nu_1^b$ (MHz)	$\nu_2^b$ (MHz)	$\nu_{p,obs}$ (MHz)	Burst ID <sup>a</sup>	$\nu_1^b$ (MHz)	$\nu_2^b$ (MHz)	$\nu_{p,obs}$ (MHz)
445	1364 (14)	1434 (5)	1399 (8)	517	1143 (30)	1476 (6)	1309 (16)
446	1330 (15)	1392 (28)	1361 (16)	518	1127 (39)	1483 (8)	1305 (20)
447	1290 (21)	1497 (4)	1393 (11)	519	1300 (69)	1384 (16)	1342 (35)
448	1187 (28)	1499 (1)	1343 (14)	520	1337 (36)	1484 (15)	1411 (20)
449	1039 (2)	1177 (9)	1108 (5)	521	1167 (13)	1450 (9)	1309 (8)
450	1324 (12)	1422 (8)	1373 (7)	522	1110 (34)	1498 (3)	1304 (17)
451	1400 (12)	1482 (6)	1441 (6)	523	1166 (28)	1267 (45)	1217 (26)
452	1131 (14)	1471 (8)	1301 (8)	524	1148 (23)	1303 (4)	1226 (12)
453	1354 (25)	1402 (3)	1378 (13)	525	1116 (9)	1193 (14)	1154 (8)
454	1093 (4)	1368 (2)	1230 (2)	526	1334 (10)	1393 (9)	1363 (7)
455	1009 (5)	1499 (1)	1254 (3)	527	1046 (5)	1159 (6)	1103 (4)
456	1389 (17)	1448 (8)	1418 (10)	528	1069 (19)	1287 (21)	1178 (14)
457	1376 (25)	1474 (17)	1425 (15)	529	1045 (9)	1250 (8)	1147 (6)
458	1028 (16)	1092 (15)	1060 (11)	530	1005 (3)	1218 (8)	1112 (4)
459	1363 (25)	1462 (32)	1412 (20)	531	1076 (53)	1497 (3)	1286 (27)
460	1062 (20)	1107 (8)	1085 (11)	532	1025 (26)	1492 (5)	1258 (13)
461	1006 (3)	1499 (1)	1253 (2)	533	1344 (25)	1457 (28)	1401 (19)
462	1315 (30)	1406 (41)	1360 (25)	534	1306 (18)	1488 (21)	1397 (14)
463	1087 (30)	1201 (13)	1144 (16)	535	1351 (3)	1398 (2)	1375 (2)
464	1067 (46)	1431 (4)	1249 (23)	536	1379 (31)	1442 (30)	1410 (22)
465	1319 (3)	1433 (4)	1376 (2)	537	1105 (18)	1345 (22)	1225 (14)
466	1123 (14)	1162 (22)	1142 (13)	538	1227 (12)	1431 (9)	1329 (8)
467	1156 (2)	1307 (4)	1232 (2)	539	1350 (31)	1411 (21)	1380 (19)
468	1345 (18)	1472 (20)	1408 (13)	540	1092 (25)	1213 (23)	1152 (17)
469	1120 (14)	1166 (5)	1143 (7)	541	1191 (32)	1431 (4)	1311 (16)
470	1053 (4)	1494 (5)	1273 (3)	542	1336 (6)	1488 (8)	1412 (5)
471	1123 (17)	1291 (20)	1207 (13)	543	1229 (4)	1447 (4)	1338 (3)
472	1318 (2)	1431 (3)	1375 (2)	544	1130 (3)	1292 (10)	1211 (5)
473	1325 (25)	1459 (26)	1392 (18)	545	1128 (21)	1349 (16)	1239 (13)
474	1120 (19)	1241 (23)	1180 (15)	546	1319 (24)	1416 (23)	1368 (17)
475	1165 (5)	1242 (3)	1203 (3)	547	1393 (3)	1460 (4)	1426 (2)
476	1292 (35)	1480 (7)	1386 (18)	548	1153 (32)	1416 (19)	1285 (19)
477	1348 (38)	1414 (27)	1381 (24)	549	1144 (5)	1320 (32)	1232 (16)
478	1343 (37)	1421 (31)	1382 (24)	550	1245 (32)	1361 (7)	1303 (16)
479	1348 (3)	1438 (3)	1393 (2)	551	1125 (11)	1247 (8)	1186 (7)
480	1353 (4)	1448 (3)	1401 (2)	552	1340 (29)	1435 (25)	1388 (19)
481	1211 (3)	1375 (3)	1293 (2)	553	1093 (12)	1180 (34)	1137 (18)
482	1080 (65)	1499 (1)	1289 (32)	554	1231 (6)	1442 (8)	1337 (5)
483	1061 (60)	1499 (1)	1280 (30)	555	1011 (9)	1469 (12)	1240 (8)
484	1009 (3)	1266 (15)	1138 (8)	556	1032 (6)	1222 (29)	1127 (15)
485	1323 (32)	1395 (15)	1359 (18)	557	1389 (22)	1454 (19)	1421 (15)
486	1304 (25)	1453 (10)	1379 (14)	558	1308 (4)	1464 (8)	1386 (5)
487	1219 (20)	1499 (1)	1359 (10)	559	1345 (2)	1436 (3)	1391 (2)
488	1252 (34)	1485 (5)	1369 (17)	560	1229 (3)	1345 (2)	1287 (2)
489	1106 (8)	1233 (5)	1169 (5)	561	1161 (17)	1440 (17)	1300 (12)
490	1201 (7)	1417 (54)	1309 (27)	562	1028 (10)	1311 (6)	1170 (6)
491	1164 (16)	1340 (10)	1252 (9)	563	1297 (14)	1489 (9)	1393 (8)
492	1310 (9)	1485 (4)	1397 (5)	564	1042 (58)	1499 (1)	1270 (29)
493	1102 (15)	1256 (16)	1179 (11)	565	1003 (1)	1499 (1)	1251 (1)
494	1097 (29)	1191 (30)	1144 (21)	566	1003 (1)	1333 (14)	1168 (7)
495	1271 (16)	1460 (21)	1366 (13)	567	1008 (5)	1499 (1)	1254 (2)
496	1252 (34)	1450 (10)	1351 (18)	568	1351 (2)	1444 (4)	1398 (2)
497	1317 (14)	1488 (3)	1403 (7)	569	1003 (1)	1499 (1)	1251 (1)
498	1116 (21)	1432 (22)	1274 (15)	570	1002 (1)	1499 (1)	1250 (1)
499	1356 (13)	1488 (6)	1422 (7)	571	1340 (5)	1410 (12)	1375 (7)
500	1247 (30)	1480 (13)	1363 (16)	572	1065 (15)	1255 (7)	1160 (8)
501	1161 (10)	1330 (7)	1246 (6)	573	1322 (88)	1447 (29)	1384 (46)
502	1265 (10)	1430 (12)	1347 (8)	574	1229 (36)	1397 (37)	1313 (26)
503	1279 (18)	1371 (12)	1325 (11)	575	1334 (2)	1403 (3)	1369 (2)
504	1067 (21)	1134 (20)	1100 (15)	576	1312 (16)	1474 (7)	1393 (9)
577	1337 (16)	1429 (10)	1383 (9)	649	1401 (27)	1476 (7)	1438 (14)
578	1077 (10)	1478 (15)	1278 (9)	650	1127 (14)	1358 (15)	1242 (10)
579	1033 (17)	1471 (16)	1252 (12)	651	1009 (4)	1319 (23)	1164 (11)
580	1392 (11)	1461 (5)	1427 (6)	652	1007 (3)	1330 (19)	1169 (10)
581	1266 (21)	1494 (5)	1380 (11)	653	1004 (3)	1340 (13)	1172 (7)
582	1012 (5)	1481 (12)	1246 (7)	654	1045 (11)	1245 (161)	1145 (81)
583	1013 (19)	1495 (5)	1254 (10)	655	1009 (5)	1463 (23)	1236 (12)
584	1323 (15)	1430 (15)	1377 (10)	656	1009 (5)	1461 (14)	1235 (8)
585	1357 (24)	1412 (26)	1384 (18)	657	1032 (4)	1198 (7)	1115 (4)
586	1371 (11)	1461 (20)	1416 (11)	658	1026 (4)	1201 (8)	1114 (4)
587	1255 (30)	1499 (1)	1377 (15)	659	1004 (5)	1499 (1)	1251 (2)
588	1365 (2)	1436 (4)	1401 (2)	660	1130 (45)	1368 (37)	1249 (29)
589	1265 (64)	1391 (18)	1328 (33)	661	1083 (24)	1495 (5)	1289 (12)
590	1301 (11)	1453 (22)	1377 (12)	662	1258 (41)	1359 (28)	1309 (25)
591	1390 (20)	1458 (20)	1424 (14)	663	1301 (10)	1477 (5)	1389 (6)
592	1320 (52)	1465 (15)	1392 (27)	664	1061 (35)	1189 (8)	1125 (18)
593	1033 (5)	1216 (13)	1124 (7)	665	1359 (8)	1497 (4)	1428 (4)
594	1312 (7)	1478 (6)	1395 (4)	666	1291 (17)	1499 (2)	1395 (9)
595	1379 (15)	1437 (13)	1408 (10)	667	1266 (14)	1451 (9)	1358 (9)

Supplementary Table 1:

Burst ID <sup>a</sup>	$\nu_1^b$ (MHz)	$\nu_2^b$ (MHz)	$\nu_{p,obs}$ (MHz)	Burst ID <sup>a</sup>	$\nu_1^b$ (MHz)	$\nu_2^b$ (MHz)	$\nu_{p,obs}$ (MHz)
596	1093 (32)	1414 (16)	1254 (18)	668	1194 (10)	1429 (9)	1311 (7)
597	1254 (8)	1354 (13)	1304 (8)	669	1334 (8)	1495 (4)	1414 (4)
598	1305 (3)	1424 (4)	1364 (3)	670	1293 (11)	1494 (5)	1393 (6)
599	1210 (12)	1336 (31)	1273 (17)	671	1409 (2)	1454 (3)	1431 (2)
600	1193 (15)	1327 (6)	1260 (8)	672	1381 (13)	1495 (3)	1438 (7)
601	1139 (11)	1261 (19)	1200 (11)	673	1329 (25)	1493 (4)	1411 (13)
602	1262 (67)	1411 (19)	1336 (35)	674	1279 (14)	1424 (19)	1351 (12)
603	1289 (32)	1397 (44)	1343 (27)	675	1302 (13)	1420 (6)	1361 (7)
604	1040 (16)	1145 (15)	1093 (11)	676	1052 (16)	1250 (5)	1151 (8)
605	1282 (47)	1366 (16)	1324 (25)	677	1352 (30)	1457 (15)	1405 (17)
606	1115 (7)	1317 (8)	1216 (5)	678	1343 (5)	1496 (4)	1420 (3)
607	1110 (11)	1321 (8)	1215 (7)	679	1339 (9)	1493 (4)	1416 (5)
608	1383 (50)	1471 (20)	1427 (27)	680	1327 (24)	1477 (8)	1402 (13)
609	1271 (49)	1458 (24)	1364 (27)	681	1195 (8)	1488 (5)	1341 (5)
610	1300 (42)	1415 (34)	1358 (27)	682	1318 (27)	1483 (7)	1401 (14)
611	1113 (42)	1190 (27)	1151 (25)	683	1356 (13)	1493 (10)	1425 (8)
612	1335 (21)	1402 (18)	1369 (14)	684	1247 (42)	1416 (9)	1331 (21)
613	1070 (24)	1353 (43)	1212 (25)	685	1324 (14)	1402 (12)	1363 (9)
614	1189 (12)	1359 (20)	1274 (12)	686	1262 (34)	1443 (12)	1353 (18)
615	1396 (15)	1449 (17)	1423 (11)	687	1260 (23)	1440 (32)	1350 (20)
616	1390 (15)	1444 (18)	1417 (12)	688	1173 (58)	1344 (37)	1259 (35)
617	1320 (22)	1472 (7)	1396 (11)	689	1332 (16)	1487 (6)	1410 (8)
618	1336 (8)	1433 (26)	1384 (13)	690	1285 (30)	1465 (15)	1375 (17)
619	1194 (35)	1342 (41)	1268 (27)	691	1237 (44)	1484 (5)	1361 (22)
620	1398 (3)	1432 (13)	1415 (7)	692	1006 (3)	1240 (12)	1123 (6)
621	1223 (93)	1440 (8)	1332 (47)	693	1192 (9)	1470 (17)	1331 (9)
622	1052 (24)	1282 (45)	1167 (26)	694	1205 (26)	1481 (11)	1343 (14)
623	1371 (2)	1444 (4)	1408 (2)	695	1325 (5)	1383 (6)	1354 (4)
624	1372 (13)	1443 (9)	1408 (8)	696	1121 (24)	1381 (39)	1251 (23)
625	1091 (18)	1184 (11)	1138 (11)	697	1409 (29)	1484 (18)	1447 (17)
626	1322 (29)	1368 (17)	1345 (17)	698	1219 (24)	1359 (7)	1289 (12)
627	1238 (10)	1324 (14)	1281 (9)	699	1105 (29)	1207 (32)	1156 (22)
628	1205 (30)	1368 (19)	1287 (18)	700	1236 (14)	1448 (18)	1342 (12)
629	1179 (18)	1469 (18)	1324 (12)	701	1269 (8)	1339 (4)	1304 (5)
630	1338 (13)	1471 (11)	1404 (9)	702	1259 (13)	1497 (2)	1378 (7)
631	1317 (21)	1398 (14)	1357 (13)	703	1294 (28)	1393 (24)	1344 (18)
632	1331 (9)	1411 (14)	1371 (8)	704	1360 (36)	1431 (21)	1396 (21)
633	1356 (20)	1480 (14)	1418 (12)	705	1112 (6)	1261 (8)	1187 (5)
634	1003 (1)	1499 (1)	1251 (1)	706	1273 (18)	1451 (10)	1362 (10)
635	1159 (99)	1499 (1)	1329 (50)	707	1019 (8)	1287 (93)	1153 (47)
636	1150 (6)	1406 (21)	1278 (11)	708	1126 (10)	1343 (9)	1234 (7)
637	1134 (15)	1428 (19)	1281 (12)	709	1150 (16)	1303 (130)	1226 (65)
638	1219 (5)	1499 (1)	1359 (3)	710	1372 (15)	1486 (7)	1429 (8)
639	1220 (6)	1499 (1)	1360 (3)	711	1257 (18)	1451 (26)	1354 (16)
640	1252 (26)	1419 (18)	1336 (16)	712	1159 (2)	1320 (2)	1239 (2)
641	1190 (38)	1430 (9)	1310 (19)	713	1364 (5)	1425 (8)	1395 (5)
642	1271 (20)	1396 (17)	1333 (13)	714	1056 (22)	1137 (31)	1096 (19)
643	1011 (4)	1499 (1)	1255 (2)	715	1229 (37)	1463 (25)	1346 (22)
644	1180 (10)	1429 (4)	1304 (6)	716	1346 (28)	1493 (5)	1420 (14)
645	1173 (13)	1421 (8)	1297 (8)	717	1155 (9)	1253 (10)	1204 (7)
646	1260 (8)	1490 (5)	1375 (4)	718	1136 (7)	1209 (11)	1173 (7)
647	1241 (8)	1487 (5)	1364 (5)	719	1354 (8)	1434 (7)	1394 (5)
648	1204 (10)	1422 (10)	1313 (7)	720	1120 (8)	1479 (8)	1299 (6)
721	1127 (6)	1316 (7)	1222 (5)	793	1389 (19)	1451 (32)	1420 (19)
722	1098 (17)	1368 (8)	1233 (10)	794	1235 (12)	1446 (6)	1341 (7)
723	1192 (31)	1486 (24)	1339 (20)	795	1226 (8)	1412 (6)	1319 (5)
724	1132 (25)	1275 (21)	1203 (16)	796	1298 (16)	1483 (19)	1390 (13)
725	1128 (10)	1299 (14)	1214 (9)	797	1246 (7)	1387 (2)	1316 (4)
726	1302 (7)	1474 (3)	1388 (4)	798	1329 (26)	1464 (27)	1397 (19)
727	1110 (6)	1433 (3)	1272 (4)	799	1034 (11)	1116 (20)	1075 (11)
728	1352 (21)	1454 (27)	1403 (17)	800	1215 (27)	1498 (3)	1356 (14)
729	1232 (23)	1404 (17)	1318 (14)	801	1361 (22)	1427 (19)	1394 (14)
730	1245 (13)	1457 (7)	1351 (7)	802	1373 (11)	1418 (14)	1395 (9)
731	1250 (13)	1402 (18)	1326 (11)	803	1107 (20)	1139 (7)	1123 (11)
732	1228 (57)	1436 (59)	1332 (41)	804	1157 (7)	1318 (12)	1238 (7)
733	1136 (12)	1499 (1)	1317 (6)	805	1044 (5)	1229 (7)	1137 (4)
734	1093 (30)	1362 (7)	1228 (16)	806	1086 (12)	1249 (14)	1168 (10)
735	1416 (6)	1462 (4)	1439 (3)	807	1103 (10)	1236 (11)	1169 (7)
736	1270 (110)	1394 (15)	1332 (55)	808	1337 (33)	1465 (23)	1401 (20)
737	1352 (24)	1480 (12)	1416 (13)	809	1404 (2)	1458 (4)	1431 (2)
738	1145 (18)	1499 (1)	1322 (9)	810	1113 (8)	1249 (7)	1181 (6)
739	1226 (22)	1495 (4)	1361 (11)	811	1372 (23)	1438 (24)	1405 (16)
740	1172 (40)	1479 (12)	1325 (21)	812	1362 (18)	1406 (25)	1384 (15)
741	1272 (13)	1487 (5)	1379 (7)	813	1134 (17)	1406 (11)	1270 (10)
742	1340 (10)	1437 (23)	1388 (13)	814	1021 (4)	1217 (14)	1119 (7)
743	1275 (39)	1440 (32)	1358 (25)	815	1338 (12)	1484 (11)	1411 (8)
744	1374 (6)	1423 (11)	1399 (6)	816	1195 (111)	1409 (22)	1302 (57)
745	1169 (38)	1430 (14)	1299 (20)	817	1285 (28)	1409 (17)	1347 (16)
746	1285 (15)	1487 (7)	1386 (8)	818	1007 (4)	1252 (6)	1129 (4)

Supplementary Table 1:

Burst ID <sup>a</sup>	$\nu_1^b$ (MHz)	$\nu_2^b$ (MHz)	$\nu_{p,obs}$ (MHz)	Burst ID <sup>a</sup>	$\nu_1^b$ (MHz)	$\nu_2^b$ (MHz)	$\nu_{p,obs}$ (MHz)
747	1322 (28)	1428 (6)	1375 (14)	819	1019 (13)	1106 (20)	1062 (12)
748	1233 (15)	1438 (17)	1336 (11)	820	1341 (37)	1437 (23)	1389 (22)
749	1131 (39)	1350 (12)	1240 (20)	821	1257 (22)	1398 (11)	1327 (12)
750	1063 (22)	1291 (18)	1177 (14)	822	1262 (20)	1408 (16)	1335 (13)
751	1183 (16)	1307 (23)	1245 (14)	823	1079 (12)	1143 (12)	1111 (9)
752	1343 (8)	1498 (2)	1421 (4)	824	1377 (13)	1431 (6)	1404 (7)
753	1149 (19)	1499 (1)	1324 (9)	825	1170 (27)	1491 (4)	1330 (14)
754	1079 (3)	1395 (64)	1237 (32)	826	1145 (14)	1491 (5)	1318 (7)
755	1087 (14)	1194 (11)	1141 (9)	827	1175 (14)	1375 (20)	1275 (12)
756	1376 (15)	1477 (22)	1426 (13)	828	1201 (49)	1477 (43)	1339 (33)
757	1126 (19)	1249 (52)	1187 (28)	829	1073 (21)	1223 (16)	1148 (13)
758	1295 (26)	1494 (5)	1394 (13)	830	1387 (27)	1449 (26)	1418 (19)
759	1083 (4)	1313 (3)	1198 (2)	831	1325 (14)	1470 (7)	1398 (8)
760	1138 (12)	1344 (15)	1241 (10)	832	1292 (5)	1481 (20)	1387 (10)
761	1082 (32)	1499 (1)	1291 (16)	833	1380 (22)	1470 (9)	1425 (12)
762	1003 (1)	1459 (6)	1231 (3)	834	1175 (8)	1414 (3)	1295 (4)
763	1378 (15)	1477 (10)	1427 (9)	835	1279 (32)	1387 (52)	1333 (31)
764	1089 (9)	1255 (31)	1172 (16)	836	1377 (2)	1447 (3)	1412 (2)
765	1251 (38)	1473 (11)	1362 (20)	837	1072 (7)	1138 (9)	1105 (6)
766	1259 (28)	1418 (11)	1338 (15)	838	1116 (18)	1348 (7)	1232 (10)
767	1178 (18)	1424 (28)	1301 (16)	839	1138 (52)	1401 (36)	1269 (32)
768	1372 (19)	1452 (36)	1412 (20)	840	1072 (22)	1201 (16)	1137 (14)
769	1227 (16)	1358 (16)	1292 (11)	841	1160 (16)	1499 (1)	1329 (8)
770	1308 (2)	1424 (5)	1366 (3)	842	1306 (2)	1419 (2)	1362 (2)
771	1046 (6)	1199 (11)	1122 (7)	843	1117 (10)	1499 (1)	1308 (5)
772	1107 (13)	1428 (4)	1268 (7)	844	1036 (38)	1498 (3)	1267 (19)
773	1359 (19)	1444 (23)	1402 (15)	845	1329 (16)	1432 (21)	1381 (13)
774	1066 (15)	1322 (25)	1194 (15)	846	1019 (11)	1141 (14)	1080 (9)
775	1063 (13)	1315 (20)	1189 (12)	847	1265 (21)	1406 (14)	1336 (12)
776	1307 (6)	1484 (3)	1396 (3)	848	1337 (13)	1486 (5)	1412 (7)
777	1018 (15)	1499 (1)	1259 (8)	849	1234 (30)	1498 (8)	1366 (16)
778	1270 (44)	1445 (21)	1357 (24)	850	1074 (53)	1482 (13)	1278 (27)
779	1058 (30)	1259 (12)	1159 (16)	851	1243 (11)	1480 (7)	1361 (6)
780	1249 (10)	1484 (5)	1367 (6)	852	1275 (16)	1444 (10)	1359 (10)
781	1275 (13)	1423 (8)	1349 (8)	853	1395 (15)	1463 (18)	1429 (12)
782	1141 (18)	1317 (22)	1229 (14)	854	1189 (9)	1485 (8)	1337 (6)
783	1022 (13)	1267 (16)	1145 (10)	855	1141 (26)	1278 (26)	1209 (18)
784	1025 (18)	1170 (14)	1097 (11)	856	1063 (14)	1264 (18)	1164 (11)
785	1366 (5)	1406 (3)	1386 (3)	857	1053 (13)	1242 (11)	1148 (8)
786	1253 (50)	1483 (17)	1368 (26)	858	1024 (21)	1314 (16)	1169 (13)
787	1098 (11)	1170 (17)	1134 (10)	859	1023 (19)	1277 (21)	1150 (14)
788	1317 (2)	1389 (3)	1353 (2)	860	1382 (15)	1486 (15)	1434 (10)
789	1349 (15)	1414 (20)	1381 (13)	861	1354 (17)	1493 (5)	1423 (9)
790	1024 (10)	1160 (8)	1092 (7)	862	1158 (28)	1306 (18)	1232 (17)
791	1299 (11)	1389 (14)	1344 (9)	863	1181 (13)	1295 (12)	1238 (9)
792	1303 (15)	1425 (9)	1364 (9)	864	1099 (5)	1162 (6)	1131 (4)
865	1226 (30)	1342 (7)	1284 (15)	937	1111 (26)	1182 (32)	1146 (20)
866	1348 (30)	1466 (24)	1407 (19)	938	1160 (22)	1318 (17)	1239 (14)
867	1334 (16)	1395 (13)	1364 (10)	939	1367 (16)	1466 (12)	1417 (10)
868	1312 (34)	1427 (18)	1370 (19)	940	1059 (8)	1363 (31)	1211 (16)
869	1084 (14)	1148 (10)	1116 (9)	941	1040 (15)	1266 (18)	1153 (12)
870	1385 (17)	1464 (18)	1424 (12)	942	1217 (13)	1497 (3)	1357 (7)
871	1294 (26)	1487 (6)	1390 (14)	943	1223 (9)	1489 (4)	1356 (5)
872	1289 (24)	1466 (9)	1378 (13)	944	1284 (31)	1375 (10)	1330 (17)
873	1148 (12)	1334 (20)	1241 (11)	945	1150 (5)	1336 (10)	1243 (6)
874	1287 (62)	1377 (15)	1332 (32)	946	1263 (13)	1391 (25)	1327 (14)
875	1195 (24)	1489 (8)	1342 (13)	947	1339 (32)	1424 (27)	1382 (21)
876	1137 (7)	1292 (6)	1215 (5)	948	1286 (20)	1472 (6)	1379 (10)
877	1323 (32)	1488 (13)	1405 (17)	949	1011 (5)	1499 (1)	1255 (2)
878	1282 (11)	1447 (8)	1364 (7)	950	1139 (78)	1337 (4)	1238 (39)
879	1012 (5)	1128 (16)	1070 (9)	951	1332 (35)	1418 (40)	1375 (27)
880	1270 (17)	1346 (4)	1308 (9)	952	1331 (53)	1488 (6)	1409 (27)
881	1349 (26)	1401 (21)	1375 (17)	953	1391 (14)	1476 (19)	1434 (12)
882	1289 (15)	1410 (10)	1349 (9)	954	1414 (22)	1482 (7)	1448 (11)
883	1039 (7)	1183 (9)	1111 (6)	955	1279 (23)	1385 (11)	1332 (13)
884	1266 (23)	1378 (17)	1322 (14)	956	1098 (46)	1356 (23)	1227 (26)
885	1171 (22)	1378 (4)	1274 (11)	957	1268 (71)	1492 (5)	1380 (36)
886	1111 (20)	1492 (6)	1301 (10)	958	1316 (33)	1484 (21)	1400 (20)
887	1080 (13)	1490 (7)	1285 (7)	959	1329 (28)	1481 (12)	1405 (15)
888	1294 (10)	1457 (14)	1376 (9)	960	1319 (9)	1492 (5)	1406 (5)
889	1210 (57)	1334 (29)	1272 (32)	961	1258 (27)	1493 (5)	1376 (14)
890	1311 (26)	1480 (13)	1395 (14)	962	1260 (6)	1408 (13)	1334 (7)
891	1096 (2)	1349 (127)	1222 (64)	963	1084 (25)	1165 (18)	1124 (16)
892	1367 (32)	1453 (22)	1410 (20)	964	1103 (23)	1254 (8)	1179 (12)
893	1010 (6)	1498 (3)	1254 (4)	965	1051 (16)	1130 (22)	1090 (14)
894	1042 (13)	1097 (10)	1069 (8)	966	1231 (12)	1454 (8)	1342 (7)
895	1210 (18)	1360 (17)	1285 (12)	967	1208 (15)	1481 (5)	1344 (8)
896	1160 (45)	1437 (33)	1298 (28)	968	1049 (13)	1120 (4)	1085 (7)
897	1259 (45)	1383 (22)	1321 (25)	969	1261 (35)	1481 (9)	1371 (18)

Supplementary Table 1:

Burst ID <sup>a</sup>	$\nu_1^b$ (MHz)	$\nu_2^b$ (MHz)	$\nu_{p,obs}$ (MHz)	Burst ID <sup>a</sup>	$\nu_1^b$ (MHz)	$\nu_2^b$ (MHz)	$\nu_{p,obs}$ (MHz)
898	1012 (4)	1479 (5)	1245 (3)	970	1357 (17)	1414 (28)	1386 (16)
899	1060 (11)	1400 (15)	1230 (9)	971	1068 (10)	1215 (7)	1142 (6)
900	1278 (36)	1473 (31)	1376 (24)	972	1136 (25)	1449 (11)	1292 (13)
901	1076 (10)	1298 (29)	1187 (15)	973	1028 (17)	1450 (4)	1239 (9)
902	1303 (10)	1363 (7)	1333 (6)	974	1320 (35)	1432 (16)	1376 (19)
903	1350 (15)	1411 (20)	1380 (12)	975	1223 (13)	1375 (9)	1299 (8)
904	1395 (17)	1452 (22)	1423 (14)	976	1135 (11)	1349 (10)	1242 (8)
905	1257 (57)	1436 (15)	1346 (30)	977	1253 (31)	1344 (14)	1298 (17)
906	1174 (19)	1309 (14)	1242 (12)	978	1133 (12)	1285 (35)	1209 (18)
907	1163 (19)	1270 (14)	1217 (12)	979	1171 (34)	1241 (18)	1206 (19)
908	1291 (14)	1485 (7)	1388 (8)	980	1284 (71)	1360 (24)	1322 (37)
909	1307 (15)	1458 (9)	1383 (9)	981	1340 (17)	1485 (6)	1413 (9)
910	1236 (15)	1454 (6)	1345 (8)	982	1034 (25)	1268 (18)	1151 (16)
911	1208 (20)	1393 (31)	1301 (19)	983	1043 (2)	1106 (3)	1075 (2)
912	1311 (4)	1498 (2)	1405 (3)	984	1022 (13)	1142 (34)	1082 (18)
913	1058 (8)	1179 (8)	1119 (6)	985	1068 (6)	1230 (11)	1149 (6)
914	1014 (5)	1185 (5)	1100 (4)	986	1095 (15)	1302 (5)	1198 (8)
915	1261 (19)	1413 (32)	1337 (19)	987	1070 (15)	1262 (20)	1166 (12)
916	1026 (5)	1156 (17)	1091 (9)	988	1386 (7)	1455 (15)	1420 (8)
917	1252 (10)	1373 (15)	1313 (9)	989	1251 (45)	1451 (11)	1351 (23)
918	1029 (9)	1222 (22)	1125 (12)	990	1223 (2)	1320 (3)	1271 (2)
919	1068 (7)	1277 (11)	1173 (7)	991	1335 (23)	1445 (23)	1390 (16)
920	1008 (5)	1398 (96)	1203 (48)	992	1368 (5)	1462 (11)	1415 (6)
921	1060 (2)	1165 (2)	1113 (2)	993	1236 (13)	1465 (14)	1350 (9)
922	1323 (16)	1485 (18)	1404 (12)	994	1237 (18)	1487 (5)	1362 (10)
923	1326 (14)	1404 (30)	1365 (16)	995	1225 (45)	1329 (34)	1277 (28)
924	1296 (13)	1461 (10)	1379 (8)	996	1242 (22)	1350 (10)	1296 (12)
925	1289 (17)	1458 (5)	1374 (9)	997	1330 (5)	1418 (10)	1374 (5)
926	1337 (17)	1393 (35)	1365 (20)	998	1134 (5)	1229 (4)	1181 (3)
927	1240 (18)	1321 (8)	1280 (10)	999	1318 (42)	1405 (25)	1361 (24)
928	1209 (36)	1370 (4)	1289 (18)	1000	1276 (54)	1415 (17)	1345 (29)
929	1154 (9)	1257 (31)	1206 (16)	1001	1213 (56)	1398 (15)	1306 (29)
930	1127 (12)	1483 (6)	1305 (7)	1002	1290 (35)	1489 (4)	1390 (18)
931	1039 (40)	1483 (27)	1261 (24)	1003	1170 (31)	1421 (28)	1296 (21)
932	1264 (19)	1409 (25)	1336 (16)	1004	1293 (28)	1446 (22)	1369 (18)
933	1324 (57)	1474 (21)	1399 (30)	1005	1085 (8)	1182 (38)	1134 (19)
934	1348 (24)	1434 (33)	1391 (20)	1006	1249 (10)	1499 (1)	1374 (5)
935	1336 (12)	1404 (8)	1370 (7)	1007	1035 (22)	1172 (38)	1103 (22)
936	1343 (15)	1471 (27)	1407 (15)	1008	1004 (2)	1499 (1)	1252 (1)
1009	1182 (10)	1391 (6)	1287 (6)	1081	1344 (7)	1474 (14)	1409 (8)
1010	1011 (4)	1496 (5)	1253 (3)	1082	1287 (14)	1481 (6)	1384 (7)
1011	1030 (7)	1116 (10)	1073 (6)	1083	1388 (9)	1481 (13)	1434 (8)
1012	1026 (10)	1131 (17)	1078 (10)	1084	1180 (62)	1431 (9)	1306 (31)
1013	1330 (8)	1463 (11)	1396 (7)	1085	1113 (17)	1319 (24)	1216 (15)
1014	1057 (16)	1387 (5)	1222 (9)	1086	1080 (10)	1234 (50)	1157 (26)
1015	1240 (42)	1456 (30)	1348 (26)	1087	1359 (41)	1459 (23)	1409 (23)
1016	1368 (16)	1477 (6)	1422 (8)	1088	1281 (34)	1417 (33)	1349 (23)
1017	1163 (26)	1457 (8)	1310 (14)	1089	1185 (18)	1283 (15)	1234 (12)
1018	1150 (29)	1273 (38)	1212 (24)	1090	1187 (29)	1332 (15)	1259 (16)
1019	1272 (11)	1497 (3)	1385 (5)	1091	1005 (4)	1499 (1)	1252 (2)
1020	1383 (30)	1442 (15)	1412 (17)	1092	1002 (1)	1306 (18)	1154 (9)
1021	1374 (5)	1454 (8)	1414 (5)	1093	1302 (10)	1478 (4)	1390 (6)
1022	1170 (17)	1319 (12)	1245 (11)	1094	1316 (22)	1431 (12)	1374 (13)
1023	1167 (17)	1310 (15)	1239 (11)	1095	1078 (2)	1154 (2)	1116 (2)
1024	1377 (7)	1487 (6)	1432 (5)	1096	1034 (18)	1094 (32)	1064 (19)
1025	1325 (15)	1397 (12)	1361 (10)	1097	1291 (28)	1417 (33)	1354 (22)
1026	1301 (14)	1379 (10)	1340 (9)	1098	1137 (21)	1396 (7)	1266 (11)
1027	1230 (39)	1372 (17)	1301 (21)	1099	1090 (38)	1285 (43)	1188 (29)
1028	1013 (9)	1276 (31)	1144 (16)	1100	1374 (12)	1436 (11)	1405 (8)
1029	1005 (3)	1168 (17)	1086 (9)	1101	1260 (44)	1424 (31)	1342 (27)
1030	1301 (19)	1435 (16)	1368 (13)	1102	1316 (14)	1387 (9)	1351 (8)
1031	1071 (12)	1445 (20)	1258 (12)	1103	1197 (22)	1392 (12)	1294 (12)
1032	1144 (3)	1397 (5)	1270 (3)	1104	1186 (18)	1421 (13)	1303 (11)
1033	1347 (13)	1471 (7)	1409 (8)	1105	1009 (10)	1078 (5)	1044 (6)
1034	1309 (43)	1433 (23)	1371 (25)	1106	1002 (1)	1164 (11)	1083 (6)
1035	1246 (16)	1357 (29)	1301 (16)	1107	1360 (29)	1423 (28)	1392 (20)
1036	1031 (17)	1192 (12)	1111 (10)	1108	1308 (30)	1475 (12)	1392 (16)
1037	1352 (21)	1421 (26)	1387 (17)	1109	1108 (21)	1482 (5)	1295 (11)
1038	1229 (9)	1317 (11)	1273 (7)	1110	1307 (8)	1498 (3)	1402 (4)
1039	1157 (15)	1309 (6)	1233 (8)	1111	1273 (21)	1498 (3)	1385 (11)
1040	1049 (19)	1191 (128)	1120 (65)	1112	1212 (8)	1499 (1)	1356 (4)
1041	1351 (25)	1481 (11)	1416 (14)	1113	1025 (17)	1174 (15)	1099 (11)
1042	1205 (75)	1493 (5)	1349 (37)	1114	1012 (7)	1235 (20)	1124 (11)
1043	1012 (4)	1453 (25)	1233 (13)	1115	1075 (15)	1313 (15)	1194 (11)
1044	1238 (10)	1469 (17)	1353 (10)	1116	1007 (3)	1259 (9)	1133 (5)
1045	1273 (14)	1408 (81)	1340 (41)	1117	1257 (48)	1405 (11)	1331 (24)
1046	1282 (30)	1408 (18)	1345 (17)	1118	1347 (19)	1416 (5)	1381 (10)
1047	1388 (16)	1441 (17)	1414 (12)	1119	1148 (8)	1302 (34)	1225 (17)
1048	1013 (8)	1361 (26)	1187 (13)	1120	1061 (4)	1250 (5)	1155 (3)

Supplementary Table 1:

Burst ID <sup>a</sup>	$\nu_1^b$ (MHz)	$\nu_2^b$ (MHz)	$\nu_{p,obs}$ (MHz)	Burst ID <sup>a</sup>	$\nu_1^b$ (MHz)	$\nu_2^b$ (MHz)	$\nu_{p,obs}$ (MHz)
1049	1236 (18)	1425 (18)	1330 (13)	1121	1028 (3)	1297 (21)	1162 (11)
1050	1122 (4)	1402 (26)	1262 (13)	1122	1064 (11)	1142 (18)	1103 (10)
1051	1307 (42)	1422 (15)	1364 (22)	1123	1267 (25)	1490 (3)	1379 (13)
1052	1073 (21)	1268 (11)	1171 (12)	1124	1088 (5)	1239 (12)	1164 (6)
1053	1098 (27)	1252 (24)	1175 (18)	1125	1052 (6)	1205 (10)	1129 (6)
1054	1354 (35)	1479 (26)	1417 (22)	1126	1037 (4)	1199 (8)	1118 (5)
1055	1340 (6)	1389 (3)	1364 (3)	1127	1179 (27)	1273 (25)	1226 (18)
1056	1133 (11)	1330 (22)	1231 (12)	1128	1082 (17)	1247 (6)	1165 (9)
1057	1261 (8)	1410 (19)	1335 (10)	1129	1233 (39)	1405 (15)	1319 (21)
1058	1250 (8)	1410 (18)	1330 (10)	1130	1012 (4)	1233 (25)	1123 (13)
1059	1160 (12)	1253 (5)	1206 (7)	1131	1126 (55)	1358 (33)	1242 (32)
1060	1014 (5)	1414 (33)	1214 (17)	1132	1240 (19)	1449 (12)	1344 (11)
1061	1203 (19)	1499 (1)	1351 (9)	1133	1046 (23)	1147 (15)	1097 (14)
1062	1261 (38)	1385 (34)	1323 (26)	1134	1288 (30)	1383 (14)	1336 (16)
1063	1123 (17)	1333 (11)	1228 (10)	1135	1029 (7)	1111 (15)	1070 (8)
1064	1303 (16)	1497 (4)	1400 (8)	1136	1340 (14)	1442 (21)	1391 (13)
1065	1100 (51)	1495 (4)	1297 (26)	1137	1355 (13)	1438 (18)	1396 (11)
1066	1082 (16)	1499 (1)	1291 (8)	1138	1283 (24)	1495 (6)	1389 (12)
1067	1007 (6)	1499 (1)	1253 (3)	1139	1050 (11)	1206 (13)	1128 (8)
1068	1078 (41)	1193 (40)	1136 (28)	1140	1015 (4)	1196 (9)	1105 (5)
1069	1194 (29)	1499 (1)	1347 (14)	1141	1349 (46)	1452 (38)	1400 (30)
1070	1152 (59)	1354 (35)	1253 (34)	1142	1186 (27)	1469 (8)	1328 (14)
1071	1303 (9)	1422 (7)	1362 (6)	1143	1047 (26)	1213 (25)	1130 (18)
1072	1341 (13)	1439 (23)	1390 (13)	1144	1101 (7)	1208 (17)	1155 (9)
1073	1170 (57)	1361 (37)	1266 (34)	1145	1282 (43)	1396 (22)	1339 (24)
1074	1249 (24)	1361 (24)	1305 (17)	1146	1318 (24)	1371 (19)	1344 (15)
1075	1123 (27)	1334 (27)	1229 (19)	1147	1346 (30)	1459 (31)	1403 (22)
1076	1269 (37)	1485 (5)	1377 (19)	1148	1248 (20)	1398 (8)	1323 (11)
1077	1105 (23)	1485 (8)	1295 (12)	1149	1109 (8)	1332 (16)	1221 (9)
1078	1255 (7)	1472 (6)	1364 (5)	1150	1099 (12)	1307 (11)	1203 (8)
1079	1206 (6)	1445 (10)	1326 (6)	1151	1122 (6)	1320 (6)	1221 (4)
1080	1118 (12)	1265 (14)	1192 (9)	1152	1350 (16)	1461 (38)	1405 (20)
1153	1346 (13)	1453 (42)	1399 (22)	1225	1376 (18)	1476 (14)	1426 (12)
1154	1378 (17)	1458 (33)	1418 (19)	1226	1196 (51)	1331 (29)	1264 (29)
1155	1236 (30)	1477 (14)	1356 (16)	1227	1319 (22)	1454 (11)	1387 (12)
1156	1139 (14)	1348 (10)	1244 (9)	1228	1093 (45)	1240 (71)	1166 (42)
1157	1142 (15)	1341 (13)	1242 (10)	1229	1111 (14)	1366 (11)	1239 (9)
1158	1290 (7)	1450 (19)	1370 (10)	1230	1354 (25)	1403 (20)	1379 (16)
1159	1063 (16)	1147 (7)	1105 (9)	1231	1328 (64)	1478 (8)	1403 (32)
1160	1247 (37)	1358 (7)	1303 (19)	1232	1021 (5)	1331 (190)	1176 (95)
1161	1156 (18)	1313 (5)	1234 (9)	1233	1010 (3)	1139 (10)	1075 (5)
1162	1198 (15)	1496 (4)	1347 (8)	1234	1132 (8)	1244 (34)	1188 (18)
1163	1122 (18)	1428 (18)	1275 (13)	1235	1326 (22)	1477 (9)	1402 (12)
1164	1115 (19)	1497 (3)	1306 (9)	1236	1249 (65)	1386 (31)	1318 (36)
1165	1164 (23)	1311 (10)	1237 (13)	1237	1315 (2)	1422 (3)	1368 (2)
1166	1342 (38)	1455 (25)	1399 (23)	1238	1160 (20)	1252 (14)	1206 (12)
1167	1071 (16)	1491 (3)	1281 (8)	1239	1051 (11)	1152 (8)	1101 (7)
1168	1050 (17)	1160 (11)	1105 (10)	1240	1060 (6)	1200 (13)	1130 (7)
1169	1192 (51)	1454 (5)	1323 (26)	1241	1152 (13)	1364 (5)	1258 (7)
1170	1281 (31)	1454 (27)	1368 (21)	1242	1137 (3)	1499 (1)	1318 (1)
1171	1325 (40)	1474 (11)	1399 (21)	1243	1158 (8)	1499 (1)	1329 (4)
1172	1217 (32)	1418 (20)	1317 (19)	1244	1202 (19)	1499 (2)	1350 (10)
1173	1333 (18)	1395 (5)	1364 (9)	1245	1137 (5)	1499 (1)	1318 (3)
1174	1038 (14)	1104 (17)	1071 (11)	1246	1010 (3)	1095 (10)	1053 (5)
1175	1201 (51)	1464 (19)	1332 (27)	1247	1420 (7)	1463 (4)	1442 (4)
1176	1128 (22)	1294 (11)	1211 (12)	1248	1327 (5)	1442 (32)	1384 (16)
1177	1065 (31)	1238 (26)	1151 (20)	1249	1176 (16)	1407 (14)	1291 (11)
1178	1029 (16)	1499 (1)	1264 (8)	1250	1282 (15)	1455 (8)	1368 (9)
1179	1003 (2)	1380 (17)	1192 (9)	1251	1003 (1)	1499 (1)	1251 (1)
1180	1180 (72)	1330 (24)	1255 (38)	1252	1354 (14)	1488 (7)	1421 (8)
1181	1008 (4)	1399 (22)	1204 (11)	1253	1339 (21)	1485 (8)	1412 (11)
1182	1040 (25)	1318 (6)	1179 (13)	1254	1307 (19)	1369 (13)	1338 (11)
1183	1267 (5)	1496 (4)	1381 (3)	1255	1132 (30)	1361 (5)	1247 (15)
1184	1293 (29)	1451 (20)	1372 (18)	1256	1302 (25)	1488 (7)	1395 (13)
1185	1039 (2)	1130 (2)	1084 (2)	1257	1275 (39)	1484 (6)	1380 (20)
1186	1006 (5)	1499 (1)	1253 (2)	1258	1265 (39)	1447 (26)	1356 (23)
1187	1008 (4)	1499 (1)	1254 (2)	1259	1325 (24)	1434 (14)	1379 (14)
1188	1338 (18)	1459 (11)	1398 (10)	1260	1093 (15)	1315 (8)	1204 (8)
1189	1226 (17)	1481 (6)	1353 (9)	1261	1049 (19)	1270 (14)	1160 (12)
1190	1007 (3)	1385 (22)	1196 (11)	1262	1281 (30)	1489 (5)	1385 (15)
1191	1297 (14)	1422 (9)	1360 (8)	1263	1300 (18)	1492 (6)	1396 (10)
1192	1370 (19)	1483 (5)	1427 (10)	1264	1189 (15)	1493 (7)	1341 (8)
1193	1365 (18)	1425 (9)	1395 (10)	1265	1379 (22)	1481 (10)	1430 (12)
1194	1308 (15)	1424 (15)	1366 (11)	1266	1312 (7)	1373 (18)	1342 (10)
1195	1297 (18)	1392 (16)	1345 (12)	1267	1316 (44)	1481 (18)	1399 (24)
1196	1349 (8)	1481 (15)	1415 (9)	1268	1297 (55)	1492 (6)	1394 (28)
1197	1219 (12)	1470 (8)	1344 (7)	1269	1305 (17)	1405 (6)	1355 (9)
1198	1264 (28)	1455 (22)	1359 (18)	1270	1313 (7)	1499 (2)	1406 (4)
1199	1296 (17)	1493 (4)	1394 (9)	1271	1322 (27)	1463 (28)	1392 (20)

Supplementary Table 1:

Burst ID <sup>a</sup>	$\nu_1^b$ (MHz)	$\nu_2^b$ (MHz)	$\nu_{p,obs}$ (MHz)	Burst ID <sup>a</sup>	$\nu_1^b$ (MHz)	$\nu_2^b$ (MHz)	$\nu_{p,obs}$ (MHz)
1200	1157 (3)	1372 (2)	1264 (2)	1272	1252 (4)	1424 (4)	1338 (3)
1201	1083 (13)	1235 (14)	1159 (10)	1273	1331 (24)	1462 (14)	1396 (14)
1202	1101 (17)	1484 (5)	1292 (9)	1274	1133 (6)	1298 (14)	1216 (8)
1203	1221 (15)	1325 (6)	1273 (8)	1275	1111 (10)	1213 (27)	1162 (14)
1204	1089 (11)	1230 (18)	1160 (11)	1276	1122 (14)	1292 (6)	1207 (7)
1205	1299 (13)	1490 (4)	1394 (7)	1277	1305 (22)	1448 (8)	1376 (12)
1206	1261 (22)	1405 (22)	1333 (16)	1278	1113 (21)	1218 (30)	1165 (18)
1207	1268 (15)	1421 (14)	1345 (10)	1279	1144 (30)	1391 (7)	1268 (15)
1208	1128 (2)	1317 (4)	1223 (2)	1280	1090 (26)	1398 (8)	1244 (13)
1209	1194 (54)	1364 (70)	1279 (44)	1281	1273 (39)	1373 (13)	1323 (21)
1210	1258 (34)	1377 (6)	1318 (17)	1282	1154 (26)	1498 (2)	1326 (13)
1211	1267 (14)	1388 (28)	1328 (16)	1283	1085 (32)	1193 (55)	1139 (32)
1212	1243 (22)	1356 (15)	1300 (13)	1284	1376 (17)	1467 (19)	1422 (13)
1213	1330 (26)	1440 (30)	1385 (20)	1285	1158 (18)	1256 (41)	1207 (22)
1214	1266 (59)	1406 (2)	1336 (30)	1286	1179 (25)	1417 (13)	1298 (14)
1215	1003 (1)	1498 (5)	1250 (2)	1287	1325 (18)	1474 (18)	1400 (13)
1216	1044 (50)	1443 (26)	1244 (28)	1288	1196 (40)	1351 (19)	1274 (22)
1217	1015 (5)	1347 (2)	1181 (3)	1289	1091 (7)	1499 (1)	1295 (4)
1218	1313 (37)	1388 (14)	1351 (20)	1290	1130 (9)	1362 (136)	1246 (68)
1219	1131 (15)	1389 (13)	1260 (10)	1291	1344 (19)	1445 (12)	1394 (11)
1220	1328 (42)	1404 (28)	1366 (25)	1292	1112 (21)	1276 (36)	1194 (21)
1221	1252 (37)	1427 (47)	1339 (30)	1293	1324 (17)	1413 (13)	1369 (11)
1222	1025 (6)	1161 (10)	1093 (6)	1294	1252 (15)	1396 (12)	1324 (10)
1223	1334 (14)	1488 (7)	1411 (8)	1295	1043 (5)	1100 (6)	1071 (4)
1224	1326 (13)	1484 (7)	1405 (7)	1296	1011 (3)	1149 (12)	1080 (6)
1297	1226 (52)	1411 (18)	1318 (28)	1369	1371 (34)	1486 (15)	1429 (18)
1298	1117 (6)	1201 (13)	1159 (7)	1370	1331 (15)	1463 (23)	1397 (13)
1299	1286 (3)	1381 (3)	1334 (2)	1371	1321 (18)	1477 (16)	1399 (12)
1300	1353 (2)	1452 (2)	1403 (2)	1372	1261 (15)	1439 (18)	1350 (12)
1301	1178 (17)	1407 (2)	1292 (9)	1373	1168 (26)	1275 (41)	1222 (24)
1302	1293 (9)	1476 (5)	1385 (5)	1374	1153 (16)	1429 (9)	1291 (9)
1303	1277 (12)	1459 (6)	1368 (7)	1375	1322 (23)	1439 (29)	1380 (18)
1304	1087 (3)	1282 (3)	1184 (2)	1376	1284 (23)	1442 (6)	1363 (12)
1305	1379 (4)	1438 (3)	1408 (3)	1377	1313 (16)	1474 (5)	1394 (8)
1306	1382 (14)	1475 (10)	1428 (9)	1378	1145 (30)	1319 (16)	1232 (17)
1307	1369 (27)	1425 (23)	1397 (17)	1379	1201 (35)	1310 (24)	1255 (21)
1308	1365 (11)	1467 (8)	1416 (7)	1380	1326 (14)	1444 (23)	1385 (13)
1309	1349 (30)	1393 (12)	1371 (16)	1381	1391 (63)	1470 (21)	1431 (33)
1310	1147 (21)	1264 (25)	1205 (16)	1382	1153 (12)	1385 (25)	1269 (14)
1311	1253 (20)	1322 (12)	1288 (12)	1383	1043 (25)	1178 (14)	1111 (15)
1312	1342 (19)	1441 (24)	1392 (16)	1384	1359 (26)	1455 (31)	1407 (20)
1313	1302 (26)	1402 (18)	1352 (16)	1385	1168 (10)	1435 (11)	1302 (7)
1314	1313 (17)	1482 (5)	1397 (9)	1386	1383 (8)	1440 (9)	1411 (6)
1315	1380 (17)	1448 (19)	1414 (13)	1387	1315 (11)	1492 (6)	1403 (6)
1316	1355 (21)	1451 (25)	1403 (16)	1388	1089 (3)	1288 (2)	1189 (2)
1317	1295 (4)	1406 (2)	1351 (2)	1389	1057 (8)	1255 (8)	1156 (5)
1318	1302 (24)	1454 (17)	1378 (15)	1390	1006 (4)	1099 (20)	1053 (10)
1319	1353 (21)	1466 (23)	1410 (16)	1391	1108 (22)	1154 (22)	1131 (16)
1320	1375 (47)	1439 (10)	1407 (24)	1392	1328 (31)	1486 (6)	1407 (16)
1321	1398 (14)	1440 (18)	1419 (12)	1393	1292 (8)	1494 (4)	1393 (5)
1322	1129 (15)	1224 (49)	1176 (26)	1394	1204 (19)	1472 (15)	1338 (12)
1323	1351 (15)	1459 (11)	1405 (9)	1395	1354 (13)	1491 (3)	1422 (7)
1324	1087 (44)	1392 (11)	1240 (23)	1396	1090 (32)	1286 (46)	1188 (28)
1325	1046 (24)	1200 (26)	1123 (18)	1397	1077 (4)	1322 (11)	1199 (6)
1326	1377 (25)	1463 (21)	1420 (16)	1398	1022 (12)	1258 (9)	1140 (8)
1327	1329 (22)	1445 (28)	1387 (18)	1399	1136 (28)	1497 (3)	1316 (14)
1328	1279 (22)	1494 (6)	1387 (12)	1400	1012 (12)	1361 (15)	1186 (10)
1329	1030 (13)	1499 (1)	1265 (7)	1401	1147 (15)	1316 (17)	1232 (11)
1330	1005 (4)	1499 (1)	1252 (2)	1402	1120 (18)	1352 (15)	1236 (12)
1331	1128 (11)	1266 (53)	1197 (27)	1403	1093 (10)	1349 (8)	1221 (6)
1332	1186 (14)	1345 (17)	1266 (11)	1404	1309 (12)	1452 (19)	1381 (11)
1333	1036 (7)	1243 (5)	1140 (4)	1405	1289 (20)	1441 (17)	1365 (13)
1334	1008 (5)	1400 (9)	1204 (5)	1406	1272 (34)	1393 (12)	1332 (18)
1335	1039 (22)	1169 (19)	1104 (15)	1407	1203 (16)	1428 (7)	1315 (9)
1336	1310 (3)	1393 (3)	1352 (2)	1408	1317 (14)	1445 (16)	1381 (11)
1337	1365 (24)	1441 (23)	1403 (17)	1409	1256 (7)	1494 (5)	1375 (4)
1338	1143 (17)	1499 (1)	1321 (9)	1410	1027 (4)	1183 (8)	1105 (4)
1339	1368 (20)	1430 (17)	1399 (13)	1411	1108 (19)	1417 (13)	1262 (12)
1340	1011 (3)	1279 (42)	1145 (21)	1412	1049 (28)	1499 (1)	1274 (14)
1341	1315 (16)	1400 (15)	1357 (11)	1413	1003 (1)	1489 (11)	1246 (6)
1342	1289 (15)	1494 (5)	1391 (8)	1414	1103 (65)	1419 (16)	1261 (33)
1343	1373 (16)	1460 (26)	1416 (15)	1415	1015 (5)	1499 (1)	1257 (2)
1344	1011 (7)	1485 (11)	1248 (6)	1416	1003 (1)	1361 (14)	1182 (7)
1345	1040 (20)	1117 (26)	1078 (16)	1417	1283 (25)	1439 (30)	1361 (19)
1346	1348 (15)	1485 (12)	1416 (10)	1418	1091 (10)	1308 (7)	1200 (6)
1347	1401 (2)	1449 (3)	1425 (2)	1419	1228 (32)	1378 (22)	1303 (20)
1348	1213 (8)	1376 (16)	1295 (9)	1420	1269 (20)	1371 (8)	1320 (11)
1349	1339 (10)	1492 (6)	1416 (6)	1421	1070 (62)	1499 (1)	1285 (31)
1350	1214 (11)	1353 (7)	1284 (7)	1422	1028 (12)	1499 (1)	1264 (6)



Supplementary Table 1:

Burst ID <sup>a</sup>	$\nu_1^b$ (MHz)	$\nu_2^b$ (MHz)	$\nu_{p,obs}$ (MHz)	Burst ID <sup>a</sup>	$\nu_1^b$ (MHz)	$\nu_2^b$ (MHz)	$\nu_{p,obs}$ (MHz)
1351	1083 (29)	1217 (14)	1150 (16)	1423	1004 (2)	1499 (1)	1252 (1)
1352	1339 (43)	1439 (52)	1389 (34)	1424	1358 (17)	1482 (14)	1420 (11)
1353	1395 (12)	1482 (10)	1439 (8)	1425	1205 (42)	1497 (3)	1351 (21)
1354	1090 (70)	1395 (20)	1243 (36)	1426	1107 (12)	1499 (1)	1303 (6)
1355	1156 (21)	1259 (24)	1208 (16)	1427	1323 (16)	1489 (5)	1406 (8)
1356	1347 (12)	1472 (7)	1409 (7)	1428	1257 (23)	1361 (23)	1309 (16)
1357	1296 (15)	1436 (15)	1366 (10)	1429	1236 (37)	1473 (4)	1355 (19)
1358	1135 (4)	1499 (1)	1317 (2)	1430	1074 (20)	1130 (12)	1102 (12)
1359	1006 (3)	1499 (1)	1253 (2)	1431	1033 (8)	1202 (10)	1117 (6)
1360	1241 (8)	1477 (12)	1359 (7)	1432	1013 (8)	1155 (26)	1084 (13)
1361	1041 (3)	1277 (50)	1159 (25)	1433	1120 (19)	1222 (32)	1171 (19)
1362	1228 (15)	1393 (9)	1310 (9)	1434	1124 (24)	1253 (9)	1189 (13)
1363	1195 (35)	1374 (10)	1284 (18)	1435	1346 (23)	1452 (27)	1399 (18)
1364	1288 (10)	1499 (1)	1394 (5)	1436	1329 (16)	1466 (25)	1397 (15)
1365	1255 (7)	1478 (7)	1367 (5)	1437	1234 (13)	1435 (14)	1334 (10)
1366	1404 (10)	1468 (5)	1436 (5)	1438	1188 (15)	1415 (6)	1302 (8)
1367	1314 (16)	1447 (39)	1381 (21)	1439	1169 (19)	1413 (9)	1291 (10)
1368	1401 (15)	1482 (10)	1442 (9)	1440	1079 (26)	1437 (17)	1258 (16)
1441	1105 (5)	1296 (11)	1201 (6)	1513	1222 (44)	1404 (11)	1313 (23)
1442	1309 (18)	1463 (9)	1386 (10)	1514	1105 (2)	1244 (2)	1174 (2)
1443	1050 (22)	1187 (7)	1118 (11)	1515	1242 (20)	1368 (22)	1305 (15)
1444	1274 (52)	1475 (6)	1375 (26)	1516	1248 (5)	1483 (5)	1366 (4)
1445	1223 (48)	1344 (32)	1284 (29)	1517	1048 (6)	1099 (7)	1074 (5)
1446	1104 (9)	1291 (40)	1197 (20)	1518	1051 (4)	1274 (19)	1162 (10)
1447	1300 (17)	1387 (15)	1344 (11)	1519	1037 (4)	1304 (10)	1171 (5)
1448	1211 (13)	1390 (20)	1300 (12)	1520	1012 (4)	1477 (6)	1245 (4)
1449	1039 (2)	1130 (2)	1085 (2)	1521	1200 (72)	1382 (51)	1291 (44)
1450	1296 (26)	1481 (5)	1388 (13)	1522	1075 (16)	1227 (108)	1151 (55)
1451	1342 (19)	1476 (23)	1409 (15)	1523	1116 (5)	1304 (14)	1210 (7)
1452	1313 (26)	1466 (22)	1390 (17)	1524	1227 (26)	1411 (21)	1319 (17)
1453	1110 (11)	1309 (26)	1210 (14)	1525	1302 (129)	1443 (20)	1372 (65)
1454	1180 (37)	1463 (29)	1321 (23)	1526	1003 (1)	1497 (8)	1250 (4)
1455	1136 (31)	1446 (35)	1291 (23)	1527	1229 (22)	1365 (14)	1297 (13)
1456	1322 (27)	1498 (2)	1410 (14)	1528	1011 (6)	1308 (29)	1159 (15)
1457	1230 (27)	1384 (13)	1307 (15)	1529	1339 (15)	1445 (17)	1392 (11)
1458	1068 (3)	1193 (2)	1131 (2)	1530	1017 (9)	1147 (28)	1082 (15)
1459	1256 (17)	1476 (6)	1366 (9)	1531	1339 (20)	1441 (33)	1390 (19)
1460	1303 (14)	1368 (13)	1335 (9)	1532	1288 (14)	1492 (6)	1390 (8)
1461	1192 (11)	1456 (10)	1324 (7)	1533	1228 (31)	1329 (17)	1279 (18)
1462	1357 (3)	1428 (3)	1392 (2)	1534	1168 (40)	1382 (26)	1275 (24)
1463	1171 (14)	1332 (6)	1252 (7)	1535	1295 (5)	1355 (6)	1325 (4)
1464	1041 (20)	1194 (25)	1118 (16)	1536	1002 (1)	1499 (1)	1251 (1)
1465	1014 (5)	1104 (12)	1059 (7)	1537	1229 (26)	1483 (19)	1356 (16)
1466	1100 (11)	1499 (2)	1300 (5)	1538	1321 (12)	1468 (5)	1394 (6)
1467	1007 (3)	1483 (10)	1245 (5)	1539	1369 (6)	1470 (6)	1420 (4)
1468	1036 (8)	1454 (28)	1245 (15)	1540	1122 (15)	1499 (1)	1310 (7)
1469	1238 (14)	1398 (12)	1318 (9)	1541	1087 (5)	1499 (1)	1293 (2)
1470	1245 (16)	1436 (13)	1340 (10)	1542	1028 (8)	1119 (13)	1073 (8)
1471	1008 (4)	1499 (1)	1254 (2)	1543	1336 (31)	1449 (37)	1392 (24)
1472	1003 (1)	1497 (6)	1250 (3)	1544	1154 (33)	1462 (5)	1308 (17)
1473	1011 (8)	1499 (1)	1255 (4)	1545	1361 (17)	1447 (22)	1404 (14)
1474	1007 (5)	1499 (1)	1253 (3)	1546	1395 (27)	1470 (20)	1433 (17)
1475	1223 (27)	1349 (17)	1286 (16)	1547	1039 (16)	1151 (22)	1095 (14)
1476	1097 (36)	1316 (44)	1206 (28)	1548	1361 (8)	1498 (2)	1430 (4)
1477	1387 (3)	1431 (3)	1409 (2)	1549	1202 (23)	1340 (13)	1271 (13)
1478	1043 (5)	1405 (11)	1224 (6)	1550	1077 (4)	1135 (22)	1106 (11)
1479	1010 (4)	1146 (22)	1078 (11)	1551	1018 (16)	1499 (1)	1258 (8)
1480	1078 (19)	1178 (72)	1128 (37)	1552	1119 (9)	1299 (10)	1209 (7)
1481	1062 (6)	1188 (15)	1125 (8)	1553	1045 (12)	1291 (13)	1168 (9)
1482	1265 (28)	1476 (8)	1371 (15)	1554	1306 (5)	1469 (20)	1387 (10)
1483	1395 (5)	1423 (4)	1409 (4)	1555	1311 (7)	1420 (24)	1365 (13)
1484	1320 (7)	1464 (20)	1392 (10)	1556	1101 (23)	1401 (20)	1251 (15)
1485	1146 (27)	1361 (18)	1254 (16)	1557	1113 (10)	1216 (13)	1164 (8)
1486	1134 (17)	1355 (12)	1245 (10)	1558	1268 (16)	1489 (5)	1379 (8)
1487	1101 (16)	1220 (15)	1161 (11)	1559	1378 (27)	1426 (17)	1402 (16)
1488	1179 (13)	1318 (26)	1248 (14)	1560	1352 (30)	1452 (40)	1402 (25)
1489	1391 (8)	1443 (17)	1417 (9)	1561	1007 (4)	1482 (16)	1245 (8)
1490	1246 (11)	1383 (34)	1315 (18)	1562	1004 (2)	1476 (17)	1240 (9)
1491	1340 (18)	1461 (6)	1401 (10)	1563	1296 (30)	1359 (28)	1328 (21)
1492	1036 (16)	1477 (9)	1257 (9)	1564	1114 (12)	1326 (8)	1220 (7)
1493	1013 (3)	1481 (7)	1247 (4)	1565	1168 (17)	1365 (9)	1266 (10)
1494	1244 (10)	1498 (3)	1371 (5)	1566	1306 (12)	1421 (9)	1364 (7)
1495	1253 (7)	1420 (4)	1336 (4)	1567	1161 (31)	1241 (13)	1201 (17)
1496	1038 (9)	1463 (16)	1250 (9)	1568	1115 (5)	1333 (5)	1224 (4)
1497	1038 (8)	1412 (16)	1225 (9)	1569	1218 (24)	1496 (4)	1357 (12)
1498	1312 (18)	1462 (7)	1387 (10)	1570	1352 (29)	1474 (22)	1413 (18)
1499	1293 (24)	1473 (6)	1383 (12)	1571	1098 (26)	1238 (21)	1168 (17)
1500	1315 (10)	1442 (23)	1379 (13)	1572	1285 (76)	1406 (38)	1345 (42)
1501	1066 (2)	1290 (61)	1178 (30)	1573	1139 (9)	1318 (8)	1228 (6)

Supplementary Table 1:

Burst ID <sup>a</sup>	$\nu_1^b$ (MHz)	$\nu_2^b$ (MHz)	$\nu_{p,obs}$ (MHz)	Burst ID <sup>a</sup>	$\nu_1^b$ (MHz)	$\nu_2^b$ (MHz)	$\nu_{p,obs}$ (MHz)
1502	1310 (22)	1486 (11)	1398 (12)	1574	1217 (8)	1499 (2)	1358 (4)
1503	1052 (34)	1458 (4)	1255 (17)	1575	1125 (4)	1499 (1)	1312 (2)
1504	1003 (1)	1409 (4)	1206 (2)	1576	1244 (31)	1488 (8)	1366 (16)
1505	1229 (4)	1494 (5)	1362 (3)	1577	1244 (9)	1481 (6)	1363 (5)
1506	1179 (27)	1475 (8)	1327 (14)	1578	1178 (24)	1465 (7)	1321 (12)
1507	1202 (16)	1407 (9)	1305 (9)	1579	1243 (19)	1457 (15)	1350 (12)
1508	1296 (35)	1414 (31)	1355 (23)	1580	1275 (36)	1336 (7)	1306 (18)
1509	1282 (44)	1351 (10)	1317 (22)	1581	1307 (4)	1465 (7)	1386 (4)
1510	1003 (1)	1499 (1)	1251 (1)	1582	1096 (8)	1248 (9)	1172 (6)
1511	1254 (4)	1423 (4)	1338 (3)	1583	1170 (22)	1478 (4)	1324 (11)
1512	1230 (45)	1422 (14)	1326 (24)	1584	1141 (5)	1353 (11)	1247 (6)
1585	1063 (15)	1419 (36)	1241 (19)	1619	1217 (31)	1490 (5)	1354 (16)
1586	1033 (16)	1107 (21)	1070 (13)	1620	1309 (21)	1492 (6)	1400 (11)
1587	1336 (24)	1475 (7)	1405 (12)	1621	1267 (20)	1496 (4)	1381 (10)
1588	1315 (23)	1482 (9)	1398 (12)	1622	1347 (29)	1475 (16)	1411 (16)
1589	1258 (12)	1328 (25)	1293 (14)	1623	1005 (2)	1271 (21)	1138 (11)
1590	1034 (17)	1192 (4)	1113 (9)	1624	1082 (29)	1414 (23)	1248 (19)
1591	1311 (22)	1456 (24)	1383 (17)	1625	1032 (9)	1395 (15)	1214 (8)
1592	1047 (4)	1328 (5)	1187 (3)	1626	1121 (23)	1481 (5)	1301 (12)
1593	1207 (15)	1290 (21)	1248 (13)	1627	1020 (8)	1100 (13)	1060 (8)
1594	1161 (41)	1334 (17)	1247 (22)	1628	1195 (19)	1316 (22)	1256 (14)
1595	1070 (14)	1222 (7)	1146 (8)	1629	1237 (58)	1484 (27)	1360 (32)
1596	1221 (31)	1359 (18)	1290 (18)	1630	1316 (22)	1450 (12)	1383 (13)
1597	1023 (12)	1122 (14)	1073 (9)	1631	1251 (19)	1497 (3)	1374 (10)
1598	1301 (12)	1437 (32)	1369 (17)	1632	1275 (23)	1489 (4)	1382 (12)
1599	1383 (15)	1483 (10)	1433 (9)	1633	1188 (15)	1471 (12)	1329 (10)
1600	1190 (4)	1478 (9)	1334 (5)	1634	1221 (30)	1499 (1)	1360 (15)
1601	1072 (17)	1473 (3)	1272 (9)	1635	1002 (1)	1489 (11)	1245 (6)
1602	1130 (7)	1499 (1)	1315 (3)	1636	1286 (22)	1432 (9)	1359 (12)
1603	1124 (11)	1418 (9)	1271 (7)	1637	1065 (9)	1114 (7)	1089 (6)
1604	1286 (31)	1485 (5)	1386 (16)	1638	1027 (2)	1090 (3)	1059 (2)
1605	1287 (18)	1499 (1)	1393 (9)	1639	1064 (6)	1419 (16)	1241 (8)
1606	1263 (42)	1466 (24)	1365 (24)	1640	1305 (13)	1488 (9)	1396 (8)
1607	1220 (32)	1363 (21)	1291 (19)	1641	1241 (19)	1472 (4)	1357 (10)
1608	1123 (8)	1242 (6)	1182 (5)	1642	1070 (15)	1168 (59)	1119 (30)
1609	1075 (55)	1412 (31)	1243 (32)	1643	1288 (23)	1465 (20)	1376 (15)
1610	1177 (14)	1485 (8)	1331 (8)	1644	1332 (15)	1492 (4)	1412 (8)
1611	1219 (18)	1499 (1)	1359 (9)	1645	1012 (4)	1260 (15)	1136 (8)
1612	1103 (32)	1499 (1)	1301 (16)	1646	1161 (10)	1297 (13)	1229 (8)
1613	1120 (53)	1433 (7)	1276 (27)	1647	1142 (7)	1390 (13)	1266 (8)
1614	1161 (15)	1385 (37)	1273 (20)	1648	1093 (10)	1373 (9)	1233 (7)
1615	1330 (14)	1495 (7)	1413 (8)	1649	1010 (3)	1388 (6)	1199 (3)
1616	1090 (23)	1235 (19)	1163 (15)	1650	1370 (10)	1421 (7)	1396 (6)
1617	1171 (19)	1483 (5)	1327 (10)	1651	1198 (13)	1275 (15)	1237 (10)
1618	1145 (8)	1469 (8)	1307 (6)	1652	1086 (13)	1487 (5)	1287 (7)

<sup>a</sup> The burst IDs are the same as those in previous work<sup>1</sup>.

<sup>b</sup> Measurements were taken across the full 1 – 1.5 GHz operating band of FAST, with better precision within the central band of 1.05 – 1.45 GHz.